C-2

ANALYSIS OF AN ULTRAFAST DISCHARGE IN AIR PRODUCED BY A MEGAVOLT PULSE SYSTEM

by

Joshua Shuchatowitz

Submitted in partial fulfillment of the requirements for the degree of
Doctor of Philosophy
in the Belfer Graduate School of Science
Yeshiva University
New York, New York 10033
September 1967

The committee for this doctoral dissertation consisted of:

David Finkelstein, Ph.D., chairman

A.G.W. Cameron, Ph.D.

Leon F. Landovitz, Ph.D.

Joel L. Lebowitz, Ph.D.

Abstract

An alternative to the Marx circuit for the production of high-voltage, high-current pulses has been developed. It employs a water immersed spiral-wound step up transformer capable of obtaining an output of one million volts from a capacitor bank charged to 100 kilovolts. A method is derived for using this transformer to efficiently pulse-charge a second capacitor bank without very tight coupling. The primary and secondary circuits each contain two resonant frequencies (each measured with the other circuit open). It is shown that total transfer of energy (except for dissipation) occurs when the two resonant frequencies of the primary and secondary are equal. The two normal mode frequencies of the coupled circuit should be in the ratio of 2:1 employing a coupling coefficient of 3/5. The design and application of such a system to produce a discharge in air a atmospheric pressure is described ($E = 10^4$ Joules, V = 720 kV). The current rises at about 5.5×10^{12} amp/sec. to a peak value of about 3×10^5 amps. When the discharge path is sufficiently narrow, the gas column contracts by magnetic pinching and then expands rapidly. An analysis of the cylindrical shock produced by this discharge shows that about 20% of the available energy is dissipated in driving the shock. The column of gas reaches an average temperature of $1.5 \times 10^{5^o}$K.

Acknowledgements

To Professor David Finkelstein, for his guidance, insight and sustaining interest, I am deeply indebted.

The many discussions with Professor Leon Landovitz and Dr. Morton Levine have proved most helpful. The contributions of Dr. Philip Goldberg to the design of Mark I are appreciated. Valuable assistance was supplied by the staff of the Plasma Physics Laboratory, Belfer Graduate School of Science, particularly Mr. Charles Young and Mr. Leon Dewan of the technical staff.

Financial support for the work covered in this report was provided by the Air Force Cambridge Research Laboratories, Office of Aerospace Research under Contract No. AF 19(628)2399.

I wish to thank the office staff, especially Miss Harriet Nachmann for typing this report. The original manuscript was prepared by Mrs. Bobbie Friedman; her efforts and suggestions are gratefully acknowledged.

Table of Contents

Diagrams and Illustrations

Tables

Part I

Analysis of the Megavolt Pulse System

1. Introduction

In recent years numerous studies have been undertaken to investigate various properties of pulsed and steady state plasmas. One type of plasma under study at our laboratories has been the type produced by a current carrying plasma column compressed by its own magnetic field. This phenomenon has been called the "pinch effect". (Fig. 1) The concept of the pinch effect was first discussed by Bennet[1] and later by Tonks.[2] The first experimental approaches to a pinch in a gas atmosphere were made by Cousins and Ware[3] in a toroidal geometry, by Kurchatov[4] et al. and by Burkhardt[5] in a linear geometry. Linhart[6] has given an approximate treatment of the constriction mechanism of the hollow pinch. The theoretical results of Leontovich,[7] derived for the normal pinch effect, give qualitative information of the contraction of the hollow pinch.

In a pinch, the resultant magnetic pressure compresses the gas resulting in a heating action which may be viewed as analogous to that produced by the adiabatic compression of a gas. Clearly, the temperature depends upon the volume change in a way such that a large increase in temperature implies a very high compression.

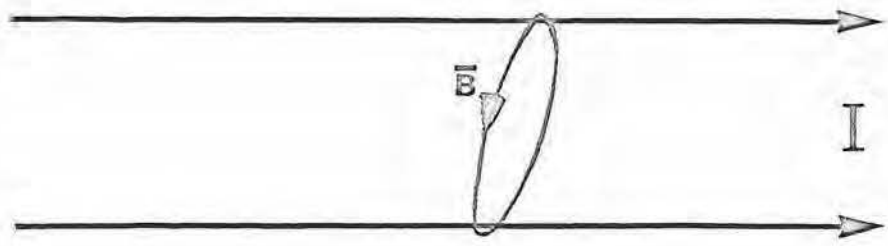

FIGURE 1 - The Pinch Effect

In almost all of the techniques proposed for producing a stably confined, high-temperature plasma, the idea is to separate the plasma from the walls of its container by means of magnetic fields in vacuum. One approach has been to ionize a low density gas with a strong electric field, compress the gas by the application of a magnetic field, and then heat the gas to a high temperature by some method. A different system has been suggested by Alfven and Smars[8] in 1960. Instead of having the plasma surrounded by vacuum they suggested that one should start out with the container filled with gas of high density and ionize and heat only a small volume of the gas in the center of the vessel using magnetic fields for confinement. The hot plasma would thus be separated from the walls of its container by a high density magnetized gas.

Their calculations using a very simple model[8] showed that the energy losses from the hot plasma region to the walls by heat conduction in the surrounding gas need not be prohibitive. In another paper Smars[9] pointed out that the obvious geometry for such a system would be a cylindrical plasma column ohmically heated by a strong current in the axial direction and surrounded by cool gas of high density. The azimuthal self-magnetic field would then be used for confinement and for limiting the heat conductivity of the plasma.

Theoretical studies[10,11] have been made to analyze the stationary and dynamic states of a cylindrical column of fully ionized high-pressure plasma. Calculations indicated that one potential advantage of surrounding the plasma with a high density gas should be its influence on plasma instabilities. Another advantage is that impurities from the walls of the confining vessel would be effectively prevented from reaching the hot plasma region. Thus, one of the greatest problems in obtaining sustained thermonuclear fusion, that of bremsstrahlung losses from a hot

plasma due to the presence of impurity ions, should be minimized. Experimental studies[12] clearly indicated an increase in stability of the current channel with increasing gas pressure. Although the results until now have not been entirely conclusive, spectroscopic observations give clear evidence that when the discharge is of the type considered above an extremely clean plasma will result.

In order to obtain high energy plasmas, high electric field gradients are required. Fried[13] has shown that a deuterium plasma of density 1.6×10^{17} particles per cm^{-3} requires electric fields on the order of 10^6 volts per cm. to produce a particle kinetic energy of 40 kev. In adiabatic heating it is important to put in the energy as quickly as possible in order to obtain a high-temperature plasma. Commercially available condenser banks with their relatively high self inductance limit the power input to magnitudes on the order of 10^{11} watts. The high temperature plasma produced by an adiabatic atmospheric pinch would be an interesting one to observe for many reasons.

(a) The requirement of high electric field gradients places particle velocities in the relativistic region. We could then investigate the relativistic plasma, a plasma whose charged particles are moving with random relative velocities comparable to the speed of light.

The plasma frequency, ω_p, is given by

$$\omega_p^2 = \frac{4\pi ne^2}{m} \tag{1.1}$$

The large electric field gradients would cause a relativistic increase in the mass of the electrons which would decrease the plasma frequency and should change the stability properties.

It has been suggested[14] that in such a pinch, relativistic effects would lead to greater stability and thereby to higher pinch temperatures.[15,16,17]

plasma due to the presence of impurity ions, should be minimized. Experimental studies[12] clearly indicated an increase in stability of the current channel with increasing gas pressure. Although the results until now have not been entirely conclusive, spectroscopic observations give clear evidence that when the discharge is of the type considered above an extremely clean plasma will result.

In order to obtain high energy plasmas, high electric field gradients are required. Fried[13] has shown that a deuterium plasma of density 1.6×10^{17} particles per cm^{-3} requires electric fields on the order of 10^6 volts per cm. to produce a particle kinetic energy of 40 kev. In adiabatic heating it is important to put in the energy as quickly as possible in order to obtain a high-temperature plasma. Commercially available condenser banks with their relatively high self inductance limit the power input to magnitudes on the order of 10^{11} watts. The high temperature plasma produced by an adiabatic atmospheric pinch would be an interesting one to observe for many reasons.

(a) The requirement of high electric field gradients places particle velocities in the relativistic region. We could then investigate the relativistic plasma, a plasma whose charged particles are moving with random relative velocities comparable to the speed of light.

The plasma frequency, ω_p, is given by

$$\omega_p^2 = \frac{4\pi ne^2}{m} \tag{1.1}$$

The large electric field gradients would cause a relativistic increase in the mass of the electrons which would decrease the plasma frequency and should change the stability properties.

It has been suggested[14] that in such a pinch, relativistic effects would lead to greater stability and thereby to higher pinch temperatures.[15,16,17]

(b) There would be an intense output of electromagnetic radiation; the possibility of the production of nuclear particles would make this a nuclear plasma. The nuclear plasma is discussed further in section 25.

(c) The interest of the spectroscopist in the spark discharge has greatly increased during the past few years[18] but in spite of this, there is no consistent theory of the spark in sufficient detail to elucidate its properties, as there is, for instance, for the arc discharge. The question arises: to what extent does the voltage of the spark affect its character, and what is necessary to obtain a "hot" spectrum?

Presently physicists believe the special nature of the spark spectrum is intimately connected with the mechanism of the formation of the channel of the spark. A detailed investigation of the physical process of the formation and expansion of the channel coupled with a hydrodynamic theory of the channel of the spark discharge would enable us to understand the mode of excitation of spectra in the spark.

(d) Relativistic plasmas may occur in nature. The Crab Nebula has a radiative pattern which strongly implies a relativistic plasma.

(e) Much is left to be discovered about the physics governing lightning and cloud formation. Until now scientists have been limited for the most part to observation of naturally occurring phenomena.[18,19] Experimentation has been limited by the lack of a device capable of producing the high electric fields and currents necessary to simulate a lightning discharge. The experimental apparatus described in this paper could be adapted to simulate true atmospheric lightning conditions.

(f) A parameter of particular interest in controlled fusion programs is Lawson's Criterion.[20] This is the product $N\tau$, where N is the density of the plasma and τ is the confinement time. It may be shown that, if a system is to be of thermonuclear interest, the product $N\tau$ must be of the order of 10^{15} sec/cm^3. An associated critical factor is the ion temperature which must be of the order of 10^4 to 10^5 electron volts. At atmospheric pressures the density is approximately 10^{19} particles/cm^3 which gives τ a value of .1 milli-seconds. The minimum confinement time can thus be considerably reduced by working at high pressures.

The technical difficulties involved in establishing fast, high energy discharges in plasmas have limited much of the research in this area.[13] In particular, the production of a relativistic plasma and study of its dynamics is the aim of several present experimental programs.[21] Various methods have been tried or proposed for similar purposes. In some of these a beam of electrons is gradually established and accelerated and subsequently neutralized.[21,22] In others an electric field is applied to a gas in order to ionize the gas and accelerate the electrons in the resulting plasma.[23,24] It was mentioned above that to establish a relativistic pinch, million volt per cm. fields applied only for very short times are required. Indeed, the acceleration ought to be complete in one or several plasma periods. An extremely high current growth rate is also necessary to achieve maximum pinch temperatures in fast pinch times: $dI/dt \sim 10^{13}$ amps/sec.[13] Therefore, the difficulty of contending with these mutual requirements may be responsible for the lack of previous work in this density and velocity regime.

2. Description of the Apparatus - The Terrawatt Pulse System

The incompatibility of the values discussed in section I.1 with the discharge times of conventional, high-energy condenser banks has led to the design of new geometries with only limited success.[13] In the present experiment we consider the simplest possible geometry to simplify so far as possible the problems connected with such large electric fields. This singles out the linear pinch geometry. In this paper we show how a conventional high-energy bank, operating at 100 KV, may be used as the first stage of a system in which the discharge is obtained from a low inductance water capacitor. This capacitor can only hold its energy for tens of microseconds, but can discharge in less than 10^{-7} seconds. Our nominal energy requirement is 10^5 joules (a power of 10^{12} watts) which must be transferred from one capacitor and stepped up in voltage from 10^5 volts to 10^6 volts. In this manner, the mutually exclusive requirements of safe energy accumulation and extremely low inductance may be successfully dealt with and a million volt, million ampere terrawatt discharge achieved.

The schematic circuit of the arrangement to produce a discharge is shown in Figure 2. It is an extrapolation in current but not in voltage of systems successfully employed at the Naval Research Laboratory and at Tech Ops, Inc.[24] It is a two stage system. Stage 1 centers about a 100 kV capacitor bank of conventional commercial capacitors. A bank of such construction can be reliable but cannot have the lowest possible inductance, as is required for shortest possible discharge times. Therefore a

second stage is added, a special water capacitor capable of holding energy for only short times (tens of microseconds) but able to discharge in times ~ 100 nsec. In this way, the mutually exclusive requirements of safe energy accumulation and extremely low inductance are separated into two systems. In addition, switches are required to transfer the energy from stage 1 to stage 2 and then from stage 2 to the plasma experiment. Moreover, it is found practical to store energy in capacitors for long times at voltages up to ~ 100 kV, but we wish a discharge at 1 MV. Therefore a transformer of some sort is required between stage 1 and 2. In the following sections we describe the design and performance of the discharge system which includes:

a) 100 kV conventional energy storage capacitor bank

b) ruptured dielectric switch

c) a unique air core pulse transformer which is able to produce a one million volt pulse by the technique of "double-resonance" pulse charging

d) specially designed water capacitor

e) air gap discharge assembly.

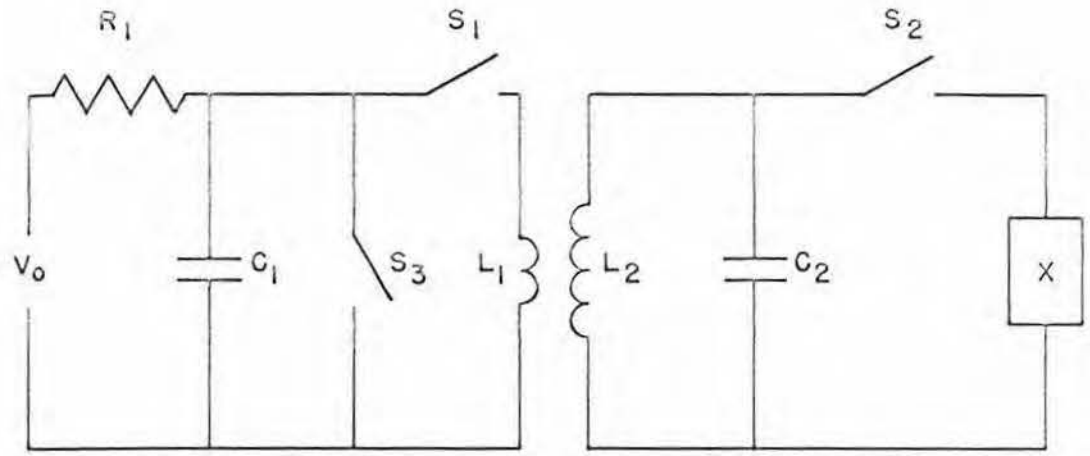

FIGURE 2

Circuit Schematic of Pulse System

V_o: charging supply, 0 - ± 100 KVDC, 100 MA.

R: charging resistor.

C_1: capacitor bank, 40 x .5μF, 100 kV

L_1, L_2: air-core transformer, L_2 = 100 L_1, k = 3/5.

C_2: water capacitor, .2μF, 1 MV.

After C_1 is charged the switches close in the following timing:

S_1 at t = 0 (V_1 = 100 kV, V_2 = 0)

S_2 at t = T_+ (V_1 = 0, V_2 = 1 MV)

S_3 at t = T_+ + 1 μsec

The "crow-bar" S_3 prevents return of charge to C_1 and is needed only in case S_2 does not fire.

3. The Capacitor Bank

The capacitor bank is shown in figures 3a-3d. The individual units are made by BICC and are rated at .5 μF @ 100 kV, and each has a ringing frequency of 490 kc/sec. Their guaranteed life is 5,000 discharges with full oscillation. With crowbar switch (S_3 in Figure 2) longer life could be expected. Each weighs 250 pounds. A detailed diagram of the BICC capacitor is shown in figure 4. Taken together the capacitors weigh five tons. They are mounted in a rack of bolted Dexion 300 steel angle iron members. The capacitors are inclined 2° below the horizontal to move bubbles to the low voltage-end. They are connected in parallel by a system of air-spaced aluminum bus-bars as shown in figure 3c. Each bus-bar is 108" x $\frac{1}{4}$" x 6". The high-voltage system of bus-bars is suspended directly from the ceramic bushings of the capacitors. The ground plane is made up of a series of $\frac{1}{2}$" aluminum rods clamped to the six screws on each capacitor as shown in figure 3b. To these rods are fastened as shown five lengths of 4" x 108" x $\frac{1}{4}$" bus-bar.

A total failure of one of the capacitors connected in parallel can permit the energy stored in the others to be discharged into the faulty unit, a well-known hazard for such capacitor banks. This capacitor bank is designed to be safe against accidents resulting from such failure. First of all, each capacitor consists of many separate sub-units in series. Even if one of these sub-units breaks down internally, the others are designed to stand the slight resulting overvoltage for a considerable time. Secondly, such an internal failure is accompanied by rapid increase in the

gas pressure within the capacitor. This activates a bellows mounted in the end of the capacitor remote from the high-voltage bushing. Should any of the forty bellows be thus exhausted, an interlock in the high-voltage system is actuated and the bank is discharged by an automatic crowbar. This requires less than .1 second. Simultaneously an indicator light shows the faulty unit. Figure 3d shows the bellows-actuated alarm system. Thirdly, no persons are permitted in the capacitor room except when the bank is shorted. At the end of each run the bank is automatically shorted to prevent any residual voltages.

Each capacitor has a self-inductance of approximately .1μH according to the quoted ringing frequency. Thus the self-inductance of the forty in parallel is necessarily at least 2.5 nH. In accordance with the two-stage principle outlined in section 2 above, we have not cut corners with the high-voltage reliability of the capacitor bank in order to trim the inductance and the discharge time. However it is elementary to extract the current from the capacitor bank at the center rather than the end of the buswork. If we neglet the distributed nature of the bus inductance and approximate it by a rectangle then the inductance of the bus system measured at the center is approximately

$$L \sim \mu_o \frac{a\ b}{4\ c} \sim 250 \text{ nH} \qquad 3.1$$

where a is the effective over-all length of 3 m, b is the air space of .3 m, and c is the sum of the bus-bar heights of .6m. (See Appendix A.1) Thus the total self-inductance of the capacitor bank measured at output terminals is dominated by the bus-bars and should then be approximately 70 kc/sec. The actual wave-form

of the current in a short circuit at the output terminal is shown in Figure 5. The measured ringing frequency is 50 kc/sec, and so the actual bank inductance is 500 nH.

As a result of this large self-inductance, the peak current that can flow during discharge even for short-circuit conditions is only one million amperes.

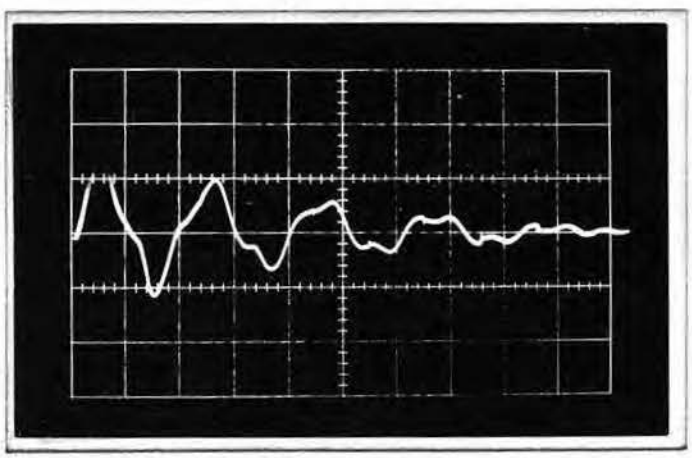

FIGURE 5

Discharge Wave-form
Bank is charged to 5 kV and switched into
3 cm length of iron wire (10^{-3} Ohm).
Time scale: 2 μsec per least division.

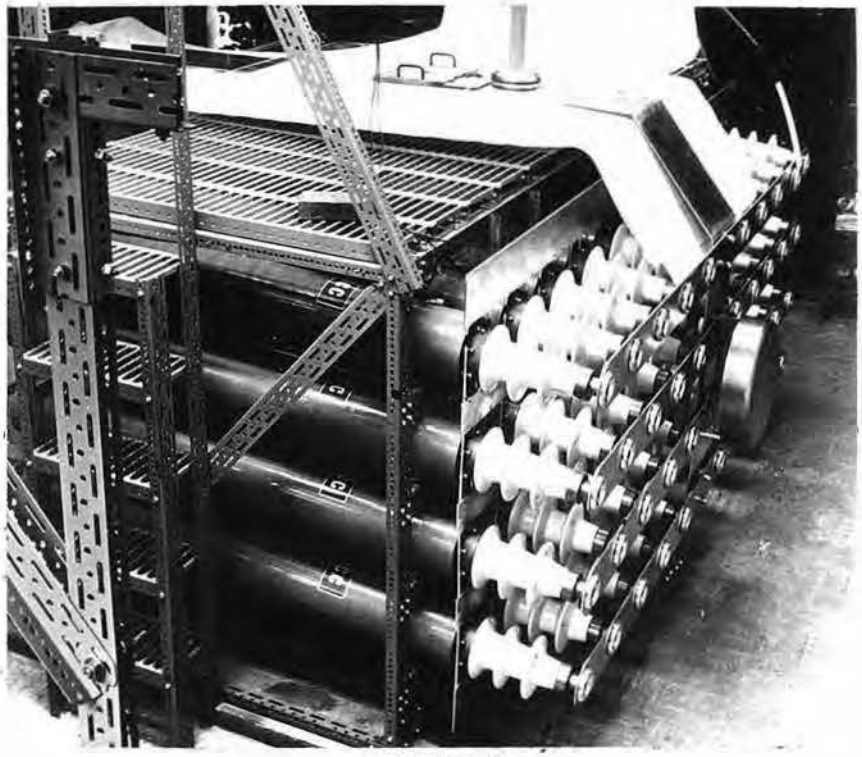

FIGURE 3a
The 100 KC Capacitor Bank

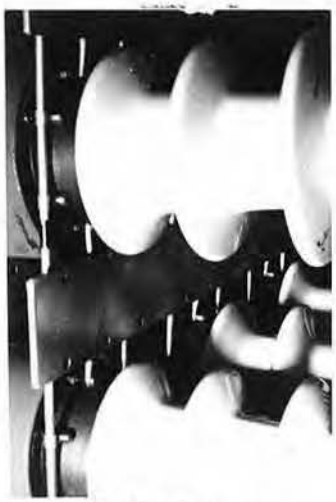

FIGURE 3b
Ground Plane Connections

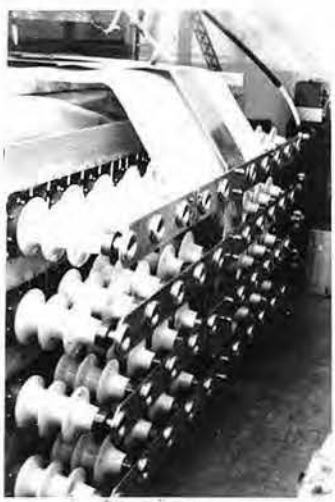

FIGURE 3c
High-Voltage Plane Connections

FIGURE 3d
Bellows Actuated
Safety System

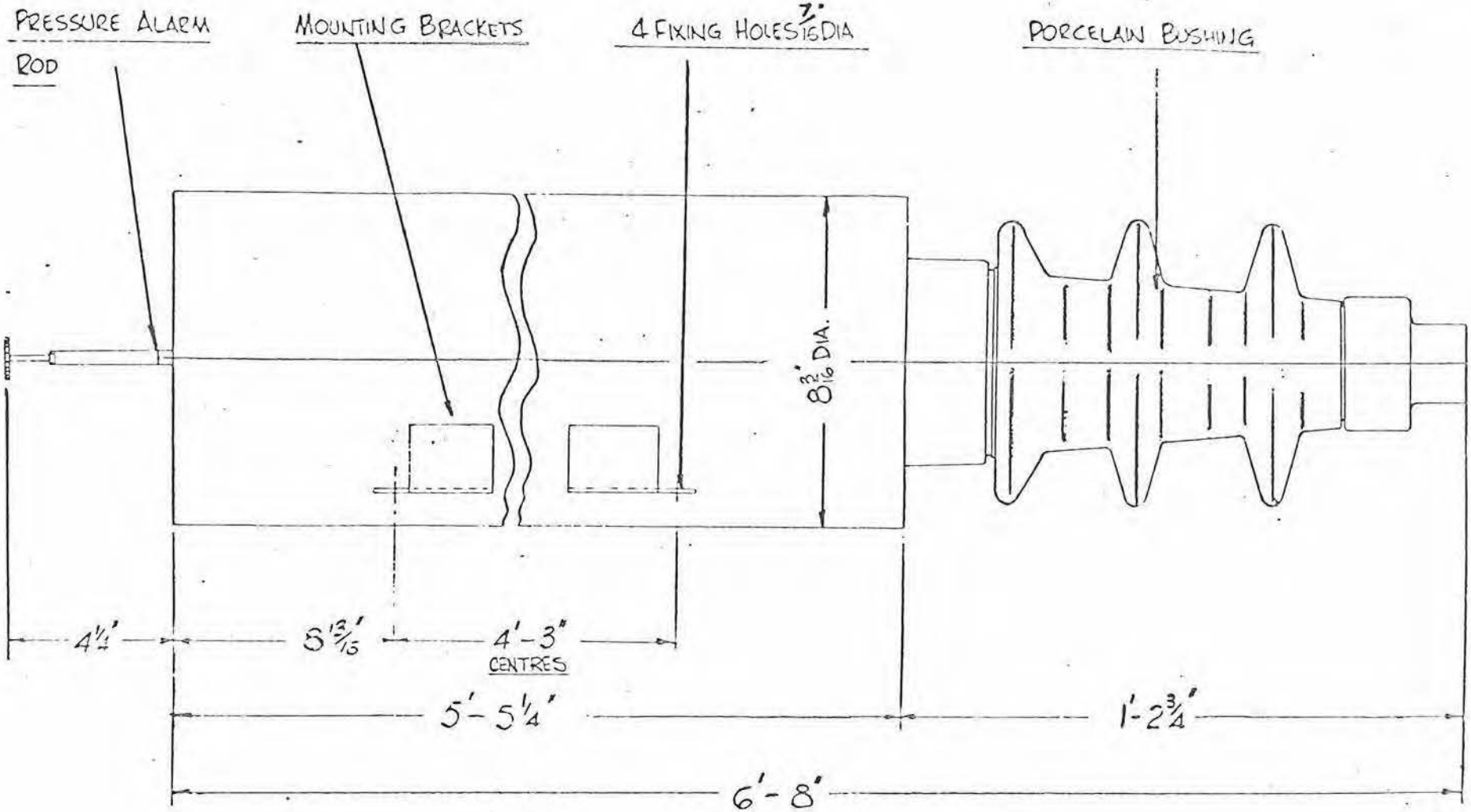

FIGURE 4

Detail Drawing of BICC 100 kV Energy Storage Capacitor

4. The Ruptured Dielectric Switch

In order to discharge the capacitor bank described in the previous section, we required a switch that would withstand a voltage rising slowly to approximately 100 kV during the charging of the capacitor and that would pass when actuated a current rising to 10^6 amps.

We selected a switch that did not require much development time though it was midly extravagant of operation time. Figure 6 shows the general plan of this kind of switch. A sheet of solid dielectric (safe for 100 kV) is sandwiched between a bus-bar carrying the high voltage from the capacitor bank and a bus-bar leading to the load. While the capacitor bank is charging its full terminal voltage appears across this dielectric. After the capacitor bank is charged the dielectric is ruptured. After each discharge the dielectric must be replaced before recharging the bank.

A prototype was tested with a smaller capacitor of .5μf at 80 kV while the main bank was being constructed. Polyethylene was the dielectric and a spring-driven needle ruptured it. The needle mechanism was replaced by a .22 caliber rifle firing a high-velocity bullet, which was placed at a greater distance from the discharge it initiated. The tests were carried out in order to see how much bracing the switch required, how thin the dielectric could be, and how long it took to make ready for the next shot. It was found that for short periods of time a safe value for the dielectric strength of polyethylene is 1000 volts/mil. Our experience indicates that an 18-24 inch border of polyethylene is sufficient up to 100 kV depending on the humidity of the air.

Intense magnetic fields are established within the switch.

When the peak current flows along the perimeter of the bullet a magnetic induction of about 50 Tesla is set up. Because of their relatively great inertia the solid parts of the switch do not accept much of the energy that is passing through it. In order to minimize the gaseous part of the circuit the polyethylene dielectric is sandwiched between 12" squares of 1" steel, the upper one of which has a 3/8" hole drilled in its center to accommodate the bullet. During the operation of the switch the sound of the rifle shot is quite unnoticeable.

From the muzzle velocity of the bullet we estimate that it takes about one microsecond for the circuit to be closed. This is a small part of the rise time of the capacitor discharge current, which is at least 5 microseconds.

If we approximate the air gap switch to be a thin wire of radius a, then the magnetic field produced by a current i is given by

$$B \sim \frac{\mu_o i}{2\pi a} \tag{4.1}$$

The inductance is given by

$$L = \frac{\phi}{i} = \frac{\ell}{i} \int B \cdot dr \tag{4.2}$$

where ℓ is the length of the discharge between the steel plates.

$$L = \frac{\mu_o \ell}{2\pi} \ell n \; r \Big|_{r_o}^{4cm} \tag{4.3}$$

$$\sim \frac{\mu_o \ell}{\pi} \sim 10 \text{ nH}$$

This is negligible compared to the inductance of the bus-bar system.

When time and resources permit it would be preferable that the rifle switch be replaced by a system of somewhat more conventional design, but this switch appears reliable and suitable for

our present needs. We have not found any need for external pre-ionization. The switch, to our delight, has proved to be far more reliable than expected.

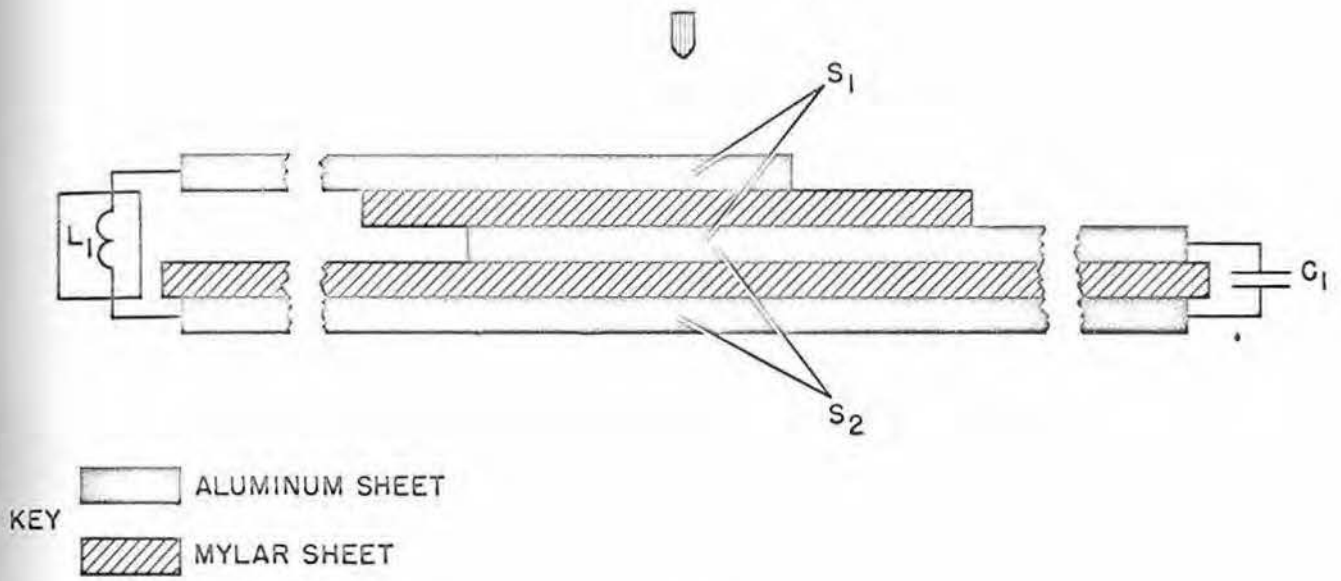

FIGURE 6
Ruptured Dielectric Switch

(S_1,S_3, in Fig. 2)

5. The Pulse Transformer

Basic Theory of the Double Resonance Principle

Introduction: The transformer couples the 100 kV capacitor bank through the switch to a water capacitor which is to be charged to one million volts. We shall first consider the selection of design parameters of the transformer and then the problem of construction. In first approximation we shall neglect losses in the capacitor bank and in the water capacitor and the interwinding capacitance. Let us take the inductance L_1 assigned in Figure 7 to the primary to include as well the inductance of the capacitor bank and the system of bus-bars and the switch. Likewise the inductance L_2 will be the total inductance of the secondary circuit. Suppose S_1 closed, S_2 and S_3 open. It will be shown that this coupled system has two modes with frequencies ω_+, ω_- different from the frequencies ω_1 and ω_2 that the primary and secondary LC circuits would have in the absence of coupling. The current that flows in the secondary will in general contain components at both mode frequencies ω_+, ω_-. It can be shown that the particular combination of modes excited by the closing of S_1 in the primary is one in which charges of both frequencies occur in the secondary with equal amplitudes and opposite initial phase. Generally therefore the charge on the water capacitor C_2 will have many local maxima of various magnitudes. In order for the largest of these maxima to occur after a small number of cycles, the two mode frequencies ω_+ and ω_- must be commensurable with small integer coefficients. The best possible case is $\omega_+ = 2\omega_-$ in which case the largest possible maxima occurs after one

period of the faster mode ω_+. It will further be shown that in order for this maxima to contain the energy stored originally in capacitance C_1 it is necessary that the primary and secondary resonant frequencies, ω_1 and ω_2, should be equal. These two conditions further imply that the coupling constant k is 3/5. Finally, in this favorable case the ratio of the peak primary and secondary voltages is simply given in terms of the corresponding inductances or capacitances:

$$V_2/V_1 = \sqrt{L_2/L_1} \quad = \sqrt{C_1/C_2} \qquad 5.1$$

The optimal coupling coefficient here is not the largest attainable, but the special value k = 3/5, which is easily possible. Notice that the selection of transformer parameters for resonant pulse-charging a capacitor is very different from coupling to a dissipative load where impedance matching and high coupling coefficient are important. In order to allow for losses in the switch and for leakage flux in the transformer, a turns-ratio of between 15 and 20 is suggested. The equivalent circuit for the system is given in Figure 7.

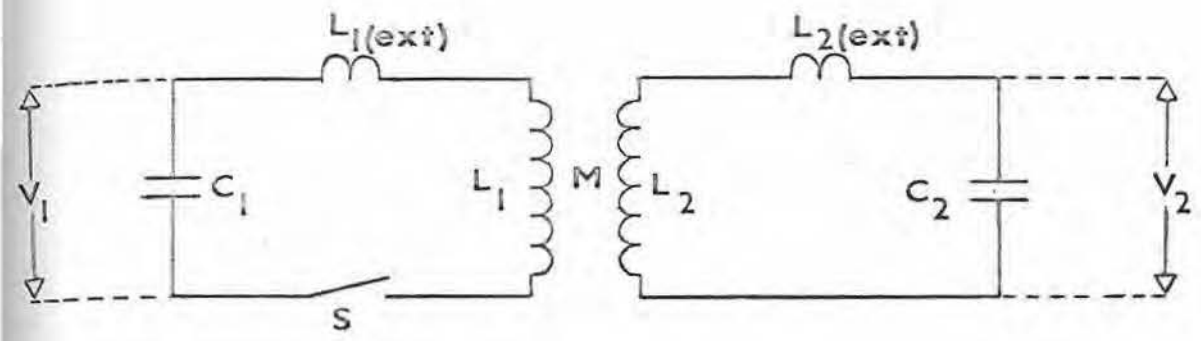

FIGURE 7

Equivalent Circuit for Pulse System

L_1	= total primary inductance
L_2	= total secondary inductance
C_1	= capacitance of high energy bank
C_2	= capacitance of water capacitor
V_1	= 10^5 volts
V_2	= 10^6 volts
S_1	= ruptured dielectric switch
M	= mutual inductance of transformer
$k = M/\sqrt{L_1 L_2}$	= coupling constant of transformer

Circuit Equations 26, 27

The circuit equations are given by

$$\left[L_1 \frac{d^2}{dt^2} + \frac{1}{C_1}\right] q_1 + M \frac{d^2}{dt^2} q_2 = 0 \qquad 5.2$$

where the subscripts 1 and 2 refer to the primary and secondary circuits respectively of Figure 7.

$$M \frac{d^2}{dt^2} q_1 + \left[L_2 \frac{d^2}{dt^2} + \frac{1}{C_2}\right] q_2 = 0 \qquad 5.3$$

The discussion of equations 5.2 and 5.3 is facilitated by using convenient units of length, time and charge. We set:

$$C_1 = 1$$

$$L_1 = 1$$

$$\omega_1 = 1/\sqrt{L_1 C_1} = 1$$

$$q_1(0) = 1$$

and

$$L_2 = L$$

$$C_2 = C$$

$$\omega_2 = 1/\sqrt{LC}$$

$$k^2 = M^2/L$$

Substituting $q_k(t) = Q_k e^{i\omega t}$ in 5.2 and 5.3 we obtain:

$$\begin{pmatrix} 1 - \omega^2 & -M\omega^2 \\ -M\omega^2 & \frac{1}{C} - L\omega^2 \end{pmatrix} \begin{pmatrix} Q_1 \\ Q_2 \end{pmatrix} = 0 \qquad 5.4$$

The non-trivial solution to 5.4 is given by:

$$(1 - \omega^2)\left(\frac{1}{C} - L\omega^2\right) - M^2\omega^4 = 0 \qquad 5.5$$

We have:

$$(L - M^2)\,\omega^4 - \left(L + \frac{1}{C}\right)\omega^2 + \frac{1}{C} = 0$$

$$(1 - k^2)\,\omega^4 - (1 + \omega_2^2)\,\omega^2 + \omega_2^2 = 0 \qquad 5.6$$

and

$$\omega^2 = \frac{(1 + \omega_2^2) \pm \sqrt{(1+\omega_2^2)^2 + 4k^2\omega_2^2}}{2\,(1-k^2)}$$

Let us designate the four roots of 5.6 by $\pm \omega_+$, $\pm \omega_-$.

The general solution to the coupled equations 5.2 and 5.3 is obtained by summing over the normal modes:

$$q_k = \sum_{j=1}^{4} Q_k^j \, e^{i\omega_j t} \qquad 5.7$$

$$i_k = \sum_{j=1}^{4} i\omega_j Q_k^j e^{i\omega_j t} \qquad 5.8$$

with the following initial conditions:

$$\text{at } t = 0 \qquad q_1 = 1 \quad q_2 = 0$$

$$i_1 = 0 \quad i_2 = 0 \qquad 5.9$$

Therefore:

$$(\omega_+ Q_k^1 - \omega_+ Q_k^2) + (\omega_- Q_k^3 - \omega_- Q_k^4) = 0$$

and

$$Q_k^1 = Q_k^2 \equiv Q_{k+}$$

$$Q_k^3 = Q_k^4 \equiv Q_{k-} \qquad 5.10$$

Using equation (5.7) at t = 0 we see

$$Q_{2+} = - Q_{2-} \qquad 5.11$$

We see that q_2, the charge on C_2, is composed of two modes, ω_+ and ω_- which contribute equal amplitudes Q_{2+} and Q_{2-}. The maximum voltage on C_2 will occur at a time T for which these modes add such that:

$$\text{at } t = T \qquad q_1 = 0 \quad i_1 = 0$$

$$q_2 = 1 \quad i_2 = 0 \qquad 5.12$$

From equation 5.7 we have at time T:

$$Q_{1+} \cos \omega_+ T + Q_{1-} \cos \omega_- T = 0$$

The two normal modes must contribute in equal amplitude to the primary oscillation as well as to the secondary oscillation, but with coincident initial phases. Then at time T the primary and secondary capacitors will have exchanged roles and we must have:

$$Q_{1+} = Q_{1-} \qquad 5.13$$

and

$$\omega_- T = n\pi \qquad \omega_+ T = (n + 2m + 1)\pi \qquad 5.14$$

Taking m = 0,

$$\frac{\omega_+}{\omega_-} = \frac{n + 1}{n} \qquad 5.15$$

As we would like T to be a minimum to reduce electrical breakdown difficulties at C_2 we choose n = 1 yielding:

$$\omega_+ = 2\omega_- \qquad 5.16$$

Figure 8 shows the charge modes at C_2.

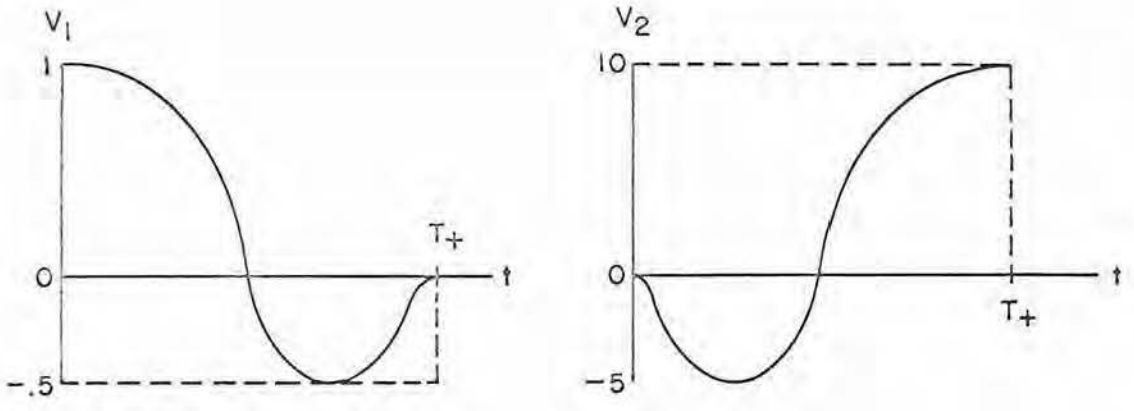

FIGURE 8

Charge Modes on the Water Capacitor

Theoretical wave-forms of V_1, V_2 during pulse-charging by the double-resonance method. Both the capacitor bank and the water capacitor are subject to one voltage reversal of 50% during pulse-charging.

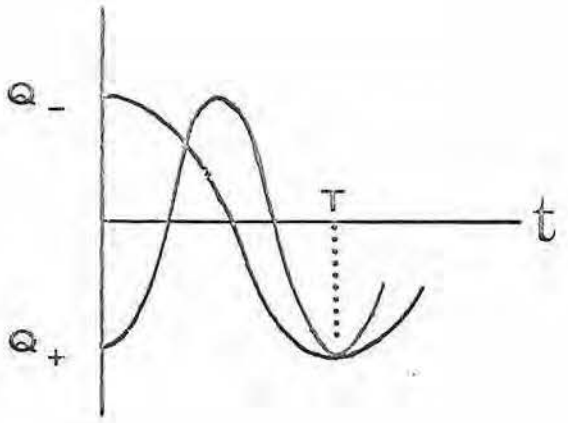

FIGURE 9

Voltage Waveforms for Double Resonance

Referring to equation 5.4 we have:

$$\frac{Q_{1\pm}}{Q_{2\pm}} = \frac{M\omega_{\pm}^{2}}{1-\omega_{\pm}^{2}}$$

Therefore,

$$\frac{(\omega_{+})^{2}}{1-\omega_{+}^{2}} = -\frac{(\omega_{-})^{2}}{1-\omega_{-}^{2}}$$

and

$$\omega_{-}^{2} = 5/8$$

5.17

$$\omega_{+}^{2} = 20/8$$

Using the second of equations (5.4) one obtains

$$\frac{\omega_{+}^{2}}{\omega_{2}^{2}-\omega_{+}^{2}} = \frac{-\omega_{-}^{2}}{\omega_{2}^{2}-\omega_{-}^{2}}$$

and

$$\omega_{2} = \omega_{1} = 1 \qquad 5.18$$

We therefore obtain maximum energy transfer under these ideal "double-resonance" conditions, $\omega_1 = \omega_2$ and $\omega_{+} = 2\omega_{-}$. Furthermore we note that the coupling constant k is determined. From (5.6) it follows that

$$\omega_{+}^{2} + \omega_{-}^{2} = \frac{1 + \omega_{2}^{2}}{1-k^{2}}$$

From which

$$k = .6 \qquad 5.19$$

We see that in resonant pulse charging, maximum energy transfer is obtained with a relatively low coupling constant. Actually, there are a discrete set of coupling constants allowable, determined by the choice of ω_+. Although we fixed $\omega_- = \frac{\pi}{T}$. ω_+ may be $2\ell\omega_-$ ($\ell = m + 1 = 1,2,3...$), each value of ω_+ corresponding to a definite value of k given by:

$$\frac{\omega_+^2}{\omega_-^2} = \frac{1 + k}{1 - k}$$

We have:

$$\begin{aligned} m = 0 \quad & \omega_+ = 2\omega_- \quad k = 3/5 \\ m = 1 \quad & \omega_+ = 4\omega_- \quad k = 15/17 \\ m = 2 \quad & \omega_+ = 6\omega_- \quad k = 35/37 \end{aligned} \qquad 5.20$$

We see therefore that $k = 3/5$, $\omega_+ = 2\omega_-$ ($m=0$) is the only practical value for a double resonant system.

The peak output voltage is given by:

$$\frac{q_2(T)}{q_1(0)} = \frac{Q_{2+} - Q_{2-}}{Q_{1+} + Q_{1-}} = \frac{Q_{2+}}{Q_{1-}} = \frac{1-\omega_+^2}{M\omega_+^2}$$

$$= \frac{-k}{M} = \frac{1}{\sqrt{L}} \qquad 5.21$$

In terms of L_1 and L_2,

$$\frac{q_2}{q_1} = \sqrt{\frac{L_1}{L_2}} = \sqrt{\frac{C_2}{C_1}} \qquad 5.22$$

Therefore

$$\frac{V_2}{V_1} = \sqrt{\frac{L_2}{L_1}} \quad \text{and } L_2 \geq 100\, L_1 \qquad 5.23$$

The voltage waveforms for the double resonance are shown in Figure 9. Note that the main bank undergoes about 50% voltage reversal during the charging of the water capacitor. The value of T is given by:

$$T = \pi/\omega_- = 2\,\pi/\omega_+ \qquad 5.24$$

In principle, perfect energy transfer is possible with still other choices of the circuit parameters. The high and low-frequency modes might reach simultaneous maxima not at the first half cycle of the low-frequency mode but at later half cycles. These conditions make for more and larger voltage reversals in both the primary and secondary capacitors, dissipating energy and deteriorating the dielectrics, and are to be avoided.

6. Design of the Mark I Air - Core Pulse Transformer

In designing the transformer the three principal considerations were electrical stress in the dielectric, mechanical stresses set up by the self magnetic fields of the currents flowing in the transformer winding, and leakage flux. In a transformer used to charge the NRL water capacitor through 1 MV, the problem of dielectric stress was solved by using a cable insulated for 1 MV throughout its entire length. There was no problem of mechanical stress because the magnetic field at the surface of the cable conductor was small. However, in our transformer the current was to be more than ten times greater and the magnetic pressure at the surface of a similar cable would be destructive (more than 100 times greater). Instead our transformer was wound with aluminum sheet 18" wide and 15 mils thick. This brought the magnetic pressure at the surface of the transformer winding to a safe value. At the same time it greatly increased the reluctance of the path taken by the leakage flux which now surrounded a conductor of perimeter 1 meter instead of the small central conductor of a cable. This meant that the entire transformer could be reduced in size keeping the same coupling coefficient. Moreover, the natural winding for the transformer was now spiral rather than helical. Therefore the stress on the dielectric surrounding each winding is only $\sim$ 100 kV instead of $\sim$ 1 MV. The thinner dielectric that this made possible provided a further reduction in size without excessive leakage flux. For the given axial length

of the spiral winding and the desired coupling coefficient, k = .6, the radius of the spiral winding should be approximately 1 m. (See Design Calculation, Section I.8 of this report.) Since we were faced by a severe corona problem in this transformer, it was immersed in an oversized tank of water. At the same time this simplified the connection of the 1 MV output. It was not necessary to use de-ionized water for this purpose because the main insulation for the transformer was provided by polyethylene. It was much more important to use de-aerated water to prevent bubble formation within the transformer because of the corona hazard. (It was found impractical to de-aerate the water by mechanical or thermal means. The best method seems to be to let the water sit undisturbed for a week or more until the trapped air rises to the surface. Attempts at using oxygen removal cartridges were only partially successful.) In the transformer used to charge the NRL water capacitor to one million volts the problem of dielectric stress was solved by using a cable winding insulated for a million volts throughout its entire length. There the problem of corona was solved at the same time because there was no air between their central conductor and the insulation surrounding it. However, without immersion there would be dangerous corona in our loose winding of aluminum sheets.

In a preliminary test a spirally wound transformer was constructed in which the dielectric consisted of six sheets of .006 in. thick polyethylene. There were 15 turns in the secondary and one turn in the primary. A ball gap as shown in Figure 10 was used to limit the secondary output voltage to 100 KV. While this prototype withstood many shots at 24 kV input voltage and no crobar, six shots at 35 kV punctured the dielectric at the edge of the winding where the electric field is greatest.

7. Description of the Mark I Air-Core Pulse Transformer

The Primary Winding: The primary winding was a single turn of a laminated dead soft aluminum strip wound on a spiral secondary. Each of the aluminum strips was 15 mils thick and 18" wide, free from sharp edges or corners.

The Secondary Winding: The conductor of the secondary winding was a continuous length of aluminum strip, 15 mils thick and 18" wide. The aluminum was reasonably free of sharp edges and points. The aluminum alloy, type 1100-F, was chosen because of its resistance to prolonged immersion in de-ionized water. The dielectric for the secondary winding consisted of 7 layers of Mylar polyester each 14 mils thick and 36" wide, free from scratches and clean. Each layer extended without breaking the full width and the entire length of the winding (approximately 50 yards). The secondary which consisted of fifteen (15) turns was wound on an acrylic squirrle cage of radius 36" plus or minus one inch. Mark II (see section 13) was shaped so as to lower the overall height but was otherwise unchanged. The secondary was wound on a cylindrical form made from $1\frac{1}{4}$" diameter acrylic rods. Then the central space of the cylinder was hollow and accessible from both ends for the insertion of turning slugs. Figure 11 shows photos of Mark I and Mark II.

Leads: The inner-most end of the secondary winding was securely attached to a $1\frac{1}{4}$" stainless steel rod 40 inches long.

The leads to the primary winding are integral extensions of the winding itself. They are brought out at right angles to the winding and are securely attached to a two inch slab of plexiglass insulation. The leads which extend 18 inches above the transformer are joined to the bus-bars by stainless-steel clamps. The clamps consist of two pieces of metal each $1\frac{1}{4}$" x 12" x $\frac{1}{4}$". One is tapped every inch for $\frac{1}{4}$-20 screws, the other has clearance holes at corresponding points. The two ends to be joined are inserted in the clamp and the screws tightened. We have found that this simple clamp arrangement is reliable for peak currents exceeding 50 kilo amps and use this method for joining all our high current leads.

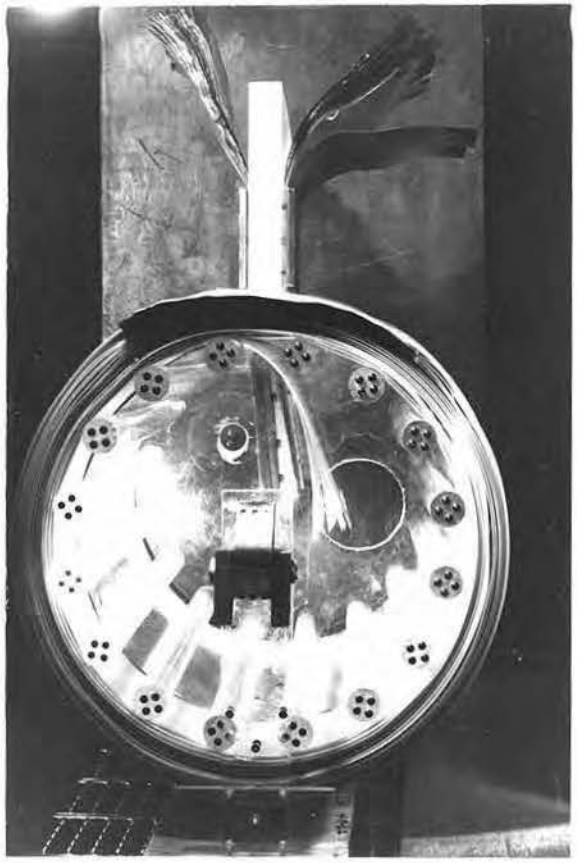

Mark I

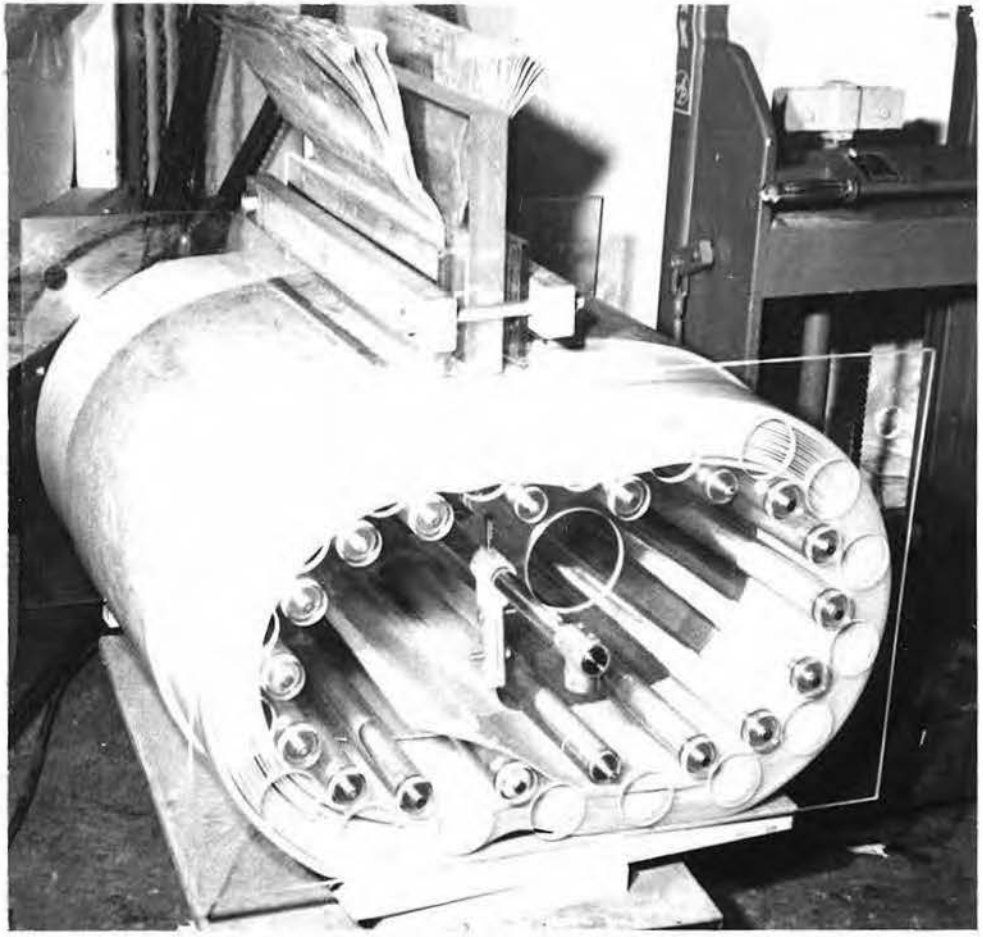

Mark II

FIGURE 11a
Air-Core Pulse Transformer

8. Design Parameters of the Mark I Pulse Tramsformer

Introduction: The inductance of the primary had to be made small enough to give a low value for T. The mutual inductance had to be large enough to account for k = .6 (note 1). The secondary radius is automatically determined by the radius of the primary and the insulation thickness.

The inductance of the Pulse Transformer is calculated from the "Nagoaka Formula"[28]

$$L = \frac{\mu_o \pi K R^2 N^2}{\ell} \qquad 8.1$$

where

N = the number of turns of the winding

ℓ = width of the winding

R = radius of the winding.

K = a geometrical factor depending on the ratio of ℓ to R.

(K is always less than 1 for a finite geometry and equals 1 for an infinite current sheet.) See figure 12 below.

Note 1: The capacitance C_1 of the storage bank is fined; in our care C_1 = 20 μf. For $L_1 \sim 1$ μH we have

$$T = \frac{2\pi}{\omega_+} = \frac{2\pi}{\sqrt{5/2}\ \omega_+} = \frac{2\pi}{(5/2\ L_1 C_1)} \simeq 18\ \mu s$$

This is about the maximum time we wish to store energy in our water capacitor. It follows from equation 5.23 that

$$L_2 \geq 100\ \mu H$$

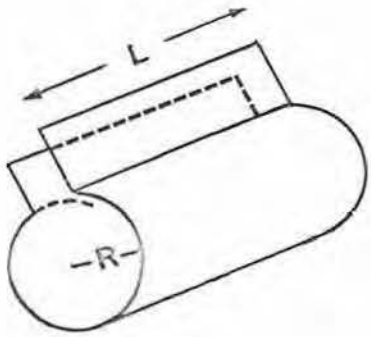

Figure 12

The current sheet used in the Nagoaka Formula

For a primary radius of 37.5 cm. where the width of the sheet is 50 cm. we have from equation 8.1

$$L_1 = .66\ \mu H \qquad 8.2$$

We must add to this the inductance of the capacitor bank and bus system. From equation A-1.5 this is .5 μH. The adjusted value of L_1 is now

$$L_1 = 1.16\ \mu H \qquad 8.3$$

Using the same formula for the secondary winding for which N = 15 turns and the radius is 33.7 cm. we obtain

$$L_2 = 126\ \mu H \qquad 8.4$$

To calculate the mutual inductance we use the standard expression for the mutual inductance between two consecutive current sheets of equal length[28]. This calculationis somewhat more complicated and only the result is stated here.

$$M = 8.7\ \mu H \qquad 8.5$$

The coupling constant is found from 8.3, 8.4, and 8.5

$$k = \frac{M}{\sqrt{L_1 L_2}} = .63 \qquad 8.6$$

Notice that k = .63 is slightly larger than the value required for double resonance. The proper value of k may be obtained by increasing either L_1 or L_2. We chose to increase the value of L_2 and adjust the value of C_2 for resonance.

Table I

Theoretical Values of the Variables of the Mark I - Yukon I Pulse Circuit

Variables	Calculated Value	Adjusted Value
L_1	.66 μH	1.16 μH
L_2	126 μH	139 μH
$V_2 = \sqrt{\frac{L_2}{L_1}}\ V_1$	1.05 MV	1.1 MV
M	7.6 μH	7.6 μH
k	.63 μH	.6 μH
$C_2 = \frac{L_1 C_1}{L_2}$	1.84 μf	.17 μf
$\omega_1 = \frac{1}{\sqrt{L_1 C_1}}$	.21 MC	.21 MC
$\omega_+ = \sqrt{\frac{5}{2}}\ \omega_1$	.34 MC	.34 MC
$\omega_- = .5\ \omega_+$	.17 MC	
T		18.8 μs

9. The Water Capacitor-Theory of Operation

The RC time-constant τ of a capacitor with homogeneous dielectric is independent of its geometry, and is just the $\rho\epsilon$ product for the dielectric (ρ = resistivity, ϵ = permittivity). (A proof of the above will be found in Appendix A-2.) For "ten megohm" water ($\rho = 10^7$ ohm-cm, $\epsilon = 82\ \epsilon_o$) this dielectric relaxation time τ is 73 μ sec. Thus even our inductance-ridden capacitor bank is fast enough to charge a water capacitor losing a fraction of the total stored energy (to joule heat in the water) that is

$$\frac{\int V^2 dt/R}{CV^2/2} = 2\,\frac{\int V^2 dt}{V^2\tau} = \frac{T}{\tau} \leq 25\% \text{ at } t = T_+ \qquad 9.1$$

(using the theoretical form $V \sim \cos \omega_+ t + \cos \omega_- t$ discussed in section 5, with $T_+ = 2\pi/\omega_+ \sim 18\ \mu s$). Much more important for the success of the project than high resistivity of water dielectric was the absence of bubbles. The wave form of the capacitor voltage include a reversal of 50% peak before full positive peak was reached, and this was likely to make corona in any bubbles present. Therefore distilled water was used; and the relatively large spacing between plates that goes with our high voltage further helped in dislodging bubbles and moving them from between the plates. The spacing of 1 to 3 cm. was much greater than the small bubbles present.

Cavitation might take place on the side of the plates where the water is subject to great negative pressure. Fortunately this was not in the region between the plates during the critical 18 μ sec charging time, and cavitation may not happen during the subsequent discharge time (< .1 μ sec.) while the large positive pressure between the plates is falling to zero.

10. Design Considerations of Yukon I

10.1 Construction Details:

The water capacitor consisted of eleven aluminum plates 41" x 13" x $\frac{1}{4}$" rivited to an alluminum plate 30" x $\frac{1}{2}$" x 41" with 3/4" aluminum angle. There was a 1" space between each plate as shown in figure 13. This web of parallel spaced plates meshed with a similar set of ground plates which were attached to the aluminum tank wall. The high voltage plate was suspended by means of arcylic rod and was adjustable in the horitzontal direction. This allowed the system to be tuned by varying the overlapping area between the plates and thus increasing or decreasing the capacitance. To the front of the hot plates was force fitted a bus-bar at the center of which was inserted a firing pin of 3/4" stainless steel rod, rounded at the tip. The distance of the pin from the tank wall was easily adjustable from the rear of the plate by means of a wheel attached to the rod. The front of the tank had a hole cut out to accommodate a 6" polyethylene disc. A stainless steel electrode ($1\frac{1}{2}$" hemisphere) was inserted through the center of the disc (figure 14). The breakdown voltage at the water gap was easily varied by changing the distance between this electrod and the rod attached to the high voltage plate. This is more clearly understood by referring to figure 15.

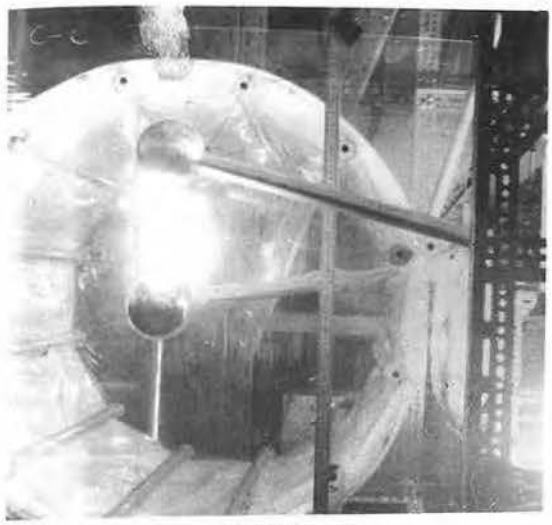

FIGURE 10
Air-core Pulse Transformer (obsolete)

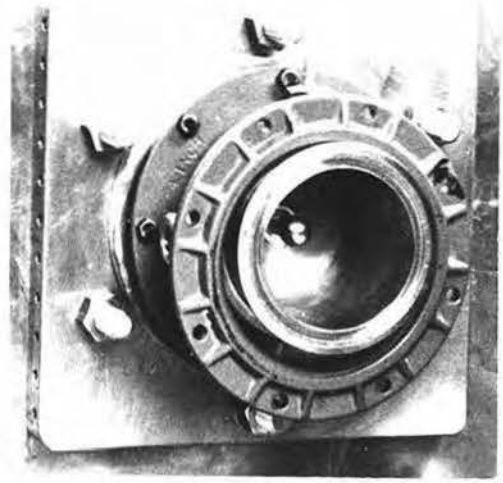

FIGURE 14b
Mounted Electrode Assembly

FIGURE 13
Photo of Yukon I During Assembly

FIGURE 14a
Polyethylene Electrode Support

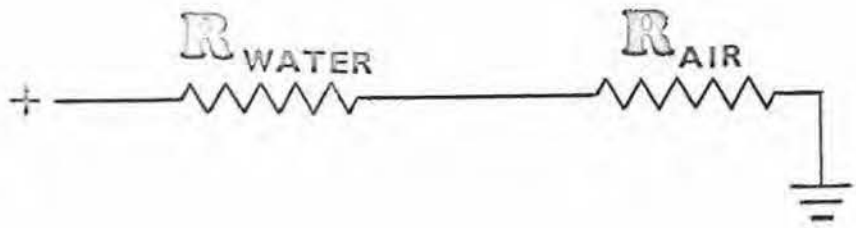

Figure 15

Pertaining to the Discharge of Yukon I

R_{air} and R_{water} are two resistances in series with the electrode. Initially the impedance of the air is small compared to the resistivity of the de-ionized water, hence the water gap alone will determine the breakdown voltage independent of the length of the air gap to ground. The breakdown was set to occur at the time T_+, when the water capacitor has reached its highest voltage.

10.2 Effect of Water Resistivity on Output Voltage:

For sufficiently high megohm water the resistance of the water can be neglected with respect to the impedance of the capacitor. A typical measurement of the D.C. Resistance across the water capacitor (C = .2 μf) was R = 100 ohms, but the impedance at a frequency of 2×10^5 cycles/sec was found to be $Z_c \simeq 2$ ohms. Clearly, since R and Z_c are in parallel, R is negligible compared to Z_c. It is just this high value for R which is so crucial to obtaining high voltage on the capacitor.

Consider a transformer where N_1 and N_2 are the number of turns on the primary and secondary respectively.

$$\frac{V_1}{V_2} = \frac{N_1}{N_2} = \frac{i_2}{i_1} \qquad 10.1$$

$$V_1 i_1 = V_2 i_2 = i_1^2 Z_1 = i_2^2 Z_2 \qquad 10.2$$

Substituting for V_1 and V_2 we have

$$Z_1 = \frac{i_2^2 Z_2}{i_1^2} = \frac{n_1^2 Z_2}{n_2^2} \qquad 10.3$$

If $\frac{n_1}{n_2} = \frac{1}{N}$ then

$$Z_1 = \frac{Z_2}{N} \qquad 10.5$$

Hence the effective impedance seen by the primary voltage source (i.e. the capacitor bank) as reflected through the Pulse Transformer, is essentially the impedance of the water capacitor divided by N^2 which here equals $(15)^2$. This is only true when $R \gg Z_c$.

The capacitor bank discharges through an air gap switch which offers an impedance Z_G essentially independent of the bank voltages.

When the impedance of the gap is small compared with the effective impedance seen at the primary of the transformer, then most of the bank voltage will appear across the transformer.

10.3 Estimate of Electrostatic and Magnetic Pressures:

It was anticipated that the operational value for the electrostatic energy density would be taken between 1 and 10 joule/cm^3. The (numerically equal) electrostatic stress on the plates would then be between 10 and 100 atmospheres negative pressure. This load of 1 to 10 tons would be troublesome if it were static, but during the time it is applied sound can only travel a small part (1/10) of the capacitor plate radius in water. Therefore most of the load would be borne by an equal and opposite positive pressure built up in the water between the plates.

The magnetic stress between the plates created during the discharge is not much greater and is in the opposite direction. Its duration is about 100 times shorter, so that a correspondingly larger fraction is born by the water, leaving only $\sim 1\%$ for the bushing. The magnetic stress on the output terminal of the high voltage plate is larger, about 100 Newton/cm^2, but this is exerted radially on a solid steel rod and is therefore negligible. This electrode was centered accurately in the surrounding conductor to reduce the unbalanced forces (which tend to center it).

11. The Output Switch, Theory of Operation

We present below a discussion of the theory governing the operation of the switch and some remarks on its potential uses.

The over-volted water-gap switch must be capable of standing off one million volts for 10 μs and then pass 10^7 amps with less than 1 μs jitter and less than 10 nsec closing time. These are not difficult requirements and the problem is to balance the demands of simplicity, low impedance, and reliability. The over-volted water-gap switch has been used successfully for our requirements. The impedance of the switch depends on the time variation of the radius and temperature of the discharge column set up in the water and therefore it is difficult to predict its reliability. If there were too much voltage jitter a triggered water gap or a pressurized gap could have been tried.

During the charging of the capacitor the impedance of the water-gap was on the order of 10^5 ohm, much less than the initial impedance of an un-ionized gas in the discharge chamber in series with the water-gap. Thus the full capacitor voltage appeared across the gas, enough to break it down at the pressures used. A current increasing to several amperes flowed through the gas and the water for several microseconds, ample to reduce the gas impedance to a level negligible compared to the water gap. This small current maintained an arc in the gas for several microseconds until the water gap was overvolted and broke down.

12. Design Modification of Yukon I

We observed that Yukon I was arcing internally. (Figure 16). This arcing was independent of the breakdown setting of the overvolted water gap switch.

Photographic analysis revealed that the breakdown was not occurring near the water gap switch but was due to arcing between the plates. In addition it was observed that the arcing was not localized but varied its position for each discharge. Careful examination of the plates further revealed that

(1) most of the arcing was in the vicinity of the edges of the plates

(2) the arcing was not, as might be expected, along the shortest line between the plates or along a horizontal path.

There were several possible explanations:

(1) breakdown was due to a fault in the basic design, i.e., the radius of curvature of a $\frac{1}{4}$" plate is too small to withstand high voltage. Any future model would have to incorporate larger radii of curvature between plates. This could not easily nor cheaply be done with any solid piece of metal.

(2) breakdown occurs between plates because of air trapped in the water which ionizes more easily than the water and causes inpredictable breakdown. This would account for the fact that the arcing was not along the shortest path. This effect was minimized in the design of Yukon II.

(3) Cosmic rays striking the water ionizes the molecules and cause unpredictable breakdown along the path of ionization. If this were true then no design would ever be able to overcome this inherent difficulty.

The breakdown of Yukon I meant that preliminary studies had to be undertaken prior to designing Yukon II. These studies had to determine a safe value for the dielectric strength of water and the minimum radius of curvature capable of preventing breakdown in water. The experimental setup is shown in Figure 17.

The pan was placed opposite a stainless steel plate in the 500 gallon water tank. The distance between the pan and the plate was adjustable. The output of Mark I was fed directly between them. In some tests a second identical pan was used in place of the stainless steel plate. Breakdown was not observed when 1 MV was pulsed between the pan and a 30" x 30" stainless steel sheet, when immersed in water with a 2" gap between them. Using the principle that the radius of curvature must always be at least 2" and convex with respect to the oppositely charged capacitor plate we arrived at the successful design for our new water capacitor.

Yukon II was designed to minimize breakdown due to trapped air or cosmic rays, as well as withstand the high voltages. The basic design consideration was to keep the electric field gradient low enough so that any localized ionization that may develop when the voltage is applied would be unable to cause breakdown between the capacitor plates. The overall height of Yukon II was considerably less than Yukon I, and although Mark I never indicated any signs of failure we redesigned the pulse transformer to conform to the lower height, making possible a lower tank height.

FIGURE 16
Photos Showing Arcing in Yukon I

Insert is a View from Directly Above the Arc

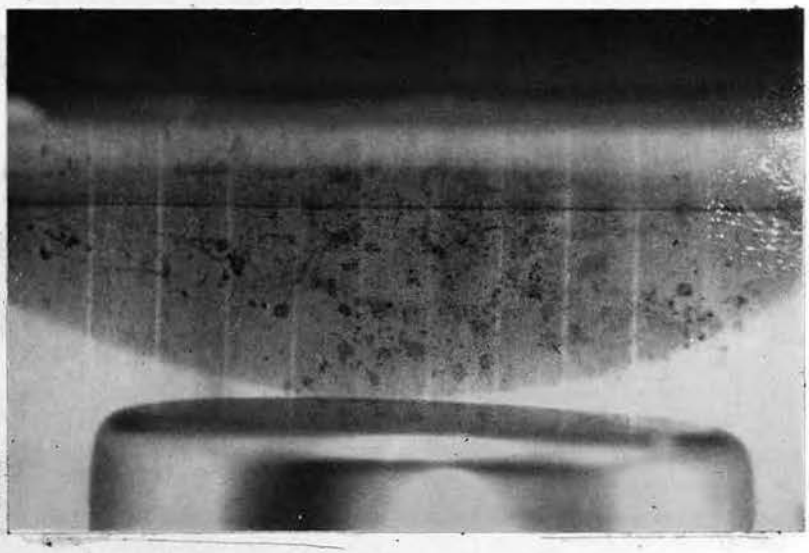

FIGURE 17
Assembly Used to Determine Dielectric Strength of Water

d - distance across bottom - 18"
r - radius of curvature of edge - 2"
h - height of wall - 4"
t - thickness of material - 1/8"

13. The Design of Mark II and Yukon II

Description of Mark II

The new tank dimensions required that the pulse transformer be less than 22" high (the height of Mark I was 33" with a mean radius of 15"). The parameters (turns ratio, coupling constant) of Mark II were identical to Mark I except for a change in shape from a circular to an oval cross section. The cross sectional area was kept constant; therefore the calculations performed for Mark I were still valid for Mark II. The windings of Mark II were made tighter thereby increasing its coupling constant. Figure 18 indicates the dimensions of Mark II.

Description of Yukon II

Yukon II consisted of three sections; two outer ground plates and one inner conducting section. Figures 19 and 20 give an overall view of the capacitor and include detail drawings.

Ground Plates:

Each ground plate consisted of a sheet of aluminum wrapped around a specially constructed frame so as to guarantee a plane surface with convex curvature at the ends. The frame consisted of two eight foot lengths of pipe welded to a pair of 4" diameter pipes, each 30" long so as to form a rectangle eight feet long and thirty inches high. The aluminum sheet was placed on the frame and the ends pulled tightly around the 4" pipe by means of a special clamping arrangement. This resulted in a plane surface 96" long x 30" high with a 2" radius of curvature at each vertical end.

Inner Plate:

The inner electrode was formed on a frame constructed from two 12' lengths of 4" diameter pipe held together by three jack screw assemblies which were designed to allow a spacing of 9" ± ½" between the pipes. The space could be adjusted by means of three allen head screws which protruded through the top pipe. A sheet of .015 mil aluminum, 120" long and 40" wide, was wrapped around the 4" pipes and anchored with stainless steel sheet metal screws which were placed in carefully aligned predrilled holes in the sheet and pipe. The spacing between the top and bottom of the pipes was 16 inches after the jackscrews were tightened. The curvature of this conductor was convex with respect to the two outer ground plates. In addition, the center conductor extended 12" beyond the end of each outer plate so as to eliminate sharp corners.

The inner conductor was supported between the two ground plates by four 1½" lucite rods and was positioned 3" from the bottom of the tank. (When the capacitor was immersed in water the 3" space prevented breakdown from the center conductor to the bottom of the tank which was assumed to be at ground potential.) The spacing between the plates is adjustable from 0-4". The entire assembly was put in a tank 16' long, 8' wide and 2' high and filled with deionized water to a level that was always 3" above the central conductor but below the outer plates. The tank was made from a reinforced plywood frame and was made watertight with a 6 mil polyethylene liner. To prevent damage to this thin liner a 20 mil sheet of polyethylene was laid on the bottom of the tank.

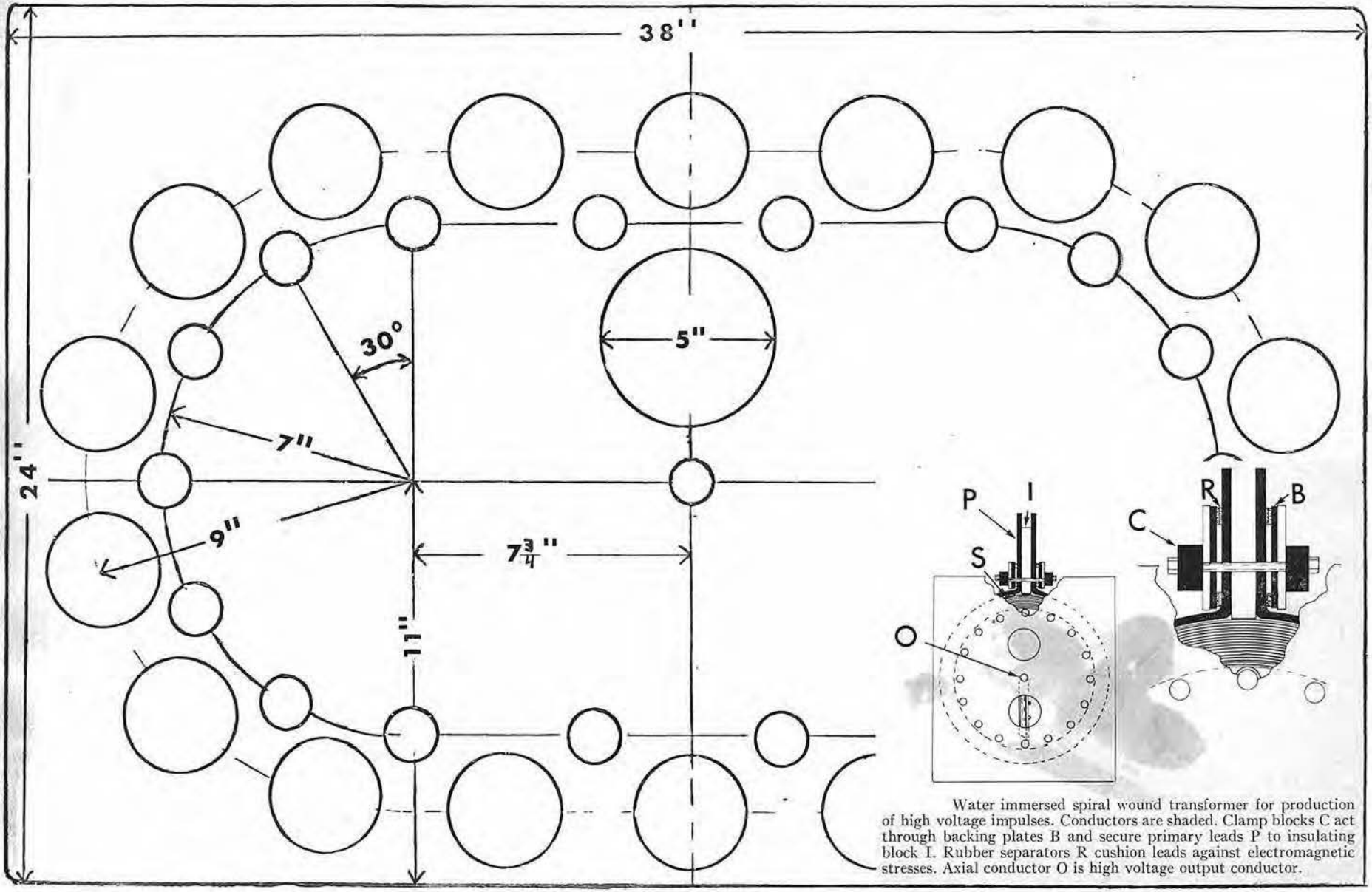

Water immersed spiral wound transformer for production of high voltage impulses. Conductors are shaded. Clamp blocks C act through backing plates B and secure primary leads P to insulating block I. Rubber separators R cushion leads against electromagnetic stresses. Axial conductor O is high voltage output conductor.

FIGURE 18

Dimensional Drawing of Mark II - Side View

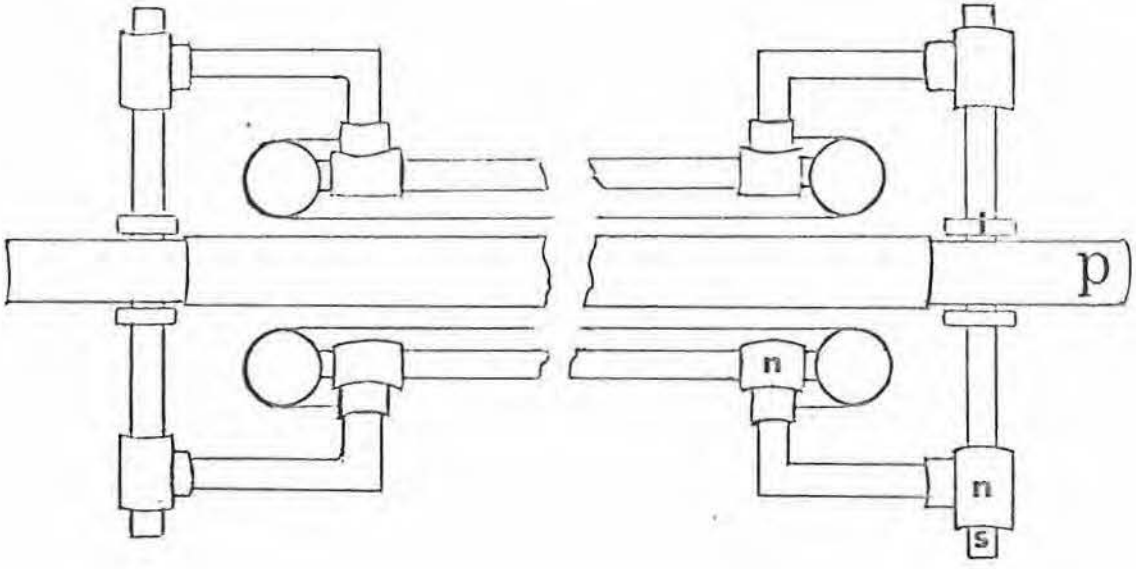

Legend

a - aluminum sheet
i - acrylic spacer
n - aluminum fitting
p - 4" aluminum pipe
s - acrylic support rod

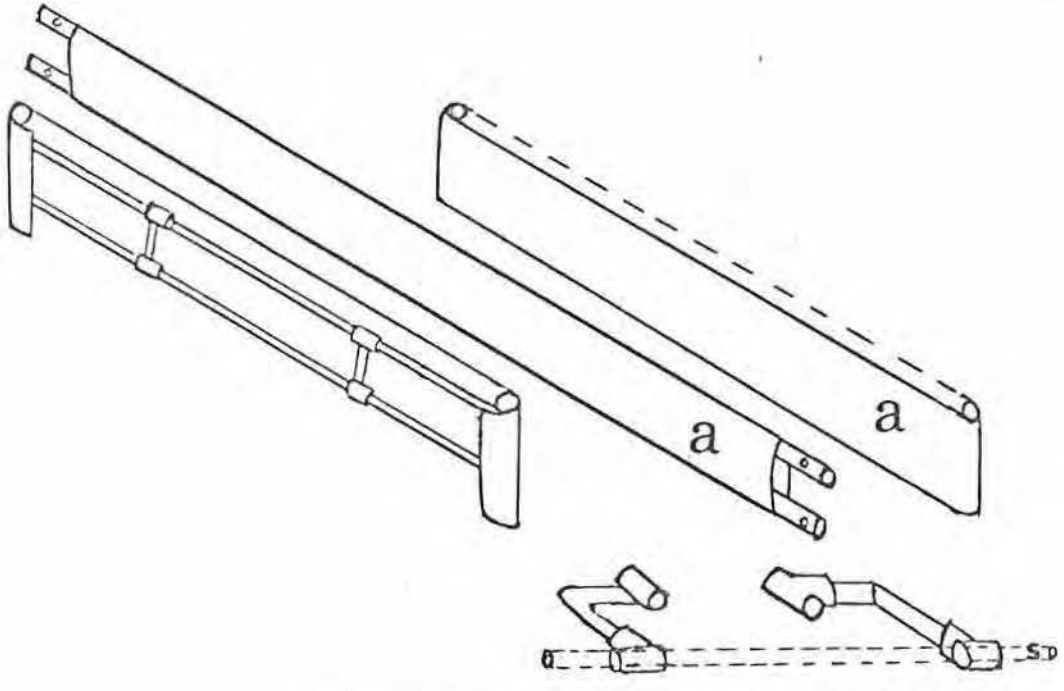

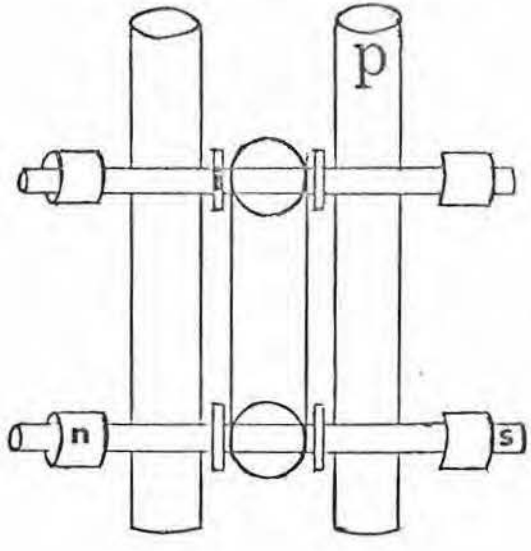

FIGURE 19 - Detail Drawings of Yukon II

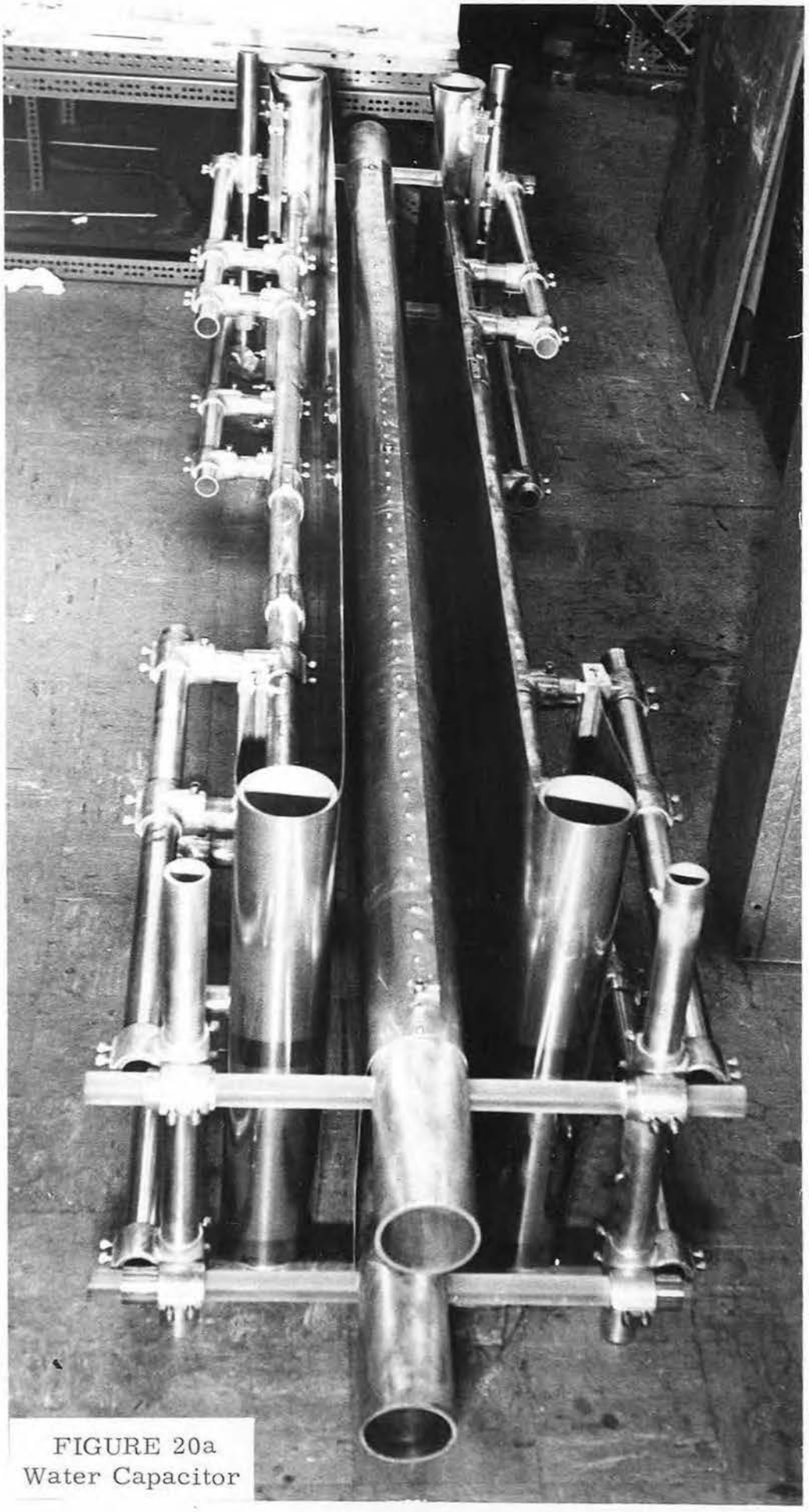

FIGURE 20a
Water Capacitor

FIGURE 20b
Center Electrode Assembly

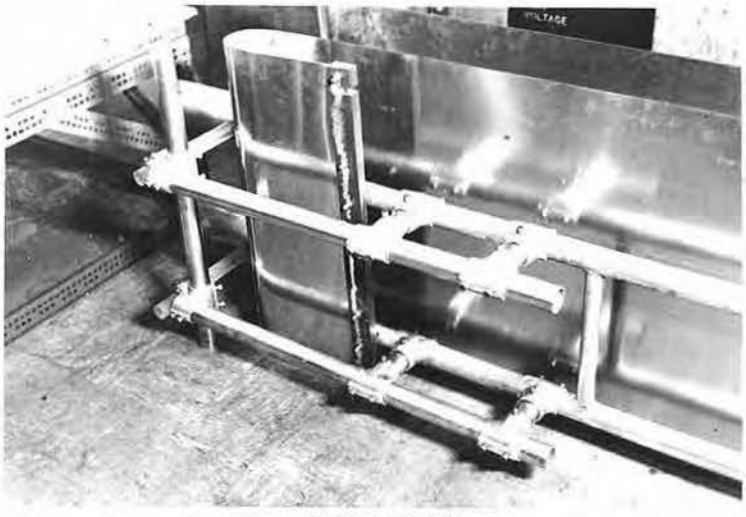

FIGURE 20c
Ground Plane Construction
Showing Support Assembly

FIGURE 20d
Detail of Clamping Device

14. Experimental Observation of Double Resonance

The desired waveform of the "double resonance" was observed in various ways.

(a) A high power pulse generator was connected across a .1 ohm resistor in series with the primary of the transformer. The oscilloscope trace of the voltage waveform of C_2 exhibited the double resonance.

(b) A grid dip meter was used to measure the resonant frequencies of the system. With a load capacitor of .215 uf, the resonant frequencies were 26 kc and 49 kc, exhibiting the 2:1 ratio required for double resonance.

(c) The capacitor bank was used to pulse charge a prototype water capacitor. The waveform showing the typical pre-reversal of the secondary is shown in Figure 21.

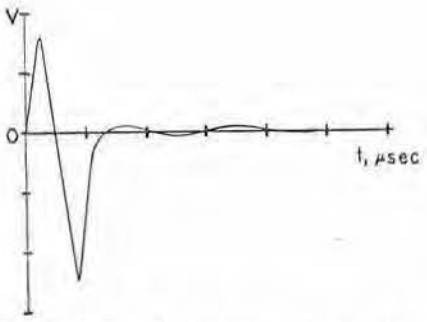

Waveform of pulse charger employing transformer and double resonance principle described in text. The secondary capacitor discharged into a water gap just before the full negative peak was reached. Signal was taken from our capacitance voltage divider. $x = 20$ μsec/div and $y = 0.5$ V/div × 19 000.

Figure 21

Experimental Observation of Double Resonance

15. Measurement of the Characteristic Parameters

15.1 The Coupling Constant:

(a) The output of a signal generator (Eico 413, checked against General Radio oscillator to be accurate to ± 2%) was fed to a 14 watt high fidelity amplifier. The amplified output was connected to Mark I as shown in Figure 22.

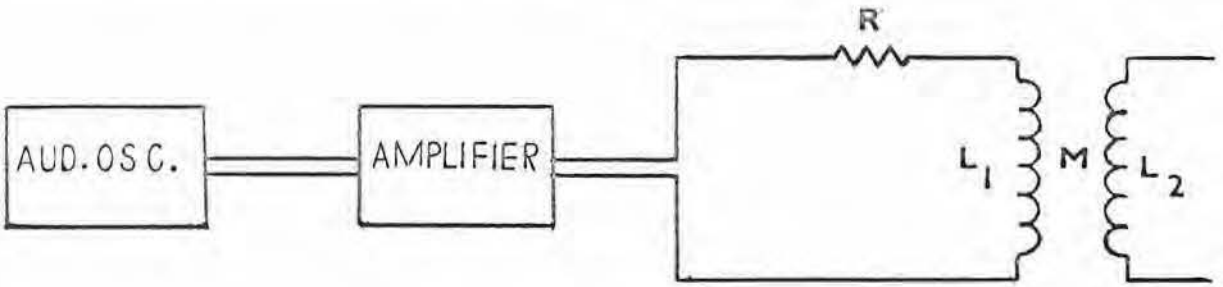

Figure 22 - Circuit Used in Determining the Coupling Constant

The voltage across R and L_1 is obtained with L_2 shorted and then with L_2 open. The current in the circuit is determined from V_R and R. It can be shown (see Appendix A-3) that for constant current

$$1-k^2 = V_{L_1}(L_2 \text{ shorted})/V_{L_1}(L_2 \text{ open}) \qquad 15.1$$

where k is the coupling constant. Equation 15.1 is symmetric in L_1 and L_2.

(b) The inductance and resistance of the shorting strip used to close L must be kept to a minimum and its effects considered when evaluating the results of any measurements. Since L_1 is small ($\sim$ .67 μH) the resistance of the shorting piece can substantially alter the correct results.

With the bus-bars attached to the transformer k is reduced because the effective inductance of the primary, L_1, is increased by L_c, the coupling inductance of the bus-bars and capacitor bank.

This is readily estimated to be on the order of .5 μH, (see Appendix A-1). Using this value for L_c we arrive at an effective coupling constant, k_ϵ.

$$k_\epsilon = \frac{M}{\sqrt{(L_1 + L_c)\, L_2}} \qquad 15.2$$

15.2 Inductance, Mutual Inductance:

(a) The following relationships are easily verified by referring to the circuit in figure 22.

$$Z = \frac{V_L}{V_R} R$$

$$L = \frac{Z_L}{\omega} \qquad 15.3$$

$$M = k \sqrt{L_1 L_2} \quad \text{by definition}$$

Since the ringing frequency of the capacitor bank is approximately 50 KC we used the value $\omega = 5 \times 10^6$ in executing our measurements.

(b) The self-inductance of the water capacitor may be determined from the ringing frequency of the capacitor if the value of C_2 is known from another measurement. A grid dip meter (Eico #613; calibrated by beating against a known F.M. station) was used to detect the resonance frequency.

15.3 Capacitance of C_1 and C_2:

Two methods were employed to determine the capacitance of C_2.

(a) An oscillator was put in series with a fixed, non-inductive resistor, R, and C_2. The voltage across R and C_2 was noted for various frequencies. The value of C_2 was computed from the following relationships:

$$V_R = iR \qquad Z_c = \frac{1}{2\pi fc}$$

$$V_c = iZ_c \qquad C_2 = \frac{V_R}{2\pi f R V_c} \qquad 15.4$$

The capacitor may be completely isolated from the pulse circuit during this type of measurement.

(b) The LC ringing frequency of the primary and secondary circuits was determined (section 15.4). With the value of $L_{1,2}$ previously known, $C_{1,2}$ may be calculated.

(c) Since the D.C. resistance of the water capacitor is negligible compared with its impedance at frequencies above 30 KC (see section 10.2) we were able to measure C_2 with a Wein Bridge. The results confirmed our other measurements.

15.4 Measurement of Resonances of Primary and Secondary Circuits

Mode Analysis:

In the theoretical discussion of section 5, we determined the optimum values for k, ω_1, and ω_2 for maximum energy transfer. These conditions were met and the double resonance was observed with Mark I. Space limitations prevented us from attaining the value of C_2 necessary for obtaining double resonance with Mark II. The value of C_2 was an order of magnitude lower than that required for maximum energy transfer. We present here a theoretical discussion of the circuit conditions determined by Mark II and Yukon II.

The general solution of $\omega_\pm$ for any coupled circuit is given by[26]

$$\omega_\pm = \left[\frac{(\omega_1^2 + \omega_2^2) \pm \sqrt{(\omega_1^2 + \omega_2^2)^2 - 4(1-k^2)\omega_1^2\omega_2^2}}{2(1-k^2)}\right]^{\frac{1}{2}} \qquad 15.5$$

where ω_1 and ω_2 are the uncoupled resonant frequencies of the primary and secondary circuits respectively and k is the coupling constant. Here

$$\omega_1 = \frac{1}{\sqrt{L_1 C_1}} = 2 \times 10^5 \quad \text{where } L_1 = 1.16\ \mu H \quad C_1 = 20\ \mu f$$

$$\omega_2 = \frac{1}{\sqrt{L_2 C_2}} = 4 \times 10^5 \quad \text{where } L_2 = 108\ nH \quad C_2 = .04\ \mu f$$

$$k = .8$$

Inserting these values in equation 14.1 we obtain the value

$$\omega_+ = 7.5 \times 10^5$$

$$\omega_- = 6.4 \times 10^5$$

which corresponds to frequencies of

$$f_+ = 120\ KC$$

$$f_- = 100\ KC$$

A beat frequency of 20 KC should be observed.

Various methods were used to determine the resonant frequencies and to observe the characteristic charging waveforms of the primary and secondary circuits. These included oscilloscope waveform analysis of the charge-discharge cycle, and analysis of Lisijous Figures. A third type of measurement consisted of placing the output of a power oscillator in series with the primary or secondary circuits. The voltage on a fixed resistor in series with the oscillator output was observed as the frequency was varied. Peak current corresponded to a resonance condition.

The above measurements gave the following results:

Mark I

Primary Resonance

$f = 50$ KC $\pm$ 3%

Secondary Resonances

$f_+ = 26$ KC $\qquad C_2 = .215\ \mu f$

$f_- = 49$ KC

This is the double resonance condition previously discussed.

Mark II

Primary Resonance

$f = 48$ KC $\pm$ 2%

Secondary Resonances

$f = 125$ KC $\pm$ 2% $\qquad C_2 = .04\ \mu f$

$f_- = 105$ KC $\pm$ 2%

Table II. Measured Values of the Variables of the Mark I and Mark II Circuits

Variables	Method of Measurement[+]	Mark I	Mark II
k_{ave} @ 50 KC	15.1a (in air)	.79	.82
$k_{effective}$	15.1a	.60	.73
M	15.2a	6.5 μH	8.7 μH
L_1 @ 50 KC	15.2a	.67 μH	.71 μH
L_2	15.2a	100 μH	108 μH
L_{C_1}	Appendix A-1	.5 μH	.5 μH
C_2	15.3a,b,c	.20 μf	Note 1
L_{C_2}	15.2b	15 nH	Note 1

Note 1: The value of C_2 was constantly varied during the experiment, therefore no direct measurement was attempted. Instead, the value of C_2 was calculated as needed for the various spacings between the plates.

[+]Numbers in this colume refer to sections of this report.

16. H.V. Measurement Techniques

The objective of any measurement is to obtain a "suitable, clean signal" which can be easily related to the quantity being measured. Several methods for measuring ultra high voltages are described in the literature.[29] Most of these techniques rely on capacitance or resistance dividers or pickup loops of one type or another. Many of these circuits fail when the probe or divider is located near sources of stray magnetic fields which can induce unwanted signal noise in the coaxial cables. Capacitance dividers can be designed to minimize this effect but at high voltages the insulation requirements become cumbersome. In our experiment the proximity of the high voltage-high current discharge to the position of the circuit under test made the design of a suitable probe difficult. Proper cable terminations had to be designed to insure signal fidelity.

Mark I

A 400:1 voltage divider for 1 MV input was made by immersing a 5" aluminum disc about 1 cm from the aluminum wall of the tank containing the transformer. A hemispherical knob with a diameter of 32 cm. placed on the output shaft of the transformer about 50 cm from the disc was the third high-voltage element of a resistor-capacitor divider formed with the disc and the tank wall. The output signal was taken from the disc at an impedance level of about 1000 ohm.

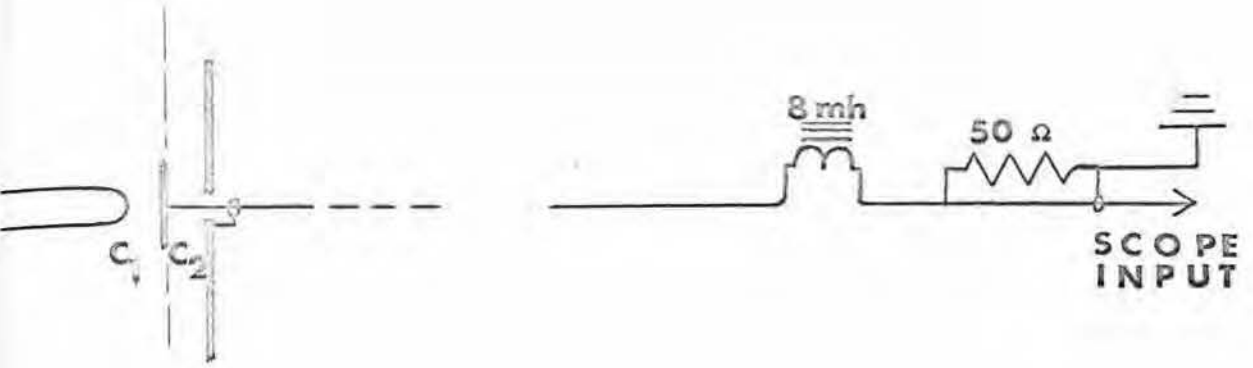

FIGURE 23

High Voltage Divider Network

Referring to Figure 23,

$$\frac{C_1}{C_2} = \frac{V_2}{V_1} \qquad 16.1$$

By moving the metal disc closer to ground the output signal, V_2, becomes continuously variable.

A known pulse voltage was put on the bushing and compared with the signal obtained from the divider. An attenuation of 19,000:1 was observed. The purpose of the 8 mH r.f. choke was to eliminate high frequency noise. The fidelity of the divider is verified in Figure 24.

Mark II

The divider for Mark II was quite similar to that used for Mark I. The design was necessarily altered due to the shape of Yukon II but the basic idea of a capacitance divider using water as the dielectric was unchanged. A screw insulated by two rubber grommets was placed in one of the support legs attached to the outside ground sheets of the capacitor. The capacitance between

the screw and the leg (ground) was much greater than the capacitance between the screw and the center plate. The voltage between the screw (which was electrically floating) and the plate, V_2, was inversely proportional to the very small capacitance between them. This imposed a requirement that the measuring device be of high impedance. A coaxial jack was mounted on the pipe above the water line and connected to the screw through a wire running inside the pipe. The signal was detected with a 25 KV Tektronix High Voltage Probe grounded only at the scope so as to avoid ground loops. The calibration, which was performed exactly as for the Mark I system, showed an attenuation of 2×10^5:1 appearing at the scope.

17. The Requirement of Deionized Water

The dielectric constant of water at room temperature is 82 [29]. The depolarization time of water is given by

$$\tau = \frac{\varepsilon \rho}{4\pi} \qquad 17.1$$

and is 73 μs for a resistivity ~ 10 megohm-cm. We have found (section 13) that the dielectric strength of water is greater than 10^6 volts/inch for times less than τ. If the capacitor is charged and discharged within this time there will not be any internal breakdown provided that the plates are perfectly smooth and that the water is kept free of all contaminents (i.e., dust particles). It should be remarked that:

(a) The dielectric constant of water helps to smooth out electric fields at the water-air interface.

(b) For a given value of capacitance the use of a water dielectric permits a smaller volume than with conventional dielectrics. The smaller volume of dielectric reduces the self inductance of the capacitor.

The use of highly deionized water is a prerequisite for this experiment. The removal of ions from the water helps to prevent internal corona and arcing at high field gradients. In addition, the high resistivity of the water insures that:

(a) The value of τ will be sufficiently large to prevent breakdown before the peak voltage is reached.

(b) The capacitor will hold its charge without large resistive losses in the water.

(c) The Q of the system will be high.

(d) The reflected impedence seen by the primary will be large compared to the impedence of the air-gap switch thus preventing a large energy loss at the air gap.

A number of other dielectric materials were considered and tested. These included some organic chemicals such as ethylene dicloride which has a high dielectric constant but broke down at relatively low voltages. Oil was ruled out because of its low dielectric constant (~ 3) and because of the poisonous gas given off under breakdown.

Treatment of Water:

Theoretically water can reach a limit of 23 megohm - cm at which time the ions and electrons dissassociate at a rate that prevents further deionization. Realistically speaking 18 megohm-cm is the highest value obtainable in the laboratory. This is done using special glass and tin plated piping throughout the system.[30]

In our first system we had hoped to reach 16 megohm-cm. but had to settle for 8-10 meg-cm. most of the time. In view of the fact that our components were constructed of aluminum and stainless steel (causing electrolytic action), that the tank contained 500 gal. of water open to air, and that we were always putting tools or our hands in the water to make adjustments we were content with 8 meg-cm. It should be mentioned that once the water was above 3 meg-cm. it quickly recovered from any contamination.

The deionizing loop for our 500 gallon tank consisted of one mixed bed, Barnstead BD-10 Super Deionizer Cartridge. The water

which was hospital-grade, double-distilled was filtered and re-circulated once every 10 hours.

The deionizing loop for the 2000 gallon tank consisted of two mixed-bed Super Cartridges connected in parallel. Their combined flow rate was 125 gallons/hr. In addition, a second pump was installed to circulate the water in the tank. The mixed bed cartridge removes metallic ions only. The oxygen removal cartridge does not remove any ions but by lowering the oxygen content in the water it slows down the formation of oxides. Our experience with oxygen removal cartridges showed them to be of little value in raising the resistivity or in preventing corrosion. We considered removing the gases trapped in the water by heating the circulating water but this proved uneconomical. Figure 25 shows how the resistivity of the water varied with time for this system. Typically, the maximum resistivity was between 5 and 7 megohm-cm.

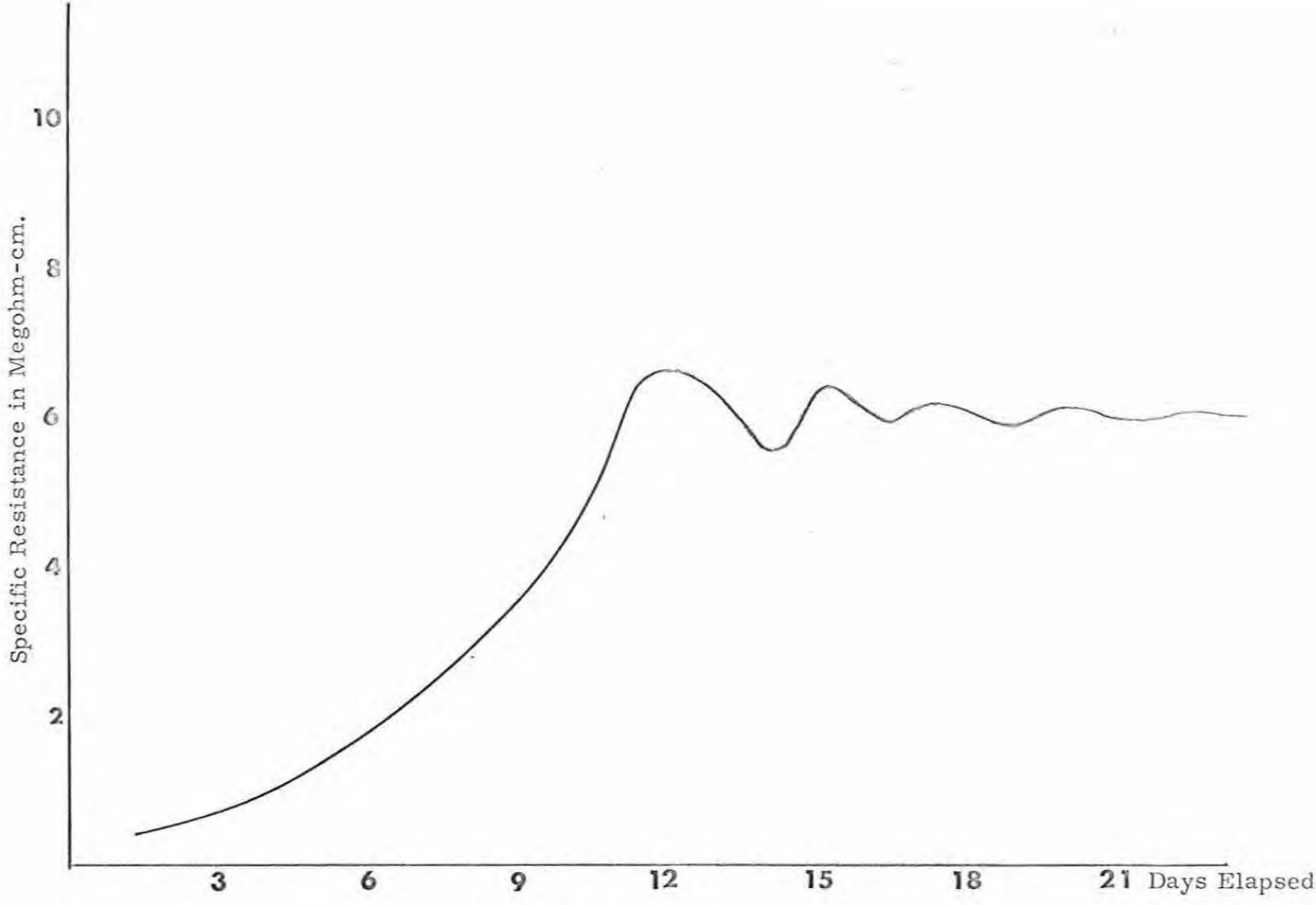

FIGURE 25

Plot of Resistivity of Water Vs. Time for Mark II System

18. Selection of Metals for Use in Water

The "300 series" stainless steel has the best corrosion resistant properties with an average corrosion rate in water of less than 5 mg/cm^2 per month. Stainless steel offers many advantages over aluminum (corrosion resistance, strength, flexibility in forming) and where cost and weight are not a factor it should be preferred.[31]

We were forced to use aluminum because of the many design considerations mentioned throughout this report. Although stainless steel offers the best corrosion resistant properties, it must be used exclusively with no less noble metal in the tank. When aluminum was put in contact with stainless steel, the aluminum corroded rapidly on the contact surface (over and above the normal corrosion rate in water) and the stainless steel formed a brownish oxidation deposition on all its surfaces which proved disastrous to the resistivity of the water. Electrolytic action in the tank can be virtually eliminated by using only one type of aluminum throughout. Although aluminum is easily cleaned by immersion in a 50% solution of Sodium EDTA in water,[32] we found from experience that once the deionizing cartridges raised the resistivity above 1 megohm the corrosion of the aluminum did not affect the resistivity and therefore there was no useful purpose in constantly cleaning the metal.

PART II

The High-Voltage, High-Current Atmospheric Discharge Experiment

19.1 Description of the Experiment

Introduction: A major part of our research effort is devoted to the observation and analysis of high-voltage, high current atmospheric discharges. It is hoped that experience gained from these studies will aid in more fully understanding the behavior and capabilities of our present pulse system. Further, the information gained from atmospheric discharges (which is an interesting study in itself) will guide us in designing a facility to observe less dense discharges in hydrogen.

The discharge was initiated between a $1\frac{1}{2}$ inch diameter hemisphere and a point electrode. The stainless steel hemisphere was attached to the top of the center section of the water-capacitor. The point electrode was secured to a 2" thick slab of stainless steel located directly over the hemisphere and supported on the two outside ground planes. (Figure 26). Although the Mark II Pulse System was capable of a million volt output it was not operated above 720 KV. For this reason all calculations concerning the atmospheric discharge experiment are executed in terms of a maximum voltage of 720 KV.

19.2 A Discussion of High-Cuttent Atmospheric Discharges

Consider two electrodes separated by a distance d with an electric field E between them. When E is made large enough there will be considerable electron ionization and a number of new electrons will be emitted from the cathode for each of the bombarding positive ions.

Loeb[34] points out that the breakdown potential is critically dependent on the condition of the electrode surface. Impurities such as fingerprints, oxide films, dust, or adsorbed gases on the electrode can lower breakdown voltage by a factor of 3 or 4.

For a pulsed field (as in our experiment) the breakdown voltage is higher than that of the static breakdown voltage because of the finite time required to produce electrons and to establish a cumulative ionization process.[35] The time lag between the instant the static breakdown voltage is reached and the instant of breakdown is less than .1 μs.[36] With sufficient overvoltage the time lag may be as little as a nanosecond.[37] A 6 cm-air gap has a breakdown voltage of about 30 kv/cm; therefore we can expect very short time lags.

The electron avalanches alone cannot account for the short time lags observed in the studies of breakdown. Loeb has proposed that the process can be brought up to the necessary speed by assuming photons formed in the avalanche ionize the gas well ahead of the luminous conducting streamers observed prior to actual breakdown. The photons initiate new avalanches along the breakdown path. The new avalanches are not always in the same path as the original one so that when the space-charge field between the head of one avalanche and the tail of a new one, somewhat ahead of it and to one side, becomes great enough, the intervening space is bridged and the irregular path observed in sparks and in lightning is produced.[38]

It has been suggested that at values of $p\,d > 1000$ mm.-cm. (p is the gas pressure, d is the gap spacing), the mechanism of static breakdown changes critically from being a Townsend type involving the action of primary and secondary processes to a Kanal or streamer type. Raether[39] has found that the electron

avalanche is accompanied by the development of a reverse streamer stretching from the anode to the cathode resulting in breakdown in the gap. The discharge mechanism is essentially the following. Irradiation of the cathode surface results in the emission of photoelectrons from various points on the surface. Thus, the paths of the secondary avalanches do not coincide. The buildup of the positive volume charge occurs initially throughout the entire volume of the interelectrode gap. This determines the dependence of the discharge voltage on the ratio of the electrode diameter D to the gap length d, since the photon losses to the surrounding space increase as the ratio D/d is increased. The avalanche diameter can be computed from the formula[40]

$$r = \frac{9}{2}\left[\frac{UX}{E}\right]^{1/2} \qquad 19.1$$

where U is the thermal electron energy in electron volts, taken as .5 ev, X is the path length in cm, and E is the field strength, 10^5 volts/cm. For a 10 cm path length, r = .3 mm.

In gaps longer than 2 cm. the initial avalanche will bring about a field distortion sufficient to localize ionization processes and to form a spark channel. The nature of this field distortion is responsible for the features observed in the development of the discharge as a thin "pinch" along the axis of the initial streamer (avalanche). It has been suggested that at atmospheric air pressures, and at gap lengths greater than .1 cm, the discharge will appear at field intensities such that only two secondary electron sources need be taken into consideration: the photo-electric effect at the cathode and photoionization in the gas volume.[41]

Discharge experiments[42] have been carried out for gap voltages up to 170 kV in air at atmospheric pressure but no evidence has been observed for the sudden suppression of the Townsend mechanism by the streamer type suggested by Raether as likely to occur at these pressures and gap spacing.

FIGURE 26a
Rifle Switch with
Electronic Controls

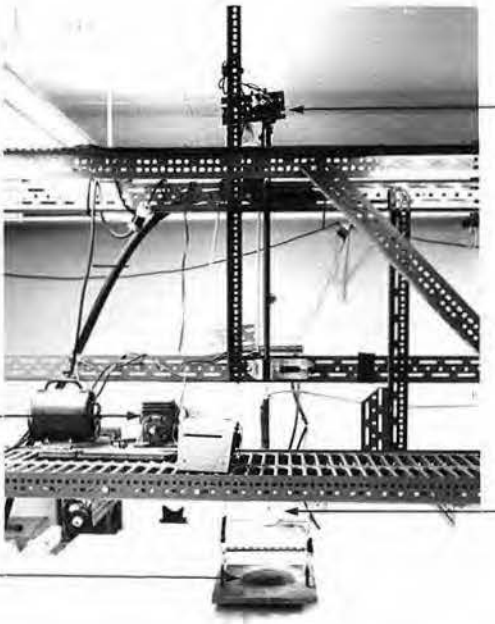

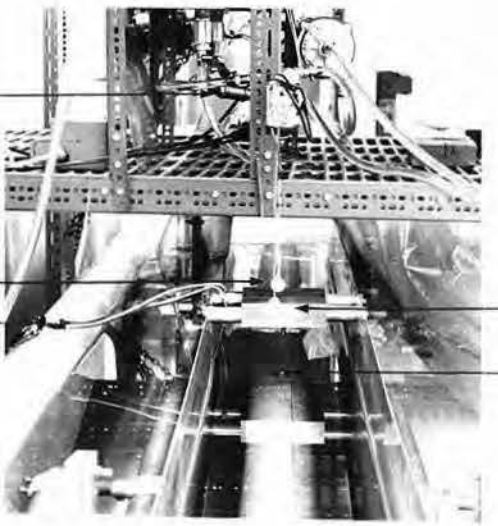

FIGURE 26b
Electrode Assembly
Yukon II

20. Theoretical Analysis of a High-Voltage,High-Current Atmospheric Dischar

To describe the dynamics of the pinch we use a simple model in which the gas is assumed completely ionized and hence highly conducting. The discharge current then flows only on the surface, resulting in a discontinuous change of the (tangential) magnetic field across the interface with a magnetic pressure $\frac{B^2}{2\mu}$, where B is the field outside the ionized gas and inside is zero. The moving interface acts like a piston and if its velocity is much greater than the initial thermal velocities of the gas, each particle struck acquires a velocity 2 v radially inward.

We have the choice of using the "free particle model", the "snow plow model", or continuum hydrodynamics. The free particle model is useful where the mean free path is large enough to neglect collisions and assumes that a particle once struck maintains a constant velocity until it strikes the interface. The snow plow model assumes that every particle struck by the interface moves with it. The use of continuum hydrodynamics is quite complicated if done correctly and its validity is not greater than the other two models if approximations are allowed. We choose to use the snow plow model because it physically allows for high densities and short mean free paths.

Table III lists the values of the important discharge parameters. When the water gap switch is triggered a discharge current I(t) flows through the air gap from the water capacitor C which is initially charged to a voltage V_o. The total self inductance of the system, L_{total}, consists of a constant external part, L_c, due to the capacitor and a variable part, L_G, formed by the air gap. The magnitude of L_G depends on the radius r(t) of the air gap.

Table III

Estimated Values of the Discharge Variables

The results below are taken from Appendix A-4.

$L_c = 30$ nH	The inductance of Yukon II
$L_G = 45$ nH	The inductance of Discharge Gap
$Z_c = 87$ nH	The characteristic impedance of Yukon II
$I_{max} = 3.6 \times 10^5$ amps	The maximum discharge current
$C = .04$ μf	The capacitance of Yukon II
$I'_o = 5.5 \times 10^{12}$ amps/sec	Initial rate of current growth
$t^* = 2 \times 10^{-9}$ sec	Minimum time discharge must exist in order to create a pinch condition

We consider here the dynamics of a cylindrical discharge which constricts under the action of its self magnetic field. The neutral gas which is encountered by the constriction is assumed to be instantly ionized and entrained by the sheet. In this model we neglect the energy needed to ionize and heat the neutral gas in the discharge. (Brown[43] has shown this energy to be ~ 100 eV for electrons produced in the neutral gas.)

Consider the discharge to be a cylinder of height l and initial radius r_o, and equate the magnetic pressure $B^2/2\mu$ to the rate of change of momentum. The equation of motion of the cylindrical shell of material (electrons, ions, and neutral particles) can be written as

$$\frac{d}{dt}\left[M\dot{r}(t)\right] = -\frac{\mu_o I^2(t) l}{4\pi r} \qquad 20.1$$

The neutral gas encountered by the moving shell is entrained by it thereby increasing the mass M continuously.

$$M = \pi \rho (r_o^2 - r^2) l \qquad 20.2$$

where ρ is the initial density of the neutral gas (air).

The current through the circuit is

$$I(t) = - CV(t) = - C \frac{d^2}{dt^2} [(LI) + \dot{Z}I(t)] \qquad 20.3$$

After breakdown the resistive effects of the water can be neglected so equation 20.3 reduces to

$$I(t) = - C \frac{d^2}{dt^2} [L(t)\ I(t)] \qquad 20.4$$

The self inductance of the system can be expressed as

$$L(t) = L_{external} + \frac{\mu_o l}{2\pi} \ln \frac{r_o}{r(t)} \qquad 20.5$$

where we have neglected the resistance. The above equations have not been solved analytically but have been evaluated by computer techniques.

An approximation has been put forth by Linhart[44]. If the relative change of the self induction is small, we introduce an average value of L, independent of time

$$L(t) = L_{ave} = \bar{L}_c + \bar{L}_G = 25\ nH + 10\ nH = 35\ nH \qquad 20.6$$

Equation 20.4 simplifies to

$$I(t) = - CL_{ave}\ddot{I} \qquad 20.7$$

with the solution

$$I(t) = I_o \sin \omega_o t \quad \text{where } \omega_o = 1/\sqrt{LC} \qquad 20.8$$

We further assume that at the start of the constriction the relative variation of the radius is small compared with the relative variation of the acceleration such that an average value $r_{ave} = 3/4\ r_o$ may be substituted. With this approximation and with the results of 20.8 equation 20.1 reduces to

$$\ddot{r}(t) = \frac{-\mu_o l I(t)^2}{4\pi M_{ave} r_{ave}} = \frac{-\mu_o l I_o^2}{4\pi M_a r_a} \sin^2 \omega_o t \qquad 20.9$$

$$= -A \sin^2 \omega_o t$$

where $M_{ave} = \pi\rho l(r_o^2 - r_a^2)$ (Note 1)

$$A = \frac{\mu_o l I_o^2}{4\pi M_a r_a}$$

The solution of 20.9 yields the constriction velocity and the radius of the shell as a function of time.

$$\dot{r}(t) = \frac{-A_o}{4\omega_o} (2\omega_o t - \sin 2\omega_o t) \qquad 20.10$$

$$r(t) = r_o - \frac{A}{4\omega_o^2} (\omega_o^2 t^2 - \sin^2 \omega_o t)$$

In solving equations 20.9 and 20.10 the maximum time used must be less than a quarter cycle of the discharge frequency. The equations themselves can be used to determine the maximum time for which the approximations are valid.

It should be remarked here that if the initial arc diameter is very wide from the beginning then the magnetic pressure at no time will exceed the particle pressure. Smars[9] describes the behavior of a 15 KV, 200 KA atmospheric discharge in the following manner.

Note 1:

Rosenbluth[45] has shown that the penetration depth of the magnetic field (the surface layer) has a thickness d given by $d = [\frac{mc^2}{8\pi N_o e^2}]^{\frac{1}{2}}$ cm. where N_o is the neutral density ahead of the layer and m is the mass of an electron. For total ionization of the surface layer the value of d is 10^{-3}mm. ($N_o \cong 10^{19}$ particles/cm^3). For partial ionization Rosenbluth (loc. cit.) shows that $d \cong 1$ mm. We may therefore replace r(t) by $(r_o - d)$ for very small t.

The discharge channel at the beginning is only a fraction of a mm., expands in about .1 μs to a diameter of a few mm. and remains there for about .2 μs. Then a very fast compression takes place in less than .1 μs immediately followed by the setting in of instabilities and a fast overall expansion of the luminous region. A review of our data (discharge wave forms, photographic and visual observation) gives the impression that the above description is applicable to our discharge.

Table IV

Theoretical Values for the Discharge Column

(From Equations 20.9 and 20.10)

The constants used in compiling this table will be found below or in Table III.

$$A = \frac{\mu_o I_{max}^2}{4\pi r_a M_a} = 1.8 \times 10^{11} \qquad M_a = 2.4 \times 10^{-6} \text{ kg.}$$

$$\omega_o = 1 / \sqrt{LC} = 2 \times 10^7 \qquad r_o = 3.7 \times 10^{-3} \text{ m.}$$

Variable	Approximation Used (for $t \leq 10^{-7}$ sec)	Value at $t = 10^{-8}$ sec.	Value at $t = 10^{-9}$ sec.
$\ddot{r}(t)$	$A(\omega_o t)^2$	7.3×10^9 m/sec.	7.3×10^7 m/sec.^{2}
$\dot{r}(t)$	$\frac{At}{2}$	9.1×10^2 m/sec.	9.1m/sec.
$r_o - r(t)$	$\frac{-At^2}{4}$	4.6×10^{-5} m.	4.6×10^{-7} m.

21. Bremsstrahlung Radiation [46,47]

X-rays are electromagnetic radiations having wavelengths of a few angstrom units (10^{-8} cm), thus having quantum energies ranging from a few thousand to millions of electron volts. The emission spectrum produced when an energetic electron beam strikes a target consists of a continuous and a line spectrum characteristic of the atoms of which the material is made. "The continuous spectrum of radiation emitted when electrons strike the metal target of an X-ray tube is the result of transitions between the unquantized positive energy levels of the electrons in the fields of the nuclei of the target atoms. This radiation is called Bremsstrahlung."[48]

The total Bremsstrahlung cross section, σ_{rad}, is defined as the fraction of the total energy $(T + m_o c^2)$ of the electron which is radiated as the electron traverses an absorber of such thickness that it contains 1 atom/cm^2. It can be shown[49] that for $T \ll 1$ mev

$$\sigma_{rad} = \frac{16}{3} \sigma_o Z^2 \quad \text{cm}^2/\text{atom}$$

where

$$\sigma_o = \frac{1}{137} \left(\frac{e^2}{M_o c^2}\right)^2 = 58 \times 10^{-29} \quad \text{cm}^2/\text{atom} \qquad 21.1$$

For $T > 1$ mev σ_{rad} is given by

$$\sigma'_{rad} = 4 \left[\ln \left(\frac{T + M_o c^2}{M_o c^2}\right) - \frac{1}{3}\right] \sigma_o Z^2 \qquad 21.2$$

For $T = 1$ mev $\sim 2m_o c^2$ equation 21.2 reduces to

$$\sigma_{rad} = 4 \left[\ln 6 - \frac{1}{3}\right] \sigma_o Z^2$$

$$= 5.84 \, \sigma_o Z^2 \ \text{cm}^2/\text{atom} \qquad 21.3$$

The difference between σ and σ' is very small. We therefore chose an average value for σ which is taken from the data found in Evans (ref. cit).

$$\sigma_{rad} = 33 \times 10^{-28} Z^2 \quad cm^2/atom \qquad 21.4$$

The fraction of the discharge energy E radiated per unit length by the electrons in passing through air is

$$\epsilon = \left(\frac{dE}{dX}\right)_{radiation} = N_A \sigma_{rad} \ cm^{-1} \qquad 21.5$$

where N_A is the number of atoms contained in a cm^3 of air. At STP the value of N_A is $\sim 10^{19}$ atoms/cm^3. The maximum fraction of the energy that can be radiated is

$$\epsilon_{max} \sim 33 \times 10^{-28} \times 10^{19} \times 52$$
$$\sim 17 \times 10^{-7} \ cm^{-1} \qquad 21.6$$

where we have taken 52 to be the square of the average value of Z for air.

Generally, the method used for measuring X-ray exposure is by means of the ionizing action of the X-rays in a particular material. The unit of exposure[15] the roentgen and is defined as that quantity of X-rays emitted such that the associated corpuscular emission per .001293 cm^3 of air produces in air ions carrying 1 esu of quantity of electricity of either sign[48]. The probability of a collision of a photon from the beam with an atom while passing through an absorber is strongly energy dependent and falls off rapidly for energies above .05 mev. Thus the roentgen is a measure of the ionizing effect of the X-rays in air rather than the direct

measure of the energy flux. It should then be clear that the same energy flux of hard X-rays gives a much lower value in roentgens than do soft X-rays.

In estimating the X-ray emission from a .1 mev or 1 mev discharge in air two assumptions will be made.

1 - There is negligible compton scattering or pair production[50].

2 - We neglect any distribution of energy and assume that all electrons have the maximum allowable energy. This will give us an estimate of the upper limit of the radiation. (Most electrons will undergo collisions. The secondary electrons liberated from these collisions produce the photons of interest.

The total energy available for our discharge is 10^{11} ergs. We multiply this by the value of ϵ obtained in equation 21.6 to find the energy radiated.

$$E_{radiation} = \epsilon E = 17 \times 10^{4} \text{ ergs} \qquad 21.7$$

The relationship between the photon energy and wavelength is given by $\lambda = \frac{hc}{E} = 1.24$ microns/volt. We find that .1 mev radiation corresponds to a wavelength of .124 A. At this wavelength one roentgen corresponds to 3,200 ergs/cm^2.[48] (The value is even higher for 1 mev radiation but is much less for radiation below .1 mev.)

At a distance of 1 cm from the discharge the radiation is equal to

$$\frac{17 \times 10^{4} \text{ ergs/cm}^2}{3200 \text{ ergs/cm}^2} = 53 \text{ roentgens} \qquad 21.8$$

At 15 cm from the discharge this corresponds to a radiation of .24 roentgens.

There exists the possibility that some electrons will have a high enough velocity such that the total cross section and collision rates for these electrons will be so small as to let these electrons accelerate right into the electrodes producing high energy X-rays.

If the total Bremsstrahlung is measured we can determine whether or not the body radiates as a black body, essentially from the surface or from throughout the volume according to the formula for Bremsstrahlung energy emitted per unit volume per unit time. The former will roughly be the case if the mean free path for energy absorption of photons is less than the diameter of the system and the latter if this mean free path is greater than the dimension. Dawson and Oberman (Princeton University Plasma Physics Laboratory Report - 101) have computed the energy absorption coefficient for Bremsstrahlung. The opacity of highly ionized air has been investigated by Kivel and Mayers.[51] An up-to-date bibliography on this subject will be found in their article.

Measurement of X-rays

The blackening of a photographic plate due to exposure to X-rays depends only on the amount of radiation falling on the emulsion and is independent of the length of exposure. If the darkening of the film is measured with a densitometer then the density of the plate, D, is defined as $D = \log I_o/I$[52] where I_o

is the incident intensity and I is the transmitted light intensity.

X-ray film (Dupont, Type 519) was placed 15 cm. from the discharge and after exposure was machine processed at a local hospital. No detectable fogging was observed. The manufacturer states that a minimum exposure of .25 roentgen is required for a net density of .1 (using a radiation source with an effective wave length of .01A). Our results are thus an indication that we have not exceeded the theoretical maximum amount of radiation.

22. Maximum Attainable Temperature

Let us assume that the two most abundant gases (oxygen and nitrogen) have been triply ionized and that one tenth the available energy has been deposited into random termal motion. The discharge column of air has a volume of 4 cm^3 with a density $\sim 10^{19}$ particles/cm^3.

The stored energy for C = .04 μf and V = 7.2×10^5 volts is

$$U = \tfrac{1}{2}CV^2 = 10{,}000 \text{ Joules} \qquad 22.1$$

If we assume an instantaneous energy transfer ($P \Delta V = 0$) then

$$\frac{3}{2} NKT = \frac{1}{10} 10{,}000 = 1000 \text{ Joules}$$

$$T \cong 10^{6} {}^{o}K \qquad 22.2$$

This, figure serves to define a maximum upper limit. It is of the same order as the results estimated from a shock wave analysis in section 24.

It has been found that the temperature of the surrounding gas departs very little from the ambient value up to a distance only a few millimeters from the luminous region. The surrounding cold gas acts as a wall to receive diffusing ions and electrons for recombination.

The energy necessary to triply ionize the discharge column will be

$$E = (\Sigma_{i\nu})N_o \qquad 22.3$$

where ν represents the species and i the level of ionization. For Oxygen, E_1 = 13.6 ev, E_2 = 35.1 ev and E_3 = 54.9 ev. For Nitrogen, E_1 = 14.54 ev, E_2 = 29.6 ev, E_3 = 47.4 ev. With these values E $\sim$ 600 joules.

23. Diagnostic Methods and Observations

23.1 Discharge Waveforms:

The existence of two frequencies in the discharge circuit corresponding to ω_1 and ω_2 was confirmed. The values agreed within 5% to those derived in section 13. The behavior of the pulse transformer was unaffected by the interwinding capacitance of Mark II. (This capacitance is about 20% that of Yukon II.) As expected, the oscillograms showed a smoothly damped ringing discharge of the water capacitor and pulse transformer. (Figure 27-a, no breakdown). At the end of each half cycle there was a period in which the current was practically zero. During this period, deionization acted to reduce the conductivity of the column. As the voltage reversed, the conductivity that existed just before the instant of zero current had to be reestablished and this required considerable voltage. Notice the gap present in Figure 27-b after 60 μs (17 KC). This corresponds to a breakdown produced by a voltage maximum due to the superposition of the two frequencies present in the discharge circuit. A typical discharge trace showed noise at the initiation of the breakdown and post breakdown charging and discharging of Yukon II as the air gap switch on the primary side died out and restruck.

The initial breakdown proceeded in less than .2 μs (Figure 27-c) in agreement with the observations of Cragg, Loeb, and Smars. The ideal LC resonance frequency of the discharge column was 3 mc. A discharge frequency of 2.5 mc was observed (Figure 27-d). An oscillogram showing the superposition of the 2.5 mc column oscillation and the 120 KC pulse system oscillation (ω_+) is shown in Figure 27-e. The output of the Rogowski Loop appears in the lower trace.

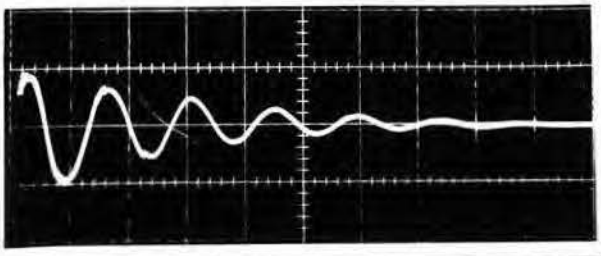

FIGURE 27a
Discharge Wave-form
Bank is charged to 8 kV
Time scale: 4 μsec per least division.
y = 75 kV per cm. (divider signal)
Comments: No breakdown
Damped Osc.

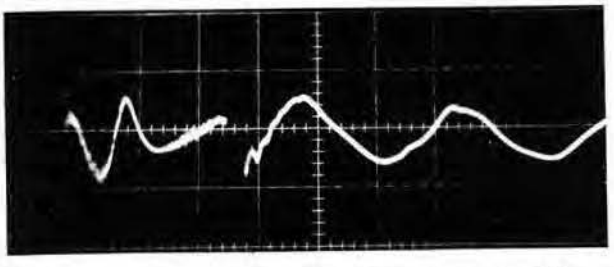

FIGURE 27b
Discharge Wave-form
Bank is charged to 40 kV
Time scale: 2 μsec per least division.
y = 400 kV per cm. (divider signal)
Comments: Time between start
of signal and gap corresponds
to beat frequency.

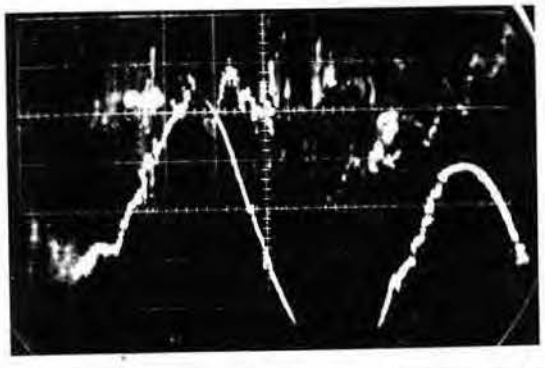

FIGURE 27c
Discharge Wave-form
Bank is charged to 60 kV

y_1 = 400 kV per cm.
x_1 = .5 μs per cm.
y_2 = 200 kV per cm.
x_2 = 5 μs per cm.

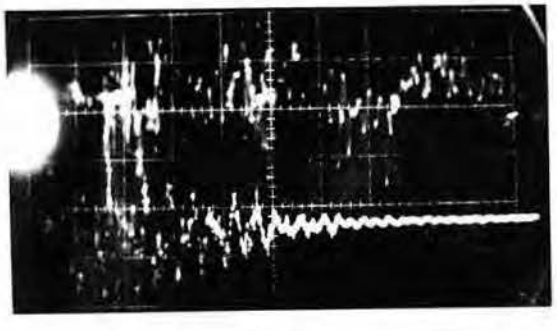

FIGURE 27d
Discharge Wave-form
Bank is charged to 50 kV

y_1 = 400 kV per cm.
x_1 = .1 μs per cm.
y_2 = 400 kV per cm.
x_2 = 1 μs per cm.

Comments: Breakdown occurs
in less than .2 μs.

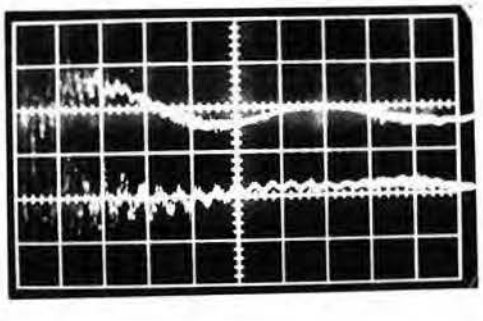

FIGURE 27e
Discharge Wave-form
Bank is charged to 35 kV
Time scale: .4 μsec per least division.
y_1 = 400 kV per cm.
y_2 = 50 v. per cm. (Rogowski
Loop)

23.2 Measurement of the Discharge Current

The discharge current was measured with a Rogowski Coil placed around one of the four bolts supporting the discharge electrode. A Rogowski Coil consists of an n turn solenoid shaped to a closed loop. The diameter of each turn is much less than the diameter of the loop. A signal V' is induced in the Rogowski coil by changes of the magnetic flux ϕ enclosed by the coil; the changes of the magnetic flux are proportional to the changes in the current I through the circuit. The signal is fed through a coaxial cable to an oscilloscope.

The induced voltage was fed to an integrating network consisting of a resistor R and a capacitor C. The integration time, RC, was chosen to be 500 μsec, which was much longer than any time of interest of the discharge phenomena. The output of the integrator, V, is proportional to the current I, and is given by:

$$V = \frac{1}{C}\int_o^t I dt = \frac{1}{RC}\int_o^t \frac{d\phi}{dt}\, dt = \frac{\phi(t)}{RC} \qquad 23.1$$

The flux at any time is related to I, the source of magnetic inductance, by an equation of the form

$$\phi(t) = KnI(t) \qquad 23.2$$

where n is the number of turns of the pickup coil (340) and K is a proportionally constant which in general depends on the geometry of the coil and the current distribution. The equation for V reduces to

$$V(t) = \frac{Kn}{RC} I(t) \qquad 23.3$$

If the turns of the coil are evenly spaced, Ampere's Law can be applied to a closed path which threads the turns of the winding

in such a manner that each element of path length is essentially perpendicular to the plane of the turn it threads. Applying Ampere's Law

$$I = \frac{1}{\mu_o} \oint \bar{B}.\, d\bar{l} = \frac{1}{\mu_o n} \oint \bar{B}.d\bar{n} \qquad 23.4$$

where l is the effective length of the deformed solenoid (mean circumference of the torus), $d\bar{n}$ is a vector in the direction of dl with magnitude $\frac{\bar{n}dl}{l}$, $\mu_o = 4\pi \times 10^{-7}$ w/amps-meter

$$I = \frac{1}{\mu_o nA} \int A\, \bar{B}\cdot d\bar{n} = \frac{1}{\mu_o nA} \int d\,\phi = \frac{l\phi}{\mu_o nA} \qquad 23.5$$

where ϕ is the total flux threading the coil and A is the cross sectional area of each turn

By comparing equation 23.3 with 23.5 the constant K is easily evaluated to be $\frac{\mu_o A}{l}$. It is independent of the manner by which the main current threads the opening.

$$I(t) = \frac{lRC\ V(t)}{\mu_o An} = 1.2 \times 10^4\ V(t) \qquad 23.6$$

To obtain the true value for the current the result of equation 23.6 was assumed to divide equally between the four bolts and the measured values was multiplied by four.

A linear response of the system is found in a certain frequency range only. The lower limit is given by the integration time RC; only sufficiently high frequencies can be measured reliably, i.e. $f > 1/RC$. The higher limit depends on the resonance frequency of the coil, which is about 10 Mc. A typical measured value of V is 6.3V which corresponds to a peak current of 300 kA. This is to be compared with the estimated ideal maximum current of 360 kA (at 720 KV).

23.3 Spectroscopic Observations:

The light emitted by the discharge was analyzed by means of a Spenser Spectrograph. The spectrum emitted during the total duration the discharge experiment was recorded on Panatomic Type B photographic film. Lines of Nitrogen, Oxygen and electrode impurities were identified with the peak intensity shifted toward the ultra violet. Continuum bands due to molecular disassociation and recombination were clearly visible. (The results are in agreement with an "optically thin" discharge and the values for the opacity of a high temperature gas given by Aller. ("The Atmospheres of the Sun and Stars", L.H. Aller, Ronald Press, New York, 1963).

No conclusions of importance could be drawn from relative line intensities since the spectra were integrated over the total duration of the luminous phenomena.

Kaiser[53] had found in 1939 that the spark is made up of two parts -- that from the discharge channel, arising mainly from the air in the gap, and the jets of electrode vapor torn off at high speed from the surface of the electrodes. It is a natural conclusion to link the light output from the spark with the high density of energy which is liberated in the channel. The value of current density attained ($\sim 10^6$ amps/cm) can account for the existence of the jets on the electrodes.

23.4 Voltage Measurement:

Measurements have been made of the discharge voltage as a function of time. The measuring circuit is described fully in section 16 of this report. A voltage gain of 11 times the bank voltage is observed. This is the actual gain after all losses are taken into account (voltage drop at bullet switch, imperfect coupling, etc.) The ideal voltage gain was found to be 12:1. This is close to the theoretical value $V_2/V_1 = kN_2/N_1 = 12$.

The voltage drop at the bullet switch varies between 2-4kV, for a bank potential above 25 K.V. Figure 28 shows the hole produced in a sheet of 40 mil polyethylene by a bullet fired at a bank voltage of 60 K.V. The smallness of the hole and the lack of damage to the surrounding material indicated a small energy loss at the switch.

23.5 Time Integrated Photography

This easy but unrefined method provides an overall check on the performance of the system. Its most valuable role is in indicating the regions on which other, more quantitative instruments should be trained.

A number of photographs of the discharge have been taken with a Faraday Cell Camera. The camera has a shutter speed of better than .8 μs and is triggered by the oscilloscope sweep. A narrow discharge channel is evident but the outside of the channel is obscurred by luminous "clouds". The photos indicate the return current path along the center of the capacitor. They also show a wavelike motion of the water. This effect has been called "Ion Drag Pumping" and has been analyzed in papers by Packard[54]. Using the formula derived by Packard we estimated the rise of the water level to be 2 cm. which agrees with the height determined from the photos. Additional photographs were taken with a Polaroid 800 camera. Photographs of the above phenomena are shown in Figure 29.

The Faraday Camera has provision for a shutter delay from the trigger signal. A discharge was evident with a 2 μs delay. This afterglow may be due to a molecular excitation or atomic relaxation.

The radius of the discharge was measured directly from the photographs by comparison with a known dismension in the same photo. The radius was found to be 3.7×10^{-3} meters ± 4%. In addition, the photos revealed thin streamers prior to the major breakdown. To understand this effect more fully a mirror was put underwater so as to permit us to photograph the underwater discharge. These pictures (figure 30) indicated an underwater corona. There seems

to be a pre-breakdown corona which ionizes the water as well as any trapped gas, and triggers the breakdown. When the capacitor arcs internally much of the energy of the discharge is lost in the water and never reaches the air. The fact that negligible damage is done to the capacitor plates when there is internal arcing indicates that the electrons are losing most of their energy in collisions with the water molecules. This is a major consideration that may limit the ultimate energy density of the discharge.

The photographic observations of the discharge suggest the following model. The initial high voltage gradients create a weakly ionized cylindrical channel with a radius r_o, a temperature T_o and a pressure P_o of 10^5 N/m^2 (1 atm.) For simplicity, we disregard variations within the channel. This cylinder is surrounded by cool gas with the same pressure. The initial current rise when the capacitor high-voltage is applied is limited at first by a resistive voltage drop, but after a time, considerably less than .1 μsec., by the inductance of the arc channel. The current starts to flow in a very narrow region and expands very fast. As the current rises, the self magnetic pressure exceeds the particle pressure and a fast contraction takes place at the time t_1. The current at that time is $I_1 = I_o't_1$. Indications are that this is completed in less than 10^{-7} sec.

When the hot gas begins to contract a relatively low pressure region is created between the surrounding cool gas and the hot contracting cylinder. This may justify comparison (in some respects) with existing theories for low pressure pinches, the main difference being that only a small and well defined central portion of the gas

is heated and compressed. As a result, impurities from outside the discharge region are effectively prevented from reaching the hot region leading to an extremely "clean" discharge. (Note 1)

The breakdown between the water capacitor and air was expected to occur along a vertical path from the center section and this was confirmed by the photographs. Due to the high ratio of the dielectric constants of water and air the electric field is internally reflected at the surface of the water except when the angle between it and the normal to the water surface is very small.

Note 1: N.J. Phillips (Department of Physics, Imperial College, London) has proposed a simple theory of the trapping of gas in a fast pinch. He shows that the efficiency of the trapping of the cold gas within the pinch during the collapse stage increases with the initial gas density.

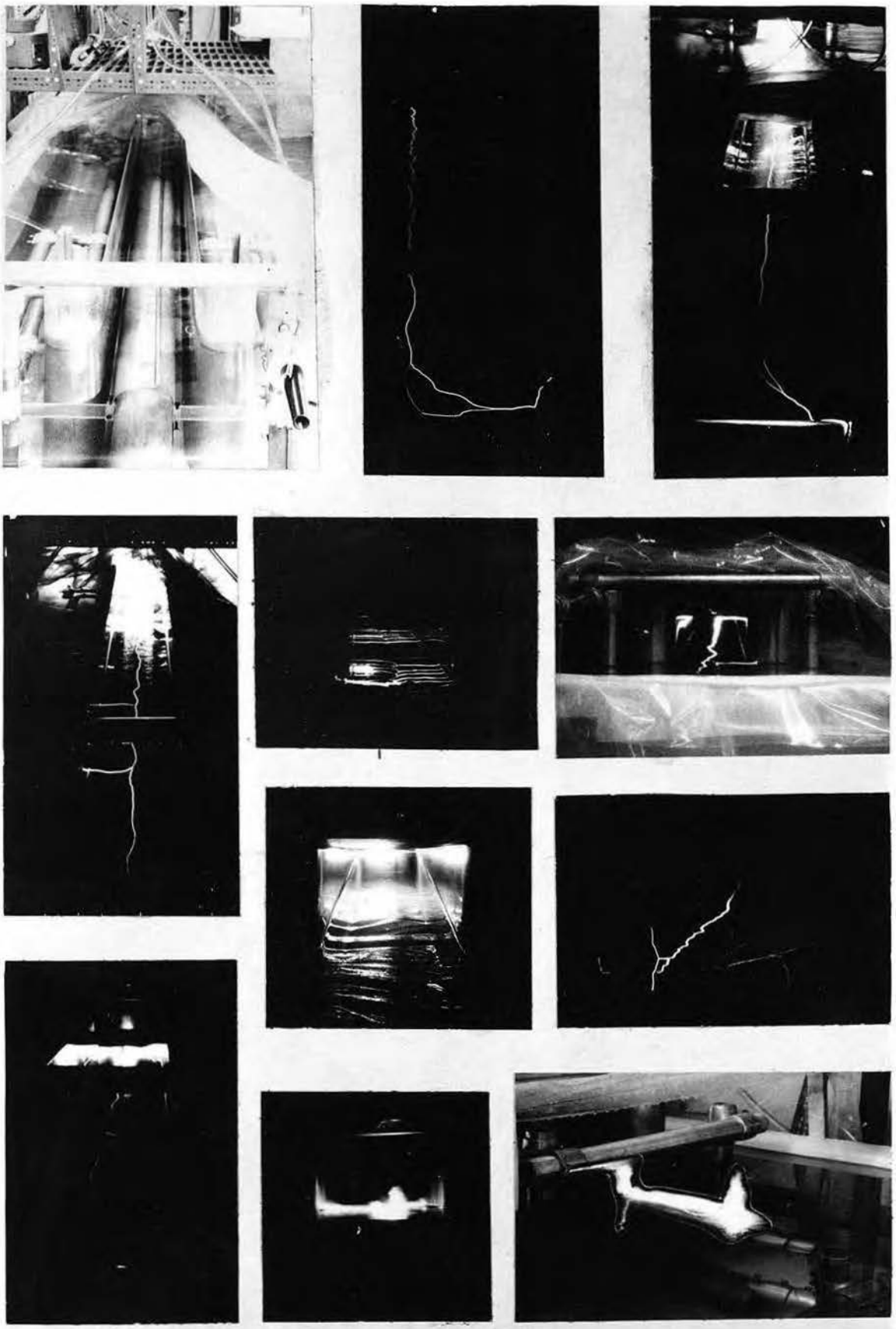

FIGURE 29

Time Integrated Photographs of Atmospheric Discharges

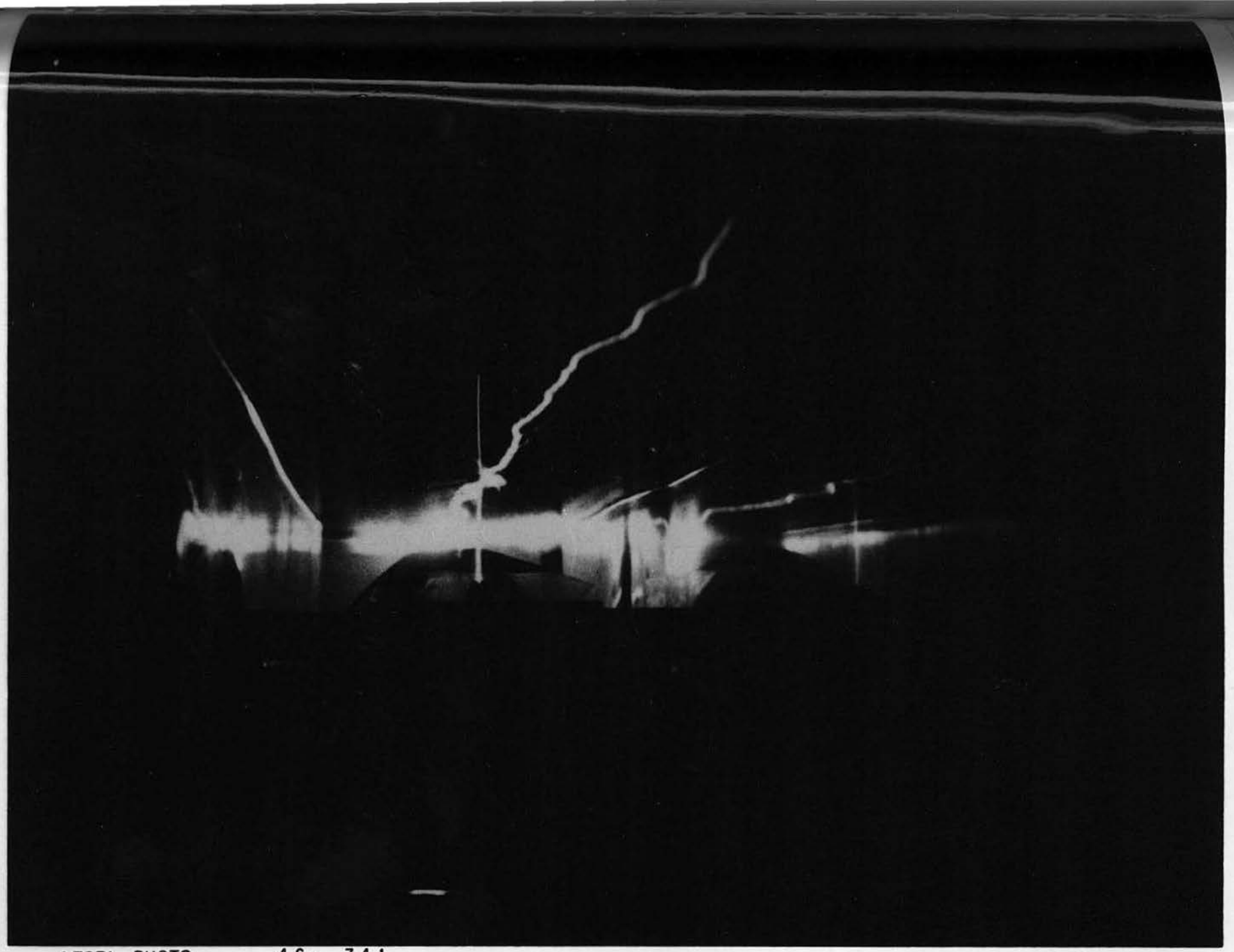

AFCRL PHOTO 46 - 741

FIGURE 29 a

FIGURE 29b

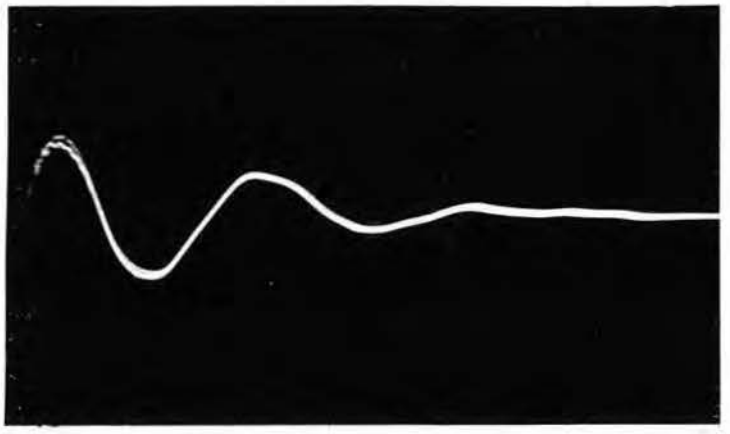

FIGURE 24

Fidelity of Signal of Mark II
High Voltage Divider

y_1 - Signal as Seen by Probe
Attached Directly to Yukon II
y_2 - Signal Appearing on Divider.
x - 10 μs/cm.

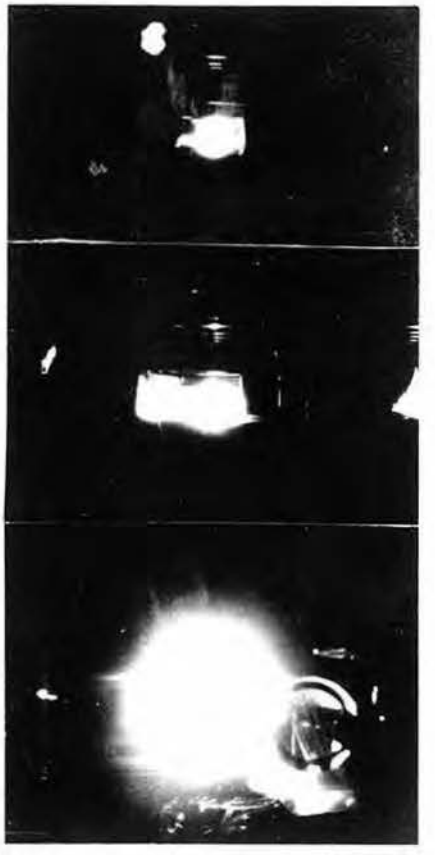

FIGURE 32
Infra-Red Photographs

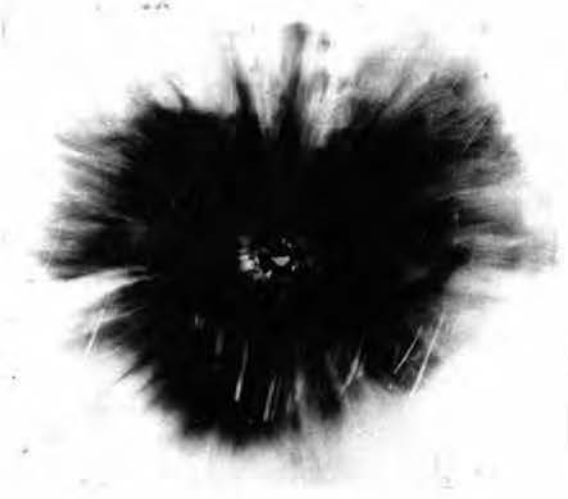

FIGURE 28
Bullet Hole In Polyethylene Sheet

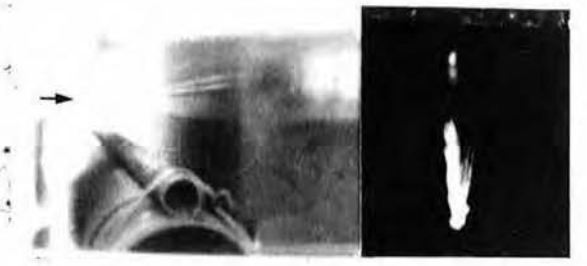

FIGURE 30
Underwater Photographs of Discharge
Arrow Indicates Water Level
Note Arc Streamers on Anode

23.6 Infra-Red Photography

The amount of infra-red radiation released during the discharge gives an indication of the location of the radiation peak as well as the average gas temperature. The spectral response of infra-red film cuts off sharply beyond .9 microns. A wratten filter placed in front of the film creates an effective narrow band filter. This is shown graphically in figure 31. Polaroid type 413 Infra-Red film was used with wratten filter #87 (passes light above 760 millimicrons) #87B (passes light above 860 millimicrons), and #87A (passes light above 950 millimicrons). The photos (see figure 32) indicate little radiation in the infra-red region. As the voltage was increased a corresponding increase in the infra-red was expected. This increase was not observed.

The infra-red photographs established the existence of a current on the surface of the water directly over the center plate. This current path (corona) occurred at all discharge voltages. Whenever a current path is established a potential exists between it and ground. A discharge can then be initiated anywhere between this current path and ground. It is plausible that this explains why discharges not occurring at the gap do not go directly from the center electrode to ground but travel along the surface of the water to ground. The photos indicate a spherical symmetry in the vicinity of the discharge.

SPECTRAL SENSITIVITY. The spectral response of Type 413 film is illustrated in Figure 1.

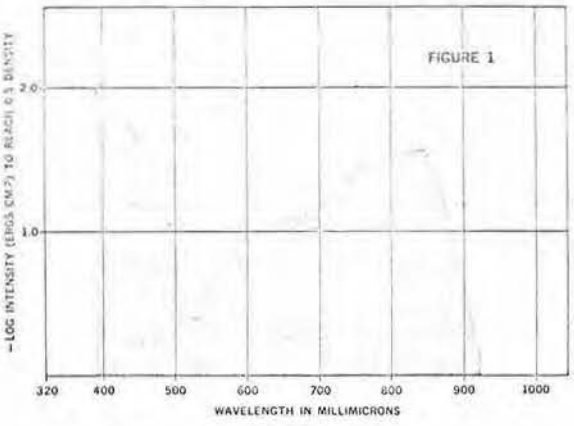

CHARACTERISTIC CURVES. Average H & D characteristics of Type 413 film are shown in Figure 2. (Tungsten light source, 3000°K.)

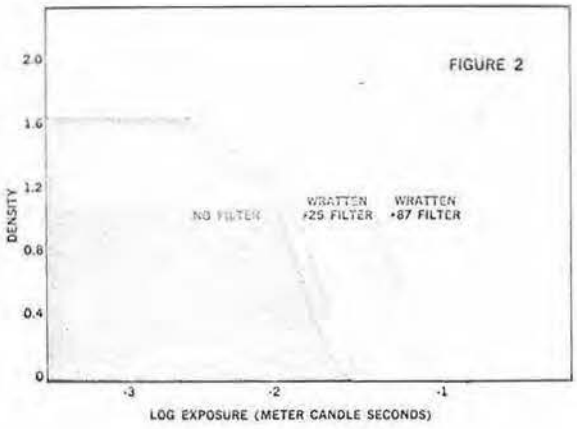

Figure 31

Spectral Characteristics of Infra-Red Film

23.7 Optical Timing Methods

Optical methods were employed to determine the instant of water gap breakdown in relation to the firing of the air gap switch. This measurement enabled us to determine (1) the duration of the discharge and subsequently di/dt, and (2) that part of the charging cycle when the discharge occurred.

The respective discharge flash of each of the gap switches was brought to focus on EGG type SD-100 photodiodes (4 nanosecond rise time). The outputs of the photodiodes were amplified and fed into separate imputs of a Tektronix dual beam scope. The time between the air gap breakdown and the water gap breakdown is recorded, from which the instant of breakdown is obtained by dimultaneously observing the bank discharge and the output of Mark I on a dual beam scope. Figure 33 shows a typical scope trace of the diode outputs. The time between the two peaks is 10 μs.

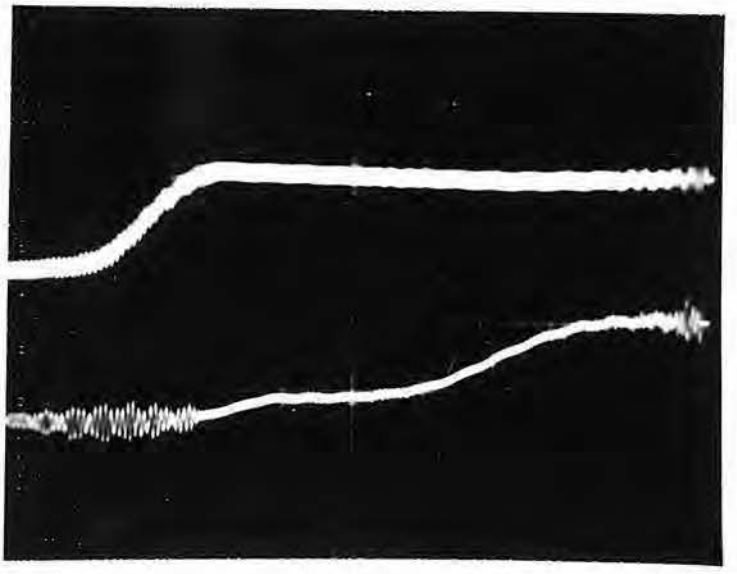

y_1 = 1.V/cm (bullet switch)
y_2 = .05 V/cm (water gap)
$x_1 = x_2$ = 2μs/cm.
Bank discharged at 40 KV.

Figure 33 - Photodiode Response

24 Analysis of the Cylindrical Shock Wave

The ratio of the probability per unit volume of finding an electron and an ion to that of finding a neutral atom (which is equal to the ratio of the product of the ion and electron density n_+ and n_- to the neutral density n_o) can be expressed by a simplified form of Saha's equation[55]

$$\frac{n_+ n_-}{n_o} = \left[\frac{2\pi m_- kT}{h^2}\right]^{3/2} \exp\left[\frac{-eV_i}{kT}\right] \qquad 24.1$$

If we express the temperature in electron volts and number densities in cm^{-3}, equation 24.1 can be expressed as

$$\frac{n_+ n_-}{n_o^2} = r_1^2 = \frac{3\times10^{21}}{n_o} T^{3/2} \exp \frac{-V_i}{T} \qquad 24.2$$

For high degree of ionization this may be written in the form

$$\frac{n}{n_o} = r_1 = \frac{3\times10^{21}\, T^{3/2}}{n_-} \exp \frac{-V_1}{T} \qquad 24.3$$

In the derivation of the above formula the following approximations were made:

1) The small interaction potential between the free ion and electron was neglected.

2) The internal degrees of freedom of all the particles were neglected.

3) The ion and atomic masses were assumed equal.

To estimate the amount of ionization produced in our discharge we note that the lowest ionization level of oxygen and nitrogen is about 15 ev. It follows from equation 24.3 that a temperature of 10^{5o}K is required for r_i to have a value ~ 100. A temperature

$\sim 10^{4}$°K will produce very little ionization ($r_i \sim 10^{-4}$). Since the ideal maximum temperature was greater than 10^{6}°K (section 22) we could expect substantial ionization of the air.

Table V states the results of S. Mandelstam[55] for the concentrations of ions of different degrees of ionization as a function of temperature for a discharge in nitrogen at atmospheric pressure. Mandelstam further showed that the time for the attainment of equilibrium between the temperatures of the gas and the electrons is 10^{-7}. This is less than a quarther cycle of our discharge.

T (°C)	N (%)	N^+ (%)	N^{++} (%)	N^{+++} (%)
20,000	1	98·7	0·3	
30,000	0·03	50	50	
40,000	—	4	93	3
50,000	—	0·4	61	38·6
60,000	—	0·02	10	90

Table V

Degree of Ionization of Nitrogen as a Function of Temperature

The Saha Equation assumes an equilibrium distribution. In order to estimate the thermal ionization for a non-equilibrium condition such as a transient electrical discharge, the Rankine Hegoniot Relations across the discontinuity must be satisfied. In general, these relations, which express the variables ρ,P,U and T as functions of their initial values are difficult to solve because the specific enthalpy ($H = \frac{1}{2} U^2$) behind a discontuity is not known exactly for a real gas.

For completeness we list the Rankine Hegonoit jump conditions across a shock front.[55]

$[\rho U] = 0$ Mass Conservation

$[\rho U^2 + P] = 0$ Momentum Conservation

$[\frac{1}{2} U^2 + \frac{\gamma P}{\rho(\gamma-1)}] = 0$ Energy Conservation

$$\frac{T_2}{T_1} = \frac{\gamma_1(\gamma_2-1)}{2\gamma_2} \quad \frac{(\gamma_2+1)^2}{\gamma_1 - 1} \frac{m_2}{m_1}$$

The temperature obtained from these equations can be used in the Saha Equation to determine the degree of ionization directly behind the shock front.

The above four equations contain five variables. It follows that only one direct measurement need be taken in order to uniquely determine all the other variables. For convenience, we chose to measure the shock speed which is usually given in terms of its Mach Number. (The Mach Number is the ratio of the speed of sound in the undisturbed material in front of the shock.)

In our experiment the Mach Number was determined by measuring the time necessary for the shock to traverse a known distance between two small crystal button microphones which were suspended on thin flexible wires at respective distances of 30.6 and 61.1 cm. The outputs from the microphones were fed into a Tektronix single beam oscilloscope with a chopped input which allowed both signals to be observed simultaneously. The sweep was triggered by the noise from the discharge of the gun switch. Careful analysis of many discharge traces suggests the following conclusions:

1) At a fixed distance from the discharge center the Mach Number varies only slightly with the discharge voltage. This follows directly from the theory of high energy shocks in air as given by Lin (see below).

2) Bennett[57] cites experimental and theoretical evidence for an inward facing second shock wave. Such a shock forms within the head wave in the early phases of the blast, is swept outward beyond the initial radius of the discharge and then propagates back to the center of the cylinder whereupon reflection occurs and it travels outward again. Care must be taken in interpreting the data to distinguish the primary shock from reflected shocks or mechanical vibration of the crystal probes.

3) The shock velocity varies roughly as $\frac{1}{r}$. This indicates that we may apply the cylindrical shock theory of Taylor[58] and Lin[59] to this dicharge. (Note 1) We assume that the elastic limit of the pressure transducer has not been exceeded and that there is a linear relationship between the voltage output and the incident pressure on the transducers.

The relationship between the Mach Number and the other variables of interest have been published for air at S. T. P. These results which are reproduced in figure 34 enable us to evaluate the average pressure and density in the region of the pressure transducers and to relate them to the temperature at that point.

Note 1 I wish to thank Mr. Marvin S. White of AFCRL for bringing these articles to my attention.

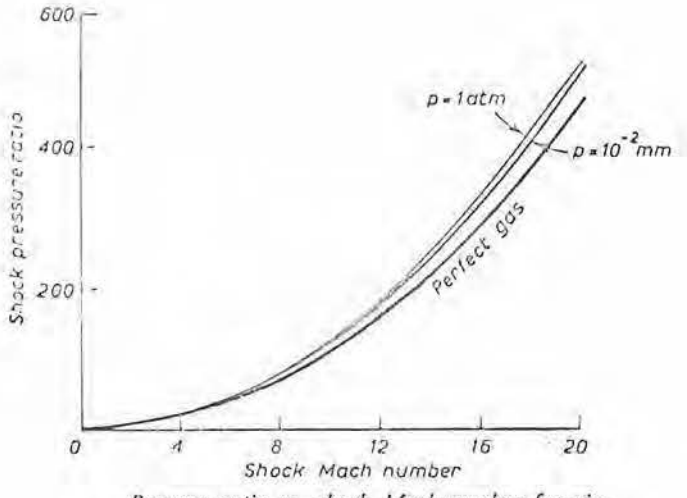

Pressure ratio vs. shock Mach number for air

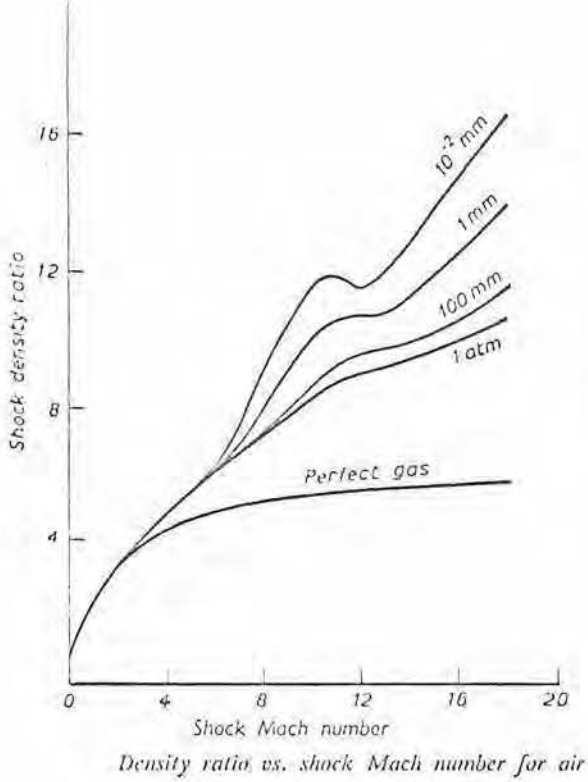

Density ratio vs. shock Mach number for air

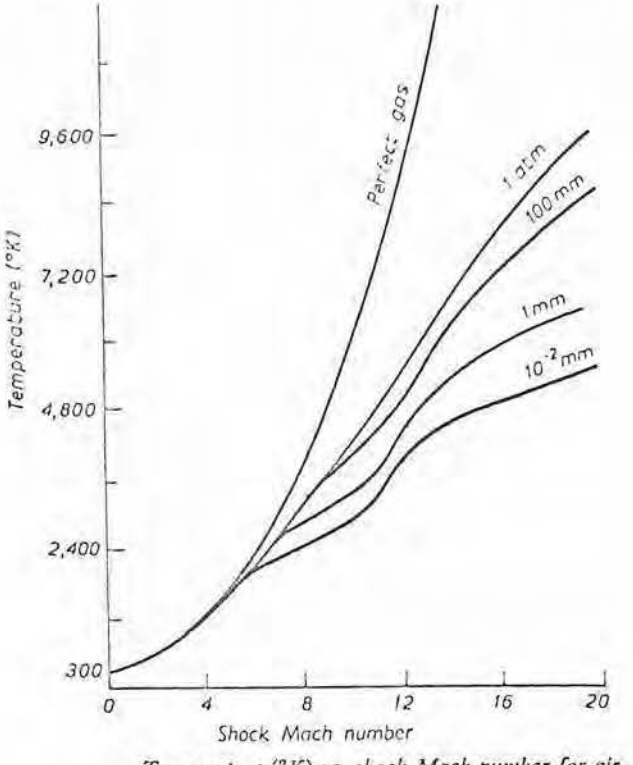

Temperature (°K) vs. shock Mach number for air

FIGURE 34 - Relation Between the Temperature, Density, and Pressure for Various Mach Numbers

Reprinted from Bradley, Shock Waves in Chemistry and Physics, John Wiley (1962).

The distance between the microphones was 30.5 cm. For a 65 K. V. bank voltage (720 kV discharge) the time required for the shock to traverse this distance was .80 μs ± 4 μs. This corresponds to a Mach Number of 1.12. (The velocity of sound in undisturbed air was taken as 34 meters/sec.)

To relate the temperature of the discharge to the velocity of the shock front at a distance R from the center of the discharge we make use of the equations derived by Lin (ref. cit.) for a strong cylindrical blast wave and Oshima[60] for a weak cylindrical blast wave. This work was an extension of the analysis by Talor (ref. cit.) of the spherical shock wave produced by the first atomic explosion in New Mexico. Taylor was able to derive a relationship for R(t) and with this result he was able to estimate (1) the energy E generated in the explosion and (2) the temperature of the explosion. The value of his estimate was critically dependent on the choice of γ, the ratio of the specific heats of air.

Taylor and Lin assumed the atmosphere to consist of perfect gases with constant heat capacities. The heat transfer (conduction, radiation, etc.,) was neglected and the flow behind the shock wave was assumed to be particle-isentropic. Because of the constant specific heat assumption these results could not be expected to be accurate where dissociation and other high temperature effects becomes appreciable. Taylor observed that the agreement between theory and experiment was surprisingly good and thought that this good agreement was probably due to the neutralizing effects of radiation and other accompaniments of high temperature, so the whole system behaved as though γ has

an effective value of 1.4 for air (diatomic gas).

Taylor's results are valid as long as the ratio of the shocked gas pressure to the undisturbed gas pressure, P/P_o, is greater than 10. When the shock strength decays to the extent that the value of P/P_o is < 10 then Taylor's equations become inapplicable and equations satisfying a weak shock condition must be used.

Based upon density measurements taken from a wide variety of cylindrical shock conditions Oshima developed a theory that is valid in the region of a weak shock. The "quasi-similarity theory" is based on the assumption that the distributions of the flow velocity, density and pressure are locally similar. (Taylor's theory of the strong shock assumed that the density ρ attained its limiting value of $\frac{\gamma+1}{\gamma-1}$ throughout the shock region. This corresponds to a Mach Number of infinity.) From experimental observations Oshima was able to describe a cylindrical blast by the following model.

The propagation of the blast wave is divided into three stages. The first is that of the strong blast wave where the Mach Number is $\gg 2$. The second stage is that of the moderately strong blast wave, where the rarefaction waves from the center occupy a considerable part of the blast wave but have little effect on the propagation and the decay of the blast wave. The Mach Number in this region ranges from about 2 to 1.15. This stage ends when the rarefaction wave overtakes the shock front. The flow pattern after this time is very complicated, due to the effects of succeeding rarefaction waves; this corresponds to regions where the Mach Number is less than 1.15.

Formula for the Cylindrical Shock

Figure 35 shows the relationship between the Mach Number, distance, and discharge energy and gives the decay of the blast wave in the weak shock region. The energy of the discharge according to the quasi-similarity theory is given by

$$R_o = \left[\frac{E}{2\pi\rho_o}\right]^{\frac{1}{2}} \qquad 24.5$$

where R_o is a characteristic length determined from E and ρ_o. A Mach of 1.12 at a distance R = 51.9 cm. from the discharge corresponds to an energy of 138 joules/cm. (R is the distance from the origin of the blast to the midpoint between the two velocity sensors.) This value of the energy is used to determine the thermodynamic properties of the strong shock region.

The value of the pressure at the surface of the discharge (R = .37 cm) is obtained from equation (4) of Lin

$$P(R) = \frac{1.167A^2P_o}{a^2R^2} \qquad 24.6$$

where A is defined for the cylindrical shock by $A^2 = E/B(\gamma)\rho_o = E/3.85\rho_o$ for $\gamma = 1.4$. a is the speed of sound in air.

For our case

$E = 1.38\times10^9$ ergs/cm.

$P_o = 1$ atm.

$\rho_o = 1.3\times10^{-3}$ gm/cm^3

$T_o = 300^oK$

$A^2 = 27.6\times10^{10}$

P(.37 cm) = 3092 atm.

This is to be compared with the maximum value of the magnetic pressure (see equation A-4.13) which is 3000 atm. The temperature at the surface of the discharge is given by

$$T(R) = \frac{T_o P(R)}{6P_o} = \frac{50P(R)}{P_o} \qquad 24.8$$

$$T(.37 \text{ cm}) = 1.55 \times 10^5 \ ^oK$$

The attainment of a high temperature in the discharge depends upon the degree of the confinement by the self-magnetic field. Under the assumption that equilibrium exists between the gas pressure and magnetic pressure Spitzer[61] gives the following expression for the temperature of the confined plasma

$$T = \frac{i^2}{2Nk} \qquad 24.9$$

where i is the current in absolute amperes, k is the Boltzman constant, and N is the number of particles (electrons plus positive ions) per unit length in the pinch.

In our case

$i = 3 \times 10^4$ abamp (measured current for 720 KV discharge)

$N = 2.4 \times 10^{19}$ particles/cm for double ionization

$k = 1.38 \times 10^{-16}$

This gives a value of

$$T_{max} = 2.73 \times 10^5 \ ^oK \qquad 24.10$$

If we assume that many of the atoms are triply ionized then

$$T_{max} \sim 10^{5o}K \qquad 24.11$$

This value is in good agreement with the results obtained from equation 24.8.

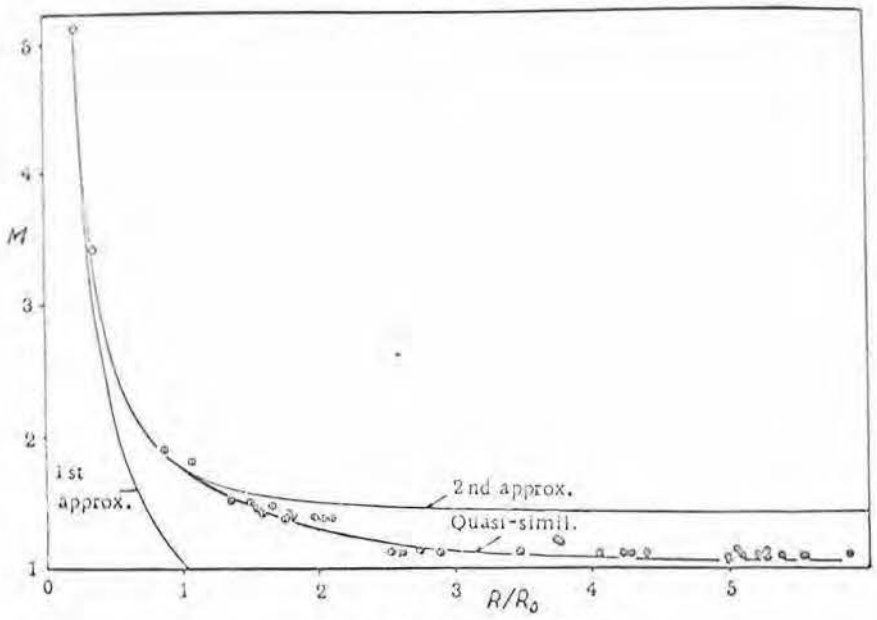

Decay of the blast wave.

Figure 35

A Few Remarks

It is remarkable that the above results are so close to the ideal values. Considering the simplicity of the experimental method this data cannot claim any high order of accuracy and only gives the order of magnitude. The energy of the shock is the thermal energy of the current which is dissipated in the conducting path produced by the breakdown. If one neglects end effects, then it appears that the discharge furnishes 20% of its energy to the wave.

An increase in capacity would cause an increase in the current, but at the same time there would be an increase in the diameter of the channel, so that the current density (which is directly related to the temperature) would not be appreciably affected. The value of the self inductance of the discharge will have the greatest influence on the current density. A reduction of the inductance will cause a rapid increase in the current density.

25. Conclusions and Recommendations

1) Gaseous Discharge Experiments

The parameters of the pulser described in this report make it possible to extend the range of voltage and currents over which most impulsive experiments on gaseous discharges have been carried out. The pulse system may be extrapolated to be used in the study of pinch studies at lower pressures and higher fields where extremely high plasma-particle energies (kinetic temperatures) may be attained, perhaps relativistic; and to pressures near atmospheric where it may become possible to simulate certain forms of lightning in which magnetofluid dynamical effects have been suggested to occur.[62]

As lower and lower pressures are used in pinch studies, the characteristic time for the development of the pinch and for its disruption by instabilities becomes shorter. As a result the energy transferred to the pinch by a given source becomes smaller. Therefore, the discharge current will often be transferred to the wall of the chamber, because the impedance of the pinch has ceased to fall. In order to couple energy into the column in a shorter time, other things being equal, a capacitor bank of higher ringing frequency is required. This makes an appropriate application for the water capacitor.

At still lower pressures and a fixed distance between electrodes of the pinch chamber, the longitudinal kinetic energy given to the electrons is not largely transferred to transverse kinetic energy and a fairly mono-energetic beam of electrons reaches the anode. If this is extracted through a hole in the anode, the dynamics of

the beam in a field-free region beyond the anode can be studied. If the electrons are relativistic and the beam current is large compared to the natural unit of current,

$$I \gg mc^3/e \sim 17{,}000 \text{ A},$$

magnetofluid dynamical forces dominate the beam behavior even in the absence of collisions.[15] The possibility then exists of creating a relativistic magneto-plasma by ionizing a gas and accelerating so many of its electrons to near the spead of light that the magnetic stress produced by these electrons is compared to the mechanical gas stress. The dynamical behavior of this magneto-plasma would make an interesting study.

The creation of a well defined and reproducable pre-ionized channel should be implemented. The line density of particles in this channel should be low in order to bring the temperature as high as possible with the available energy input. One method of creating such a channel is to use a vortex stabilized d.c. arc as described in the paper by Pfender and Bez.[63]

Consideration should be given to the possibility of stabilization of the discharge pinch column with an external B_z field. This external field would have to be on the same order as the self magnetic field.

It would be worthwhile to investigate what proportion of the total potential drop across the air gap is associated with the electrodes and with the gas in the column; ultimately the efficiency will depend upon minimizing losses at the electrodes.

2) Energy Losses

Energy losses in the system must be considered in evaluating its performance. This problem has been analyzed in various sections of this report. For completeness we summarize our results here.

Sources of Energy Losses

1) Ruptured Dielectric Switch
2) Underwater Corona
3) Surface Current Flow
4) Ionization of Water Gap
5) Molecular Disassociation and Recombination
6) Imperfect Impedance Match to Air Column
7) Imperfect Energy Coupling in Transformer
8) Energy Stored in the Magnetic Field
9) Energy Dissipated by Shock Wave

It is recommended that in future experiments an attempt be made to match the impedance of the discharge and the water capacitor more closely so as to allow a greater fraction of the energy to be transferred to the discharge before the circuit current reverses. The discharge impedance results primarily from the inductance of the arc and thus may be varied by changing the spacing between the discharge electrodes.

3) Neutron Production.

After the collapse of the pinch the various instabilities that can develop in the arc column may produce localized electric field gradients in excess of ten times the applied electric field. An interesting phenomena will be observed if the discharge is performed in hydrogen instead of air. Deuterium has a photoneutron threshold (γ,n) of $(2.226 \pm .003)$ Mev. and produces 1 neutron per 1000 gamma-rays.[64] A suitable neutron detector (electronic or neutron activation foil) will yield information about the maximum energy of the photons produced by the discharge.

4) Modification of the Pulse System

The problems presented by the return current along the surface of the water can be aleviated by extending the ground plane over the surface of the water with a hole cut out to allow a discharge to an overhead electrode.

The principle of the Mark II transformer may be extended to a 10 mev. pulse transformer. Insulation requirements dictate that the new transformer be of the same geometry as Mark II. (It would be impractical to design a pulse transformer with a primary attached to the output of Mark II). To keep the inductance within tolerable levels the width of the windings will have to be increased to 24" from the present 18".

5) A Comment on the Dynamical Model

If the constriction doesn't take place within a time interval which is short compared to a quarter of a cycle of the current oscillation, the approximation $I = I_o' t$ used in section A-4 is not valid. The theoretical results derived for a number of further approximations can only be looked upon as qualitative indications. In our derivation the onset time and the energy input necessary to heat the neutral gas has been neglected and therefore in most cases the results are not applicable to the experiment. The constriction should proceed slower than predicted.

6) Instrumentation

The simplicity and relatively low cost of optical methods suggest that they should be used here to determine the duration and the instant of maximum intensity of the discharge. With various interference filters a somewhat detailed spectroscopic analysis could be made of the discharge (i.e., absorption and transmission of various wavelengths can be used to determine the electron density.)

Consideration should be given to the application of Laser Holography Techniques in analyzing the arc channel. The availability of a Framing Camera and low level radiation detectors would be most helpful in gaining insight into the fine structure of a terrawatt discharge. Relative intensities of spectra lines will yield a more accurate picture of the temperature, density and opacity than has been realized in this report.

A controllable air spark gap should be used in place of the present bank switch. This would allow all measurements to be made with reference to the time at which the switch was triggered. Such a switch with a jitter less than 5 nsec. is described in the May 1965 issue of Inst. & Exp. Tech. (translated from Russian).

Appendix A-1

Parameters of Capacitor Bank

(a) Inductance of Bus-Bar System with Leads at Center

We approximate the bus-bar system as a rectangular ground plane with an opposing rectangular H.V. plane 3 meters long by .6 meters high with a .3 m. separation. See Figure 36 below.

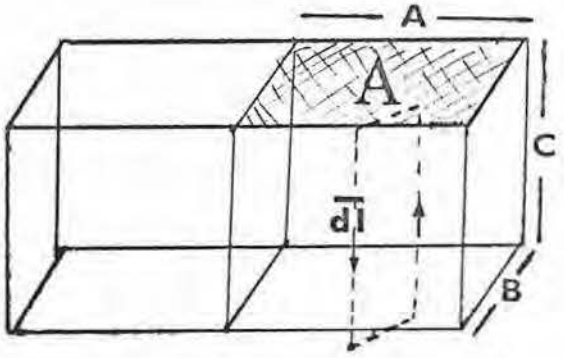

Figure 36

Pertaining to the Calculation of the Inductance of the Capacitor Bank

The flux ϕ between the plates is given by

$$\phi = Li = BA \qquad \text{A-1.1}$$

We then solve for the field $\bar{B}$

$$\int \bar{B} \cdot \bar{dl} = \mu_o i$$

$$B = \frac{\mu_o i}{l} = \frac{\mu_o i}{C} \qquad \text{A-1.2}$$

Combining A-1.1 and A-1.2 we obtain for the inductance of each half taken separately:

$$L = \mu_o A/C = \frac{4\pi \times 10^{-7} \times .3 \times 1.5}{.6} = .94\ \mu H \qquad \text{A-1.3}$$

The true value of the inductance, L', is just the parallel sum of two inductances

$$L' = \tfrac{1}{2}L = .47\ \mu H \qquad \text{A-1.4}$$

The capacitor bank with its associated leads has a short circuit ringing frequency of 50 KC ± 3% (see figure 5). This agreed with results obtained by observing Lisijous Figure patterns produced with a variable frequency signal generator. Using the formula $f = 2\pi\sqrt{LC}$ where C = 20 μf and f = 50 KC the value of L is found to be:

$$L_{Bank} = .51\ \mu H \qquad \text{A-1.5}$$

This is in good agreement with our previous estimation.

(b) Pressure Exerted on Bus-Bar System

The self-magnetic field of the bus-bars is given by

$$B = \mu_o i/l \qquad \text{A-1.6}$$

The current and the magnetic field it produces are mutually perpendicular to each other, hence the resultant force of their interaction is given by

$$F = iB\ kg \qquad \text{A-1.7}$$

but

$$B = \mu_o i/l$$

hence

$$F = \frac{\mu_o i^2}{l} \sim 50 \text{ atm. pressure} \qquad \text{A-1.8}$$

The magnetic stress presented is easily sustained by the aluminum.

A-2. The Depolarization Time of Water (Derivation)

Consider two arbitrary equipotential surfaces ϕ_1 and ϕ_2 with a dielectric of resistivity ρ and dielectric constant K as in Figure 37.

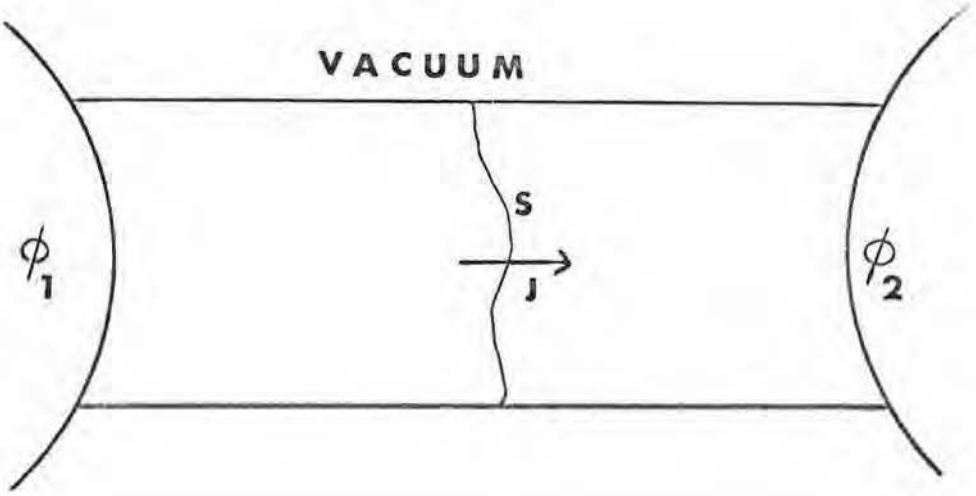

Figure 37

Pertaining to the Derivation of the Depolarization Time of Water

The dielectric is bounded by ϕ_1 and ϕ_2 and vacuum. The electric field vector $\overline{E}$ has only a tangential component along the vacuum —dielectric interface.

Inside the dielectric there are no sources or sinks, hence Maxwell's equation takes the form

$$\nabla \cdot \overline{j} = 0 \qquad \text{A-2.1}$$

but $$\overline{j} = \sigma \overline{E}$$

$$\therefore \quad \nabla \cdot \overline{E} = 0 \qquad \text{A-2.2}$$

This implies $E = -\nabla \phi$ from which

$$\nabla^2 \phi = 0 \qquad \text{A-2.3}$$

The current acts as any intersecting surface s is given by

$$I = \int \bar{j} \cdot \hat{n} \, ds \qquad \text{A-2.4}$$

But by definition

$$\phi_2 - \phi_1 = \bar{E} \cdot \bar{ds} \qquad \text{A-2.5}$$

Hence $$\frac{\phi_2-\phi_1}{R} = I = \int \bar{j} \cdot \hat{n} \, ds = \sigma \int \bar{E} \cdot \hat{n} \, ds \qquad \text{A-2.6}$$

also $\sigma = 1/\rho$

$$\therefore \frac{\phi_2-\phi_1}{R} = I = \frac{1}{\rho} \int E \cdot n \, ds \qquad \text{A-2.7}$$

From Gausses Theorem

$$\sigma = \frac{\bar{D}\cdot\hat{n}}{4\pi} \qquad \text{A-2.8}$$

hence

$$Q = \frac{1}{4\pi} \int \bar{D}\cdot\hat{n} \, ds = \frac{\epsilon}{4\pi} \int \bar{E}\cdot\hat{n} \, ds \qquad \text{A-2.9}$$

From the definition of capacitance we have

$$\frac{Q}{\phi_2-\phi_1} = C \qquad \text{A-2.10}$$

combining equations 2.7, 2.8 and 2.9 we have

$$\frac{\phi\epsilon}{4\pi} = RC \qquad \text{A-2.11}$$

Putting in $\epsilon/4\pi = K\epsilon_o$, the desired result follows

$$RC = \tau = \rho \, K\epsilon_o \qquad \text{A-2.12}$$

RC is the time constant of the system. Where the dielectric is water the constant RC is referred to as the depolarization time of the water. The depolarization time is the maximum time that the system can hold its charge before the dipole moment breaks down and the dielectric (water) becomes a conductor. Note the important result that the value of RC depends on ρ and K and is totally independent of the configuration of the system.

A-3. Proof: $1-k^2 = V_{L_1}$ (L_2 closed)$/V_{L_1}$ (L_2 open)

We write the differential equation for the case L_2 closed in Figure 38.

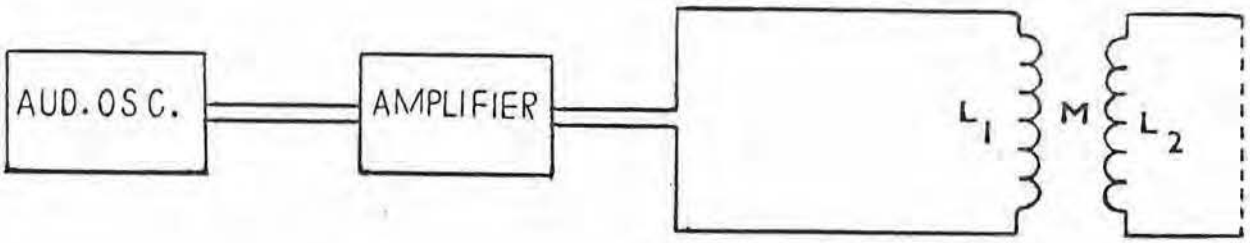

Figure 38

Pertaining to the Derivation of an Expression for the Coupling Constant of the Pulse Transformer

$$L_1 \frac{di_1}{dt} + \frac{Mdi_2}{dt} = \epsilon_1 \qquad L_2 \text{ closed} \qquad \text{A-3.1}$$

$$L_1 \frac{di'_1}{dt} = \epsilon_1' \qquad L_2 \text{ open} \qquad \text{A-3.2}$$

$$L_2 \frac{di_2}{dt} + M \frac{di_1}{dt} = 0 \qquad L_2 \text{ closed} \qquad \text{A-3.3}$$

Putting A-3.3 in A-3.1 we have

$$L_1 \frac{di_1}{dt} - \frac{M^2}{L_2} \frac{di_1}{dt} = \epsilon_1 \qquad \text{A-3.4}$$

but for $i_1 = i_1'$ we have from 3.2

$$L \frac{di_1}{dt} = \epsilon_1' \qquad \text{A-3.5}$$

By definition k is given by

$$k = \frac{M}{\sqrt{L_1 L_2}} \qquad \text{A-3.6}$$

Hence

$$L_1 (1-k^2) \frac{di_1}{dt} = \epsilon_1 \qquad \text{A-3.7}$$

$$(1-k^2)\ \epsilon_1' = \epsilon_1 \qquad \text{A-3.8}$$

It follows that

$$1-k^2 = \frac{\epsilon_1}{\epsilon'_1} \qquad \text{A-3.9}$$

This result is correct only when the current in L_1 is held constant.

A-4. Calculation of Discharge Parameters

To estimate the maximum discharge current we must know the discharge inductance, the maximum voltage appearing at the gap, the discharge radius, and the rate of the current rise with time, $\frac{dI}{dt}$.

The current flow during the discharge is radially towards the discharge electrode. This flow is similar to that produced by the discharge of two semi-circular charged plates with a radius equal to the effective radius of our capacitor plates. The water capacitor can be imagined as the parallel combination of two of these circular capacitors. It is clear that the inductance of such a capacitor is twice the inductance of a parallel plate circular capacitor.

The magnetic field B produced by the discharge current I in the semi-circular plate capacitor shown in figure 39 below is easily derived from Ampere's Law,

$$\pi \int \bar{B} \cdot \bar{dr} = \mu_o \left(I - \frac{\pi r^2}{2} j \right) \qquad \text{A-4.1}$$

where j is the displacement current density, and r is the effective radius defined above. We neglect edge effects.

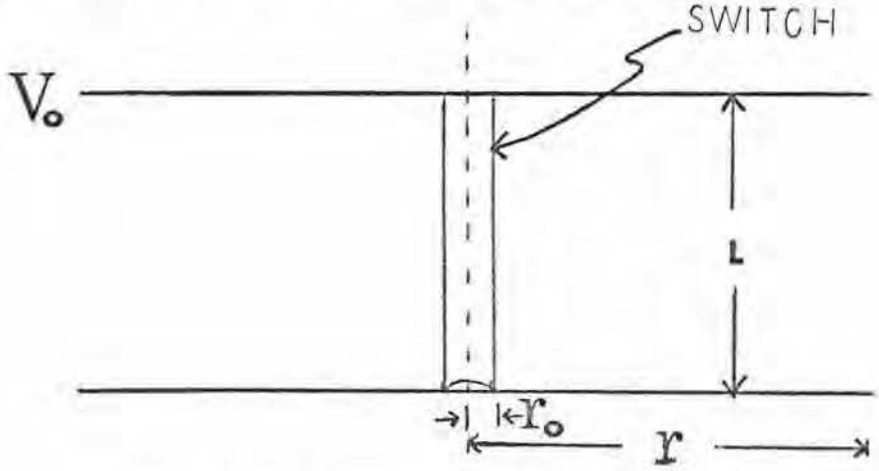

Figure 39 - Radial Condenser Approximation

Solving equation A-4.1 for B, we obtain

$$B(r) = \mu_o[\frac{I}{\pi r} - \tfrac{1}{2} rj] \qquad \text{A-4.2}$$

At the edge of the plate $B(r) = 0$,

$$0 = \frac{I}{r_o} - \tfrac{1}{2} rj \qquad \text{A-4.3}$$

from which we solve for j

$$j = \frac{2I}{r^2} \qquad \text{A-4.4}$$

The flux will be given by

$$\phi = \int B \cdot dA = \mu_o \int (\frac{I}{\pi r} - \tfrac{1}{2} rj) l\, dr$$

$$= \mu_o l(\frac{I}{\pi} \ln \frac{r_o}{r} - \tfrac{1}{2} jr^2) = \mu_o l(\frac{I}{\pi} \ln \frac{r_o}{r} - \frac{I}{\pi}) \qquad \text{A-4.5}$$

$$= \mu_o \frac{lI}{\pi}(\ln \frac{r_o}{r} - 1)$$

We put in the following values

$$\mu_o = 4\pi \times 10^{-7}$$

$$l = .03 \text{ meters} \qquad \text{A-4.6}$$

$$r = .38 \text{ meters}$$

$$r_o = .0037 \text{ meters (determined from photographs)}$$

$$\ln \frac{r_o}{r} \sim \ln 100 \sim 4.6$$

$$L' = \frac{\phi}{I} = \frac{\mu_o \ell}{\pi} (\ln \frac{r_o}{r} - 1) \sim 60 \text{ nH} \qquad \text{A-4.7}$$

Since we have two inductances in parallel, the true inductance is one half this value

$$L_c = 30 \text{ nH} \qquad \text{A-4.8a}$$

The Gap Inductance as computed from the formula in Terman is

$$L_G = 45 \text{ nH} \qquad \text{A-4.8b}$$

The value of the capacitance between the plates of Yukon II is given by

$$C = 2K \frac{\epsilon_o A}{d} \sim .04 \ \mu f \qquad \text{A-4.9}$$

where $\epsilon_o = 8.85 \times 10^{-2} \ \frac{\text{coul.}^2}{\text{n-m}^2}$

$A = .94 \text{ m}^2$ (96" x 15")

$d = .037$ m ($1\frac{1}{2}$" spacing between plates)

The characteristic impedance of Yukon II is that of a transmission line and is given by

$$Z_c = \sqrt{\frac{L_c}{C}} = \left(\frac{3.0 \times 10^{-8}}{.04 \times 10^{-6}}\right)^{\frac{1}{2}} = .87 \text{ ohm} \qquad \text{A-4.10a}$$

The Gap Impedance is given by

$$Z_G = \omega L_G = 1.1 \text{ ohm} \qquad \text{A-4.10b}$$

The maximum current of the discharge will be

$$I_{max} = \frac{V_{max}}{Z_c + Z_G} = \frac{7.2 \times 10^5}{2} = 3.6 \times 10^5 \text{ amps.} \qquad \text{A-4.11}$$

The time necessary to reach maximum current is given by equation A-5.1

$$T = \frac{r_o}{2} \sqrt{LC} \sim 66 \text{ ns} \qquad \text{A-4.12}$$

where $r_o = 2.40$ m is the length of the capacitor plate;

$L = L_c + L_G = 75$ nH; $C = .04 \ \mu f$.

At a time t^*, the instant of the onset of the pinch, the inward magnetic pressure will be in equilibrium with the kinetic pressure of the gas. The current shell as a whole can only start to move inward at the moment the magnetic pressure $P_B(r)$ exceeds the gas pressure. The equilibrium conditions at t* can be expressed by the following equation.

$$P_B(r) = \frac{\mu_o I^2}{8\pi^2 r^2} = P_{atmosphere} = 1.01 \times 10^5 \ n/m^2 \qquad A\text{-}4.13$$

We recall from section 20 that the discharge current I may be approximated by $I'_o t$ where $I'_o = dI/dt$.

From the results obtained from equation A-4.11 and A-4.12 we have

$$I'_o = 5.5 \times 10^{12} \text{amps/sec.} \qquad A\text{-}4.14$$

Putting this in equation A-4.13 and solving for t* we obtain

$$t^* \simeq 2 \times 10^{-9} \text{ sec.} \qquad A\text{-}4.15$$

This is the length of time the discharge must exist in order to obtain the pinch condition. During compression the variation of pressure follows an adiabatic law. After the onset of constriction the magnetic pressure increases much faster than the gas pressure. The effect of the gas pressure can therefore be neglected in the description of the constriction mechanism.

A-5. The Application of Transmission Line Theory to Yukon II

We wish to consider the behavior of Yukon II when the discharge is treated as that of a transmission line.

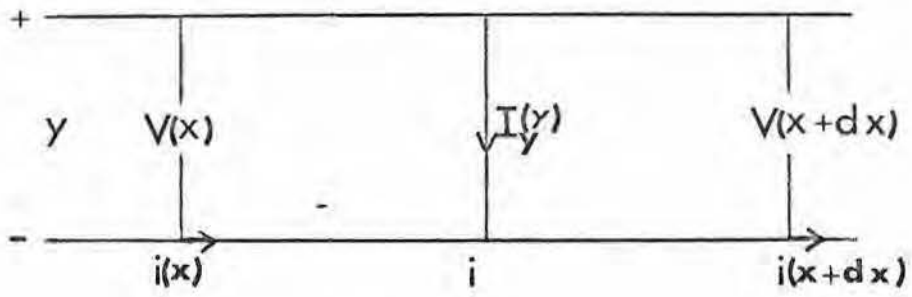

Figure 40

Pertaining to Transmission Line Theory of Yukon II

Referring to figure 40 above the equation for the conservation of charge in the x direction is

$$i(x) = I_y(x) + i(x + dx) \quad \text{(the X direction)} \qquad \text{A-5.1}$$

In the y direction the equation becomes

$$YV(x) = I_y(x)dx \qquad \text{where } Y = \frac{1}{Z} \text{ per unit length} \qquad \text{A-5.2}$$

By Taylors Expansion we may write

$$i(x + dx) = i(x) + \frac{\partial i}{\partial x} dx \qquad \text{A-5.3}$$

An expression for i(x) may be obtained by combining 5.1, 5.2, and 5.3

$$i(x) = YV(x)dx = i(x) + \frac{\partial i}{\partial x} dx \qquad \text{A-5.4}$$

which reduces to

$$\frac{\partial i}{\partial x} = -Y\ V(x) \qquad \text{A-5.5}$$

In the X direction we have

$$V(x + dx) - V(x) = i(\ddot{x})Zdx \qquad \text{A-5.6}$$

Using Taylors Expansion this simplifies to

$$\frac{\partial V}{\partial x} = -i(x)\ Z \qquad \text{A-5.7}$$

Upon differentiating A-5.5 and substituting A-5.7 into the result we obtain

$$\frac{\partial^2 i}{\partial x^2} = -Y\ \frac{\partial V}{\partial x} = YZi(x) \qquad \text{A-5.8}$$

or

$$\frac{\partial^2 i}{\partial x^2} - YZi(x) = 0 \qquad \text{A-5.9}$$

The capacitative impedance per unit length is given by

$$Z_c = \frac{1}{Y} = \rho + \frac{1}{i\omega C} \qquad \text{A-5.10}$$

where C is the capacitance in the Y direction per unit length and ρ is the resistivity. Solving for Y we have

$$Y = \frac{1}{\rho + \frac{1}{i\omega C}} \qquad \text{A-5.11}$$

Similarly, the inductive impedance per unit length, L, is given by

$$Z_L = \rho + i\omega L \qquad \text{A-5.12}$$

If we can neglect ρ as compared with $\frac{1}{\omega C}$ and ωL then A-5.11 and A-5.12 reduce to

$$Y = i\omega C \qquad \text{A-5.13}$$

and

$$Z_L = i\omega L \qquad \text{A-5.14}$$

Similarly

$$YZ_L = -\omega^2 LC \qquad \text{A-5.15}$$

We assume a solution of A-5.9 to be of the form

$$i = i(x)\ \epsilon^{-i\omega t} = i_o e^{-\gamma x + i\omega t} \qquad \text{A-5.16}$$

which upon substitution into A-5.9 gives

$$\gamma = \sqrt{YZ} = i\omega\sqrt{LC} \qquad \text{A-5.17}$$

therefore the current can be expressed by

$$i = i_o e\, \exp\left(-i\omega\left(\sqrt{LC}\, x - t\right)\right) \qquad \text{A-5.18}$$

The current will reach its maximum when the value of the exponent is zero. From this we obtain the velocity of the current along the transmission line.

$$v = \frac{x}{t} = \frac{1}{\sqrt{LC}} \qquad \text{A-5.19}$$

A-6. Comparison of Energy Storage Methods[65]

The four most useful devices for storing large quantities of electrical energy appear to be: capacitors, inductances, rotating machinery and storage batteries. For certain applications the choice between competing methods can be made primarily on the basis of cost, but in most situations factors other than the cost per watt-second are at least of equal importance.

Probably the most important differentiating characteristic between these systems is the length of the discharge time. When the discharge interval must be short compared to a millisecond, capacitors have the advantage. For cases in which the discharge interval is of the order of milliseconds, the inductance coil is particularly attractive. For slower rates of discharge, corresponding to an interval of perhaps a second, rotating machinery is advantageous, while for still longer discharge periods (and long storage periods), storage batteries have an unusual advantage. In brief, as a rough rule of thumb, the four systems might be characterized by their possible minimum discharge periods: capacitor, microseconds; inductance, milliseconds; machinery, seconds; battery, minutes.

While capacitors have a unique advantage in their short discharge time, they suffer from a serious economic limitation in comparison to inductance coils, machinery, and batteries in that they cannot be temporarily overloaded no matter how low the duty cycle may be. The cost of a capacitor bank varies linearly with

the amount of energy to be stored. At the present time, energy storage capacitors cost about six cents per watt-second. The cost of the complete installation is much greater than these figures would indicate because of space requirements, shelf-type mounting arrangements, and wiring which requires an extensive protective system of relays and interlocks.

In comparing capacitive vs. inductive storage, the differences in circuit behavior of the two systems may be a deciding factor. For instance, when a capacitor bank is discharged through a high-pressure electric arc, the arc cannot extinguish until all the stored energy has been expended. In general, the capacitor tends to act as a voltage generator and the current is determined by the load characteristics, while the inductance tends to act as a current generator and the voltage is determined by the load characteristics.

Bibliography

Theory of High Current Discharges

Aicher, L.C., Variations in the Dielectric Strength of Air, Third Quarter 1949, Allis-Chalmers Electrical Review, pp. 12-17.

Aicher, L.C., Corona, Fourth Quarther 1950, Allis-Chalmers Electrical Review.

Block, Neville, Dynamics of a Pinch Discharge by a High Current Pulse Forming Network, Report #778, Department of Aerospace & Mechanical Sciences, Princeton University.

Cobine, Gaseous Conductors Theory & Engineering Application, Dover, 1958.

Loeb, L.B., Electric Breakdown of Gases with Steady or Direct Current Impulse Potentials, Handbuch Der Physik, Vol. XXII, 1956, pp. 445-530.

Meek & Graggs, Electrical Breakdown of Gases, Oxford, 1953.

Atmospheric Phenomena Involving High Current Discharges

Lawson, J.D., Journal of Electronics & Control 3, 587, 1957; 5, 146, 1958.

Malan, J.D., Physics of Lightning, English Universities Press.

McEachron, K.F. & Patrick, K.G., "Playing with Lightning", Random House, 1940.

Norinder & Karstan, "Experimental Lightning Discharges", Journal of F.I., 253, 3, March 1952, p. 225.

Schonland, Dr. B.F., "Flight of the Thunderbolts", Oxford 1950.

Viemeister, Peter E., The Lightning Book, Doubleday, 1961.

Radiation and Its Detection

Bellamy, E.J., Infra-Red Spectra of Complex Molecules, Wiley.

Berger, H., Neutron Radiography, Elsevier, 1965, chapter III, Photographic Neutron Image Detectors.

Birkhoff, "Passage of Fast Electrons through Matter", Handbook of Physics - Volume XXXIV, p. 53.

Birks, Theory & Practice of Scintillation Counting, Pergamon Press, 19.

Bovey, F.A., The Effects of Ionizing Radiation on Natural and Synthetic High Polymers, Interscience, 1958, chapters 1 and 2.

Cameron, J.R., et. al., Radiation Dosimeter Utilizing the Thermoluminescence of Lithium Fluoride, Science, August, 1961.

Charlesday & Woods, International Journal of Applied Radiation & Isotopes, Pergamon, 14, pp. 413-419, 1963.

Cumming, Annual Review of Nuclear Science, 1963.

Henby & Ruchman, Annals of Analytical Chemistry, 28, 1956.

Miller, Herman L., Summary of Neutron Measurement Methods, Bulletin No. 35, United States Atomic Energy Commission.

High Voltage Measurement

Craggs, High Voltage Laboratory Techniques, Buttersworths Scientific Publs., 1954.

Edwards, F.S., and Smee, J.F., The Calibration of the Sphere Spark-Gap for Voltage Measurement up to One Million Volts, Journal Institution of Electrical Engineers 82,655-657, 1938.

Griscom, S.B., Voltage Divider for Measuring Impulse Voltages on Transmission Lines, AIEE Trans. 73, pt. III-A, 228-237, 1954.

Griscom, S.B., The Kine-Klydonograph -- A Transient Waveform Recorder, AIEE Trans. 79, pt. III, 603-610, 1960.

Harris, F.K., Electrical Measurements, John Wiley, 1952, 673-687.

Energy Storage

Brotherton, M., Capacitors, D. Van Nostrand, 1946.

Dietz, A., A High Voltage Radio Frequency Variable Capacitor Using a Liquid Dielectric, Report No. MATT-341, Plasma Physics Laboratory, Princeton University.

Powell, S.T., "Water Conditioning for Industry", McGraw-Hill.

Struble, R.W., Materials for Handling De-Ionized Water, Technical Memorandum No. 51, Princeton University, (Project Matterhorn).

Van Vleck, J.H., Electric & Magnetic Susceptibilities, Claredenon Press, Oxford, 1932, pp. 87.

Warner, D.F., The Application of Large Capacitors for Use in Energy Storage Banks, IRE Transactions on Component Parts, August 1956.

Transformer Design

Blume, L.F., Transformer Engineering, John Wiley & Sons, 1938, chapters IV, V, VI.

Insulation Strength of Transformers, AIEE Transformer Subcommittee, AIEE Trans. 56, 749-754, 1937.

Lewis & Wells, Millimicrosecond Pulse Techniques, Pergamon Press, 1959, chapter 3, Transformers, 3.4, Tapered Lines.

M.I.T. Staff, Magnetic Circuits and Transformers, Wiley, 1943, chapter 28.

Terman, F.E., Radio Engineering Handbook, McGraw-Hill, 1943, pp. 109-112, 119-128.

References

1 Bennett, W. H., Phys. Rev. 45 (1934) 90

2 Tonks, L., Trans. Electrochem. Soc. 72 (1937) 167

3 Cousins, S. W., Ware, A. A., Proc. Phys. Soc. B 64 (1951) 159

4 Kurchatov, I. V., Atomnaya Energya 1 (1956) 65

5 Burchkhardt, L. C., et. al., J. Appl. Phys. 28 (1957) 519

6 Linhart, J. G., Plasma Physics (North-Holland Publ. Cy., Amsterdam) 1960; Nuclear Fusion 1 (1961) 78

7 Leontovich, M.A., Osevets, S. M., Atomnaya Energya 1 (1956) 81

8 Alfven, H. and Smars, E., Nature 188, 801 (1960)

9 Smars, E., Arkiv For Fysik 29, No. 9 (1965)

10 Falthammar, C. G., Phys. Fluids 4, 1145 (1961)

11 Murty, G. S., Arkiv Fysik 19 (1961) 511

12 Smars, E. and Johansson, R. B., Phys. Fluids 4 (1961) 1151

13 Fried, B. D., ARL Report 7-60, Ramo-Woolridge Corp. (1957)

14 Budker, G. J., and Naumov, A. A. CERN Symposium 1 (1956) 65

15 Finkelstein, D. and Sturrock, P., Plasma Physics, J. Drummond Ed., McGraw Hill, 1961

16 Harrison, E. R. Journal of Nuclear Energy C4 (1962) 7

17 Finkelstein, D., Physics Today 15, No. 12, Dec. 1962

18 Meek & Craggs, Electrical Breakdown of Gases , Oxford (1953) ch. 4

19 Malan, D. J., Physics of Lightning, The English Universities Press, ch. 8

20 Bishop, A. S., Physics Today 17, 3, March, 1964

21 Bennett, W. H., Proceedings of the Second U.N. Conference on the Peaceful Uses of Atomic Energy 31 (1958)

22 Christofilos, N. C., Proceedings of the Second U. N. Conference on the Peaceful Uses of Atomic Energy 32, 279 (1958)

23 Rogers, K., Finkelstein D., et. al., Second U.N. Conference on the Peaceful Uses of Atomic Energy, P/2432, Geneva (1958)

24 Onkawa, T., CERN Report 60-35 (1960)

25 We are indebted to Drs. J. O'Rourke and V. Scherrer for Discussions of their work from which grew many of the ideas attempted here.

26 For a complete discussion of coupled circuits see for example: Page and Adams, "Electricity and Magnetism", D. Van Nostrand Co., ch. 15, "Coupled Circuits."

27 This section is based on an article by D. Finkelstein, P. Goldberg, and J. Shuchatowitz, Rev. of Scientific Instruments, Feb. 1966.

28 See for example, Inductance Calculations, Grover, Van Nostrand

29 Craggs, High Voltage Laboratory Techniques, Buttersworths, Scientific Publications, 1954.

30 Von Hipple, Dielectric Materials and Applications, John Wiley, 1954.

31 Technical Report IE-13-55, Roam & Hass Co., July 1960.

32 Fagen, W., Argon National Report, ANL-5079

33 Personal communication with Madhav Ghate; this method was used to clean the reactor at the Atomic Energy Laboratories, Bombay, India

34 Loeb, L. B., Fundamental Processes of Electrical Discharge in Gases pg. 451-461

35 Loeb, L.B., ref. cit., pg. 441-448.

36 Cobine, Gaseous Conductors Theory & Engineering Application, Dover, 1958

37 White, H. J., Phys. Rev. 40, 507, 1936 CRFA Talk

38 Rudenberg, R., Wiss. Veroff. ad. Siemens-Konzern 9 (Part I) 1, 1930

39 Faether, H., Electron Avalanches and Breakdown in Gases, Washington Buttersworths, 1964.

40 Meek & Craggs, ref. cit.

41 Aleksandrov, B. N., Soviet Physics-Technical Physics, 19, 5 Nov. 1965

42 Davies, W.E., Nature 205, 4976, March, 1965, pg. 1092

43 Brown, S., Basic Data of Plasma Physics, Wiley, 1959

44 Linhart, J.C., Nuclear Fusion 1 (1961) 78

45 Rosenbluth, LASL Report, LA-1850, 1954

46 Handbook #76, National Bureau of Standards, Medical X-Ray Protection Up to Three Million Volts

47 NBS Monograph 1, Energy Dissipation by Fast Electrons, Spencer, L. V.

48 Condon & Adishew, Handbook of Physics, Section 7, pg. 124, McGraw Hill, New York, 1958

49 Evans, The Atomic Nucleus, McGraw Hill, 1955, ch. 20

50 Thomas C., Physics of Radiology, pg. 49, 2nd ed., H.E. Johns Inc., 1961

51 Kival and Mayers, J. Quant. Spect. Radiative Transfer, G. B. Vol. 5, 13-38, Jan.-Feb. 1965

52 Bill, British Journal of Radiology, 9, 587, 1936

53 Kaider, H., Ann. Physik, 34, 297 (1939)

54 Ion Drag Pumping, Pickard, W. F., JAP, 34, 2, Feb. 1963

55 Thompson, W. B., An Introduction to Plasma Physics, Addison Wesley

56 Mandelstan, 5, Spectrochimica Acta, 1959, pgs. 255-271

57 F. D. Bennett, Physics of Fluids, 1, 4, July, 1958

58 G. I. Taylor, Proc. Roy. Soc. (London) A201, 159 (1950);

59 S. C. Lin, Journal of Applied Physics, 25, 1 January 1954

60 Koichi Oshima, in "Exploding Wires", Vol. 2, Chace and Moore (eds.) Plenum Press, New York, 1962, pg. 159

61 Spitzer, L., Physics of Fully Ionized Gases, Interscience, 1956, pg. 43

62 Carpenter, D. G., Ball Lightning, Iowa State University, Ames, Iowa, 1962 (unpublished thesis)

63 Pfender, E. and Bez, W. Proc. V Int. Conf. on Ioniz. Phen. in Gases , Munich, 1961, Vol. II, pg. 897, North -Holland Publ. Comp., Amsterdam, 1962

64 Segre, E., Experimental Nuclear Physics, Vol. II, Wiley, 1953

65 Early and Walker, AIEE Transactions Paper No. 57-59